Post Little Ice Age rock wall permafrost evolution in Norway

Justyna Czekirda[1,*], Bernd Etzelmüller[1], Sebastian Westermann[1], Ketil Isaksen[2], Florence Magnin[3]

[1]Department of Geosciences, University of Oslo, 0316 Oslo, Norway
[2]Department of Research and Development, Norwegian Meteorological Institute, 0313 Oslo, Norway
[3]EDYTEM, Université Savoie Mont-Blanc, CNRS, 73000 Chambery, France

Correspondence to: Justyna Czekirda (justyna.czekirda@geo.uio.no)

Keywords: *Rock walls, Mountain Permafrost, Norway, Thermal modelling, Permafrost modelling, Climate change*

Abstract

The ground thermal regime and permafrost development have an important influence on geomorphological processes in periglacial regions and ultimately landscape development. Around 10 % of unstable rock slopes in Norway are possibly underlain by widespread permafrost. Permafrost thaw and degradation may play a role in slope destabilization and more knowledge about rock wall permafrost in Norway is needed to investigate possible links between the ground thermal regime, geomorphological activity and natural hazards. Here, we assess spatio-temporal permafrost variations in selected rock walls in Norway over the last 120 years. We model ground temperature using the two-dimensional ground heat flux model CryoGrid 2D along nine profiles crossing monitored rock walls in Norway. The simulation results show the distribution of permafrost is sporadic to continuous ~~permafrost~~ along the modelled profiles. ~~Ground~~Overall, our simulations suggest that ground temperature at 20 m depth in steep rock faces increased by 0.2 °C decade^{-1} on average since the 1980s~~. Rates~~, and rates of ground temperature change increase with elevation within a single rock wall section. ~~Multi-~~Heat flow direction is often vertically one dimensional ~~thermal effects are in general smaller~~ within mountains in Norway ~~than in e.g. the European Alps due to gentler mountain topography and less aspect-related variations in ground surface temperature.~~. Nevertheless, ~~the steepest mountains are~~narrow ridges may still be sensitive to even small differences in ground surface temperature~~.~~ and may have horizontal heat fluxes. This study further demonstrates how rock wall ~~permafrost distribution and/or rock wall~~ temperature increase rates and/or rock wall permafrost distribution are influenced by factors such as surface air temperature uncertainties, surface offsets arising from the incoming shortwave solar radiation, snow conditions in, above and below rock walls, rock wall geometry and size, together with adjacent blockfield-covered plateaus or glaciers.

1 Introduction

Numerous studies infer that thawing permafrost induced rapid mass movement events around the world, e.g. in the European Alps (Dramis et al., 1995; Fischer et al., 2006; Ravanel et al., 2010), the New Zealand Southern Alps (Allen et al., 2009), Alaska (Huggel et al., 2010) and the Caucasus (Haeberli et al., 2004). ~~Concerns arise because inventories~~Inventories from the European Alps document an enhanced frequency of rockfalls and rock avalanches from permafrost rock walls since around 1990/2000, especially at the lower permafrost limit,~~ since around 1990/2000~~ in response to accelerated global warming (Ravanel and Deline, 2011; Fischer et al., 2012). An example of a fast response was exceptional rockfall activity ~~that was~~ reported during the extremely hot summers of 2003 and 2015 in the European Alps, likely ~~because of~~due to permafrost degradation (Gruber et al., 2004; Ravanel et al., 2017). Deep permafrost requires longer timescales to degrade and its warming or degradation ~~likely resulted in~~may have influenced the activation of ~~the~~ slowly creeping rock masses in the warmer period of the Holocene Thermal Maximum, thousands of years after local deglaciation (Lebrouc et al., 2013; Böhme et al., 2019; Hilger et al., 2021). The stability of cliffs underlain by permafrost~~-underlain cliffs~~ with the consequent hazards, such as rockfalls or rock avalanches, is of growing concern considering global surface warming projections. Rock wall permafrost is highly susceptible to climate deterioration because: (1) ~~ice contents are typically low in bedrock causing a quicker~~small latent heat effects and high thermal conductivity cause more rapid ground temperature (GT) increase (Gruber and Haeberli, 2007), (2) ~~surface temperature change enters several mountainsides and results in~~the three-dimensional nature of heat flow leads to faster degradation of deeper permafrost in some locations than would be the case in flatter terrain (Noetzli et al., 2007), and (3) thermal conditions in steep bedrock and the atmosphere are strongly coupled since steep slopes are typically ~~covered with~~have shallow snow~~, debris~~ or ~~soil~~surface material, if any (e.g. Boeckli et al., 2012; Myhra et al., 2017).

~~Several authors have linked permafrost degradation and destabilisation of slopes (e.g. Davies et al., 2000; Davies et al., 2001; Gruber and Haeberli, 2007; Krautblatter et al., 2013). Conductive warming of ice-filled fractures, which are believed to stabilise permafrost-underlain mountains (e.g. Dramis et al., 1995), may result in: (1) loss of joint bonding and reduction of shear strength of the joint due to water release through ice melting, (2) shear strength changes due to mechanical ice properties that are a function of the normal stress and temperature (Davies et al., 2001). Furthermore, advective heat transport by percolating meltwater might result in rapid, local degradation of rock wall permafrost, which can trigger rockfalls even in cold permafrost areas (Hasler et al., 2011b). Krautblatter et al. (2013) noticed, in addition, that rock-mechanical properties themselves depend on rock temperature; hence, thawing can lead to a significant drop in rock strength. Frost weathering processes caused by ice segregation and/or volumetric expansion are believed to contribute to the generation of weakness planes or widening fractures in frost-affected rocks (Gruber and Haeberli, 2007; Krautblatter et al., 2013).~~

~~Some impacts of permafrost~~ Permafrost degradation is suggested to have had an impact on the dynamics of recent rock~~-~~ slope failures ~~are likely~~ for a few sites in Norway, e.g. the Gámanjunni-3 instability in ~~the~~ Northern Norway that accelerated recently (Böhme et al., 2019; Etzelmüller et al., 2022), the Polvartinden rock avalanche in~~ the~~ Northern Norway that occurred in 2008 (Frauenfelder et al., 2018) or possibly for the north-facing Veslemannen in ~~s~~Southern Norway that fell in 2019, where at least seasonal freezing controlled the rock stability (Kristensen et al., 2021). Moreover, Blikra et al. (2006) discussed permafrost thawing as a possible triggering mechanism for rock~~-~~ slope failures ~~that~~which have occurred ~~after~~since the deglaciation ~~in~~of Norway. Hilger et al. (2021) modelled permafrost distribution in the Holocene and suggested ~~that~~ permafrost ~~had~~ likely had a stabilising effect on some rock slopes in Norway for several millennia after deglaciation. Magnin et al. (2019) estimated that 11 % of potentially unstable slopes in Norway are currently underlain by at least discontinuous permafrost.

Numerous studies concerning permafrost in the ~~gentle~~flatter parts of the Scandinavian Mountains have been published since the 1980s, attributing variations in mountain permafrost occurrence ~~owing~~ to mean annual air temperature (Etzelmüller et al., 1998), elevation (Sollid et al., 2003; Heggem et al., 2005), snow cover (Farbrot et al., 2008; Farbrot et al., 2011; Isaksen et al., 2011; Gisnås et al., 2017), blockfield cover or ~~surficial~~

~~sediments~~surface materials (Farbrot et al., 2011; Gisnås et al., 2017), and vegetation cover (Farbrot et al., 2013; Gisnås et al., 2017). Studies indicate that recent atmospheric warming has led to the degradation of mountain permafrost in ~~gentle~~flatter terrain in Norway, especially since the 1990s (Isaksen et al., 2007; Hipp et al., 2012; Westermann et al., 2013; Etzelmüller et al., 2020).

The earliest rock wall permafrost studies in Norway provided: 1) first rock wall temperature measurements from rock faces in the Jotunheimen Mountains, central-~~s~~Southern Norway (Hipp et al., 2014), and from small rock cliffs in Troms,~~ the~~ Northern Norway (Frauenfelder et al., 2018), 2) first-order rock wall permafrost map for mainland Norway based on ~~the~~a statistical permafrost model relating permafrost distribution to both elevation and potential incoming short-wave radiation (Steiger et al., 2016), and 3) first 2D modelling for three north-facing rock walls in Norway, based on the interpolated air temperature, variable snow cover and presence of glaciers (Myhra et al., 2017). Systematic field observations using *Geoprecision, M-Log 5W Rock* rock wall loggers ~~that~~(at least 0.1 °C at 0 °C accuracy) were ~~installed~~taken at selected sites in ~~Norway in 2010 in~~ the Jotunheimen Mountains (Hipp et al., 2014~~) and from~~). From 2015 through 2017 ~~at~~ other sites across ~~s~~Southern and ~~n~~Northern Norway were also logged (Magnin et al., 2019~~) allowed later~~), allowing for the improvement of ~~the~~ earlier approaches ~~of~~by Hipp et al. (2014) and Steiger et al. (2016~~)~~). Improvements helped to calibrate a near-surface thermal regime model for rock wall permafrost in Norway, by using mean annual air temperature (MAAT) as an explanatory variable instead of elevation. ~~In~~

The aim of this study~~, we~~ is to improve knowledge about the spatio-temporal variations in ground temperature in steep rock walls in Norway on the inter-decadal scale. We employ the 2D slope-scale transient heat flow model CryoGrid 2D (Myhra et al., 2017) to simulate the thermal ~~state~~evolution of mountain permafrost since 1900 along nine transects crossing the instrumented rock walls in mainland Norway~~ since 1900~~. We advance the methods presented in the study by Myhra et al. (2017), by ~~the~~an observation-constrained ~~modelling,~~model for ground surface temperature (GST), i.e. including the field observations from rock walls in various expositions. All sites presented in this study are monitored by at least one rock wall logger in a vertical rock face, and three of the unstable sites are constantly monitored by the Norwegian Water and Energy Directorate (NVE). Thus, this study aims to be an important baseline for the development of the ground thermal regime in steep mountain terrain, which is possibly unstable. ~~As presented in Magnin et al. (2019) lower elevation limits of near-surface permafrost vary between southern- and northern-facing slopes in Norway by several hundred metres, even though the elevation difference is less pronounced than e.g. in the European Alps. We included nine transects in the present study to improve the knowledge of permafrost geometries and over a century long permafrost development in steep rock faces across Norway. These results are a prerequisite for stability assessment in the Norwegian rock walls.~~

2 Study areas and field installations

2.1 Western Norway

~~The~~ Western Norway is characterised by alpine mountains, deep glacial valleys and fjords, which were formed after multiple mountain and full-sized Fennoscandian ice sheets linearly eroded the pre-existing fluvially eroded valleys (Kleman et al., 2008). The region’s climate ~~in the area~~ is maritime with annual total precipitation ~~sums~~ of more than 2000 mm (Lussana, 2018). Normal mean annual temperature (the normal period 1971-2000) varies between -5 - -4 ºC at the highest mountain peaks to 6 - 8 ºC in the coastal areas (Lussana, 2020) and ~~an~~the annual range of mean monthly air temperature ~~of~~is less than 18 ºC (Tveito et al., 2000). ~~Permafrost~~The permafrost limit is higher in this part of Norway as high-elevation areas are often occupied by glaciers or deeper winter snow, which ins~~o~~ulates the ground ~~in many places~~ (Etzelmüller et al., 2003). ~~The areas where permafrost research was conducted include sporadic permafrost at Finse at the Hardangervidda Mountain Plateau (Gisnås et al., 2014) and during~~During 2015–2017 nine rock wall loggers have been installed at selected ~~sites in the~~ rock walls to measure surface temperature in Western Norway (Magnin et al., 2019). ~~Lower~~The lower rock wall permafrost limits in the area can be at present expected at 1300–1400 m elevation in north-facing slopes (Magnin et al., 2019).

We choose four profiles in ~~the~~ Western Norway for this study: (1) Mannen (Figure 1G), (2) Hogrenningsnibba (Figure 1B), (3) Kvernhusfjellet (Figure 1B) and (4) Ramnanosi (Figure 1C). The name Mannen is used for both a mountain peak at 1294 m elevation and a large active rockslide ~~in the Møre og Romsdal county.~~. Over the last few years, ~~it~~the Mannen instability has been moving with a velocity of more than 20 mm a^{-1} in the upper part of the slope above about 1000 m elevation (Etzelmüller et al., ~~2021). The Mannen instability activated during the Holocene Thermal Maximum around 8 ka (Hilger et al., 2021), leading to the formation of a 20 m high backscarp. The rockslide developed in the Caledonian metamorphic rocks of the so-called Western Gneiss Region, within a quartz-rich gneiss unit with sillimanite and kyanite minerals (Saintot et al., 2012). Hogrenningsnibba (1670 m) and Kvernhusfjellet (1740 m) are two mountains located above the Raudalen Valley north of the Jostedalsbreen Ice Cap, on the eastern side of Lovatnet Lake and next to the Tindefjellbreen Glacier. On the other side of Lovatnet Lake, two of the worst natural disasters in Norwegian history occurred in 1905 and 1936 when rock avalanches from Ramnefjell Mountain ("Loenulykkene") generated tsunami waves and killed many people living in the valley. Bedrock at Hogrenningsnibba is mapped as quartz monzonite, whereas Kvernhusfjellet is mapped as composed mainly of granitic gneiss (Lutro and Tveten, 1996). Ramnanosi (1421 m) is a mountain peak in the Flåm Valley in the former county of Sogn og Fjordane. Ramnanosi peak is part of the larger unstable rock slope Stampa, which includes the continuously monitored Joasetbergi instability around 3 km north of Ramnanosi. Around the Ramnanosi Mountain,~~2022). Hogrenningsnibba (1670 m) and Kvernhusfjellet (1740 m) in the Loen area are two mountains located north of the Jostedalsbreen Ice Cap. Around the Ramnanosi Mountain (1421 m), both gravitational faults and fractures were mapped in the phyllite nappes. Below a west-facing 200 m high slide scar, there are deposits from the rock avalanche/rockfall events (Blikra et al., 2006; Böhme et al., 2012; Böhme et al., 2013).

2.2 The Jotunheimen Mountains

The Jotunheimen Mountain Range is located in the central part of ~~s~~Southern Norway and represents one of the highest mountain areas in Norway, including ~~the~~its highest peak ~~in Norway~~, Galdhøpiggen (2469 m). ~~Till deposits are more common in the Jotunheimen, where glacial erosion has been small compared with the Western Norway due to its proximity to the ice divide (Olsen et al., 2013). At high-mountain plateaus, blockfields were preserved beneath non-erosive ice sheets (Sollid and Sørbel, 1994; Goehring et al., 2008), where negative thermal anomaly in blockfields could enhance the formation of permafrost and cold basal conditions (Juliussen and Humlum, 2007).~~ The Jotunheimen area receives less precipitation than ~~the~~ Western Norway with normal (1961-1990) mean precipitation typically less than 1000 mm per year ~~in the normal period 1961–1990~~ (Lussana, 2018~~) and~~). Normal mean annual air temperature (1971-2000) is under -6 ºC at the highest mountain peaks to 0-2 ºC in the valleys (Lussana, 2020). The area has an annual range of mean monthly air temperature~~ of~~ normally greater than 18 ºC (Tveito et al., 2000). Most mountain permafrost research in ~~s~~Southern Norway has been conducted in ~~the Central~~central and ~~E~~eastern Norway, especially in the Jotunheimen Mountain Range (Ødegård et al., 1992; Farbrot et al., 2011; Isaksen et al., 2011). In 1982, the first 10 m deep borehole at 1851 m elevation was drilled in ~~the ~~Jotunheimen (Ødegård et al., 1992) and then in August 1999, the deepest permafrost borehole (129 m) in Norway was drilled in the continuous permafrost zone at Juvvasshøe (1894 m) as part of the PACE project (Figure 1D; Sollid et al., 2000; Harris et al., 2001). ~~Six additional~~Additional boreholes have been drilled at various elevations in the Juvvasshøe area on its north-eastern slope in August 2008 (Figure 1D; Farbrot et al., 2011). The measured GTs show that ~~discontinuous ~~permafrost occurs ~~down to~~in all boreholes at ~~least the borehole drilled in the bedrock at ~~and above 1559 m elevation~~ (Juv-BH4)~~.~~ For the second lowest borehole (Juv-BH5) and nearby gentle slopes, geophysical surveys performed in 1999 to delineate the elevation limit of mountain permafrost were repeated in 2009 and 2010 and indicated the degradation of permafrost over the intervening decade (Isaksen et al. 2011). At the highest elevations (above ~1850 m elevation) permafrost has likely been present throughout the whole Holocene (Lilleøren et al., 2012). ~~Magnin et al. (2019)'s statistical model results suggested that the lower limit of rock wall permafrost in the Jotunheimen area is at approximately 1550 and 1150 m elevation in the south- and north-facing rock walls, respectively. ~~ ~~We define two profiles in Jotunheimen in this study (Figure 1D) for (1) Veslpiggen (2369 m) and (2) Galdhøe (2283 m).

~~We define two profiles in the Jotunheimen in this study (Figure 1D) with (1) Veslpiggen (2369 m) and (2) Galdhøe (2283 m). The selected profiles are mostly within the tectonic unit of the Jotun-Valdres Nappe Complex and the bedrock along the profiles is composed of pyroxene granulite (Lutro and Tveten, 2012).~~

2.3 Northern Norway

The geomorphology of Northern Norway is in general similar to ~~s~~Southern Norway with multiple glaciations leading to the formation of fjords and U-valleys ~~and the depositional areas further inland, e.g. at Finnmarksvidda~~ (Kleman et al., 2008; Olsen et al., 2013). The climate in~~ the~~ Northern Norway is mostly subarctic in the lowland and tundra type in the mountains. The climate varies from maritime in the coastal areas, with the ~~largest~~highest annual total precipitation ~~sums in the Nordland county~~reaching > 2000 mm in 1961–1990 (Lussana, 2018), to a more continental character ~~at Finnmarksvidda~~further inland, where annual total precipitation ~~sums were~~averaged less than 750 mm in 1961–1990 (Lussana, 2018). Normal ~~Several permafrost studies have been conducted in the Northern Norway, where both miniature~~~~M~~mean annual air temperature ~~dataloggers and borehole temperature strings were installed~~(~~for the normal period ~~1971-2000) is between -6 - -5 ºC at the highest mountains to ~~monitor ground thermal conditions (Isaksen et al., 2008; Christiansen et al., 2010; Farbrot et al., 2013). Farbrot et al. (2013) distinguished three permafrost regions in the Northern Norway (excluding Nordland): (1) maritime mountain permafrost in the western part of Troms county, (~~2~~) continental permafrost in Finnmark, mainly in palsa mires, and (3) Low Arctic permafrost at the Varanger Peninsula.~~-6 ºC in the coastal areas (Lussana, 2020). For the gentle terrain, the permafrost limits decrease from 800–900 m elevation in the western areas of ~~Troms~~Northern Norway to around 200–300 m elevation ~~in the continental parts of Finnmark and Troms~~further inland (Farbrot et al., 2013). Three transects in the coastal areas of~~ the~~ Northern Norway are extracted in this study: (1) Gámanjunni 3 (Figure 1A), (2) Ádjit (Figure 1E), (3) Rombakstøtta (Figure 1F). Gámanjunni 3 (Figure 1A) ~~in the Manndalen Valley,~~

~~west of Tromsø,~~ is one of the most unstable rock slopes in Norway, moving recently up to 60 mm a^{-1} ~~–~~(Böhme et al., 2016a; Böhme et al., 2019; Etzelmüller et al., 202~~1~~2). The unstable part has moved approximately 150 m downslope since the end of the Holocene Thermal Maximum (Böhme et al., 2019; Hilger et al., ~~2021). The upper part of the profile (>300–500 m elevation) is composed of mica schists that are part of the Kåfjord Nappe, whereas the lower parts of the profile are mapped as calcareous mica-schist within the Váddás Nappe and superficial deposits of Quaternary age (Quenardel and Zwaan, 2008).~~ 2021). Ádjit (Figure 1E) is a mountain ridge ~~in the Skibotn Valley, Troms~~, where below its south-western rock wall several periglacial and mass movement landforms were mapped, such as ~~e.g. active and inactive talus-derived rock glaciers (Nopper, 2015; Eriksen et al., 2018). The mountain is located within the Kåfjord Nappe and meta-arkose to feldspathic quartzite, together with mica or garnet-mica schists dominate along the profile (Boyd et al., 1985; Quenardel and Zwaan, 2008). Rombakstøtta (Figure 1F) is a steep mountain top at 1230 m elevation located a few kilometres east of Narvik, Nordland. Geologically, Rombakstøtta profile is within the Narvik Nappe Complex, and the rock types mapped along the profile are garnet or kyanite-garnet two-mica schist, quartzite and quartzite schist (Karlsen, 1991). The north-facing part of the mountain, east of our profile, displays open tension cracks and it has been subject to investigations due to its instability potential (Gauer et al., 2016; Morken, 2017).~~ active and inactive talus-derived rock glaciers (Nopper, 2015; Eriksen et al., 2018). .

3 Methods

3.1 CryoGrid 2D

A transient 2D heat conduction model, CryoGrid 2D (Myhra et al., 2017), is employed to model GT evolution along the selected profiles. The subsurface temperature is modelled by solving the heat diffusion equation following Fourier's law of heat conduction with the material- and temperature-dependent thermal parameters. The effective volumetric heat capacity, which includes the latent heat effects due to water/ice phase transitions, and the thermal conductivity are functions of volumetric contents of soil/rock components (mineral, water/ice, air, organic) and their individual thermal properties, as defined in the one-dimensional CryoGrid 2 model (Westermann et al., 2013). In CryoGrid 2D, the MATLAB-based finite element solver MILAMIN package (Dabrowski et al., 2008) generates an unstructured triangular mesh for a given slope geometry and is used for space discretisation, whereas time discretisation is based on the finite-difference backward Euler scheme. The spatial resolution in ~~the~~ CryoGrid 2D is prescribed by the maximum triangle area (MTA), i.e. a maximum area for the three node triangular elements. Dirichlet boundary conditions are used at the upper model boundary and the model is forced by GST at the air-ground interface, i.e. temperature below the snowpack. A more thorough description of the model and equations can be found in Myhra et al. (2017). Note that since CryoGrid 2D is a conductive model~~, hence~~, convective or advective heat transport is unaccounted for. The model is constructed as a 2D slice through a slope, assuming translational symmetry along the third dimension.

3.2 Model geometry and ground stratigraphy

The upper boundary for the selected profiles was extracted from the 0.5–1 m digital elevation models (DEMs) available from the Norwegian Mapping Authority at www.hoydedata.no, whereas the lower boundary extends down to 6000 m below sea level. Most profiles are approximately 2.5–4 km long, except for the ~7.5 km long profiles in ~~the~~ Jotunheimen (Figure 2). Because profiles in ~~the~~ Jotunheimen, together with the profile at Kvernhusfjellet traverse glaciers, we compute glacier bed elevation by extracting glacier thickness provided by ~~the Norwegian Water Resources and Energy Directorate (~~NVE~~)~~, where ice thickness was estimated using a distributed model described in detail in Andreassen et al. (2015). At Kvernhusfjellet, we add a 5 m thick snow patch on the top plateau as observed on the orthophotos from the Norwegian Public Roads Administration, the Norwegian Institute of Bioeconomy Research and the Norwegian Mapping Authority (www.norgeibilder.no). Meshes for each profile are constructed with nodes at a 0.05 m distance at the upper boundary and MTA that increases with depth. The constructed meshes have MTA of 0.05 m^2 between the ground surface and 2 m depth, 0.20 m^2 at depths between 2 and 10 m, 0.50 m^2 at depths between 10 and 20 m, 5.00 m^2 at depths between 20 and 100 m, and 50 m^2 below 100 m depth. The model domains consist of approximately 500,000 vertices, except for the longer profiles in ~~the~~ Jotunheimen, where each mesh has ~1,250,000 nodes. No mechanical aspect is considered in this study; hence, the meshes remain static throughout the ~~whole~~entire simulation period.

A digital map of ~~superficial deposits~~surface materials is available for ~~the entire~~all of Norway from the Geological Survey of Norway (~~NVE~~NGU) at 1:250.00 scale. Due to the small scale of the map, we refine the geomorphological mapping along the upper profile boundaries based on the available orthophotos from www.norgeibilder.no. The ground composition (Supplementary Table ~~1~~S1) is based on the sediments mapped on the surface for most profiles, where we define hard vertical boundaries between the sediment classes also at depth because such an approach allows for an effective and almost automated generation of nodes for an unstructured mesh. Similar volumetric contents and layers for the NVE sediment classes are assumed as in Westermann et al. (2013) for the one-dimensional CryoGrid 2. However, we apply a higher rock porosity than Westermann et al. (2013) and follow the higher porosity of 5 % vol. to account for rock discontinuities as Myhra et al. (2017). The thermal conductivity for the mineral fraction is extracted from the same data as in Westermann et al. (2013) and varies for the sites between 2.3 and 3.1 W m^{-1} K^{-1} (Supplementary Table ~~A1~~S2). For the Jotunheimen profiles, we used a value of 2.7 W m^{-1} K^{-1} (Hipp et al., 2012). The NVE sediment classes and their stratigraphy as defined in Westermann et al. (2013) lack a suitable representation for some sediments mapped along the profiles. Therefore, we added a few sediment classes to fill this gap (Supplementary Table ~~1~~S1). The Ádjit profile intersects a rock glacier at lower elevations, where we used a similar geometry, as presented in Eriksen et al. (2018). For Gámanjunni we use a slightly modified version of a geological profile for the unstable part (Böhme et al., 2016b), in conjunction with the geomorphological mapping outside of the geological model. The scree class is defined with the same parameters as in Myhra et al. (2019). At Ramnanosi, very thick 30 m thick colluvium deposits are assumed just below the rock wall down to around 600 m elevation and 4 m thick regolith is assumed at the plateau. Bedrock stratigraphy is assumed to be below glaciers and perennial snow.

3.3 Model forcing

3.3.1 Surface air temperature

The modelled daily surface air temperature (SAT) data set for ~~the~~ mainland Norway, hereafter seNorge, is available for 1 km^2 grid cells for the period 1957–present (Lussana, 2020). However, the seNorge data set overestimates SAT trends and often shows ~~increasing~~positive SAT trends with elevation for our study sites, leading to e.g. 3 °C SAT increase in ~~the~~ Jotunheimen between the 1980s and ~~the~~ 2010s. This is the result of the inhomogeneity in the network of meteorological stations, particularly the lack of meteorological stations at mountain plateaus in some periods. Cold periods are overestimated if the gridded data set is based mainly on meteorological stations in valleys, where air temperature inversions are frequent during winter. Therefore, we choose to force the model with the regional monthly data set at 2 km spatial resolution provided by the Norwegian Meteorological Institute, described in detail in Hanssen-Bauer et al. (2006). This regional model yields robust temporal estimates at a regional scale; ~~nevertheless,~~however, the data provides rather poor ~~spatial coverage~~temperature series at local scales. Therefore, we superimpose a local component on the regional data. Regional SAT data sets were provided for valleys at the bottom of each profile. We use the following procedure for each ~~data set~~profile:

(1) Since we~~ want to~~ begin to run the model at the end of the Little Ice Age (LIA) in Norway and the regional SAT data sets start in 1900, we reconstruct SAT back in time by using SAT from the long-term meteorological stations described in ~~Table 2.~~Supplementary Table S3. The latter data allows for SAT reconstruction back to 1861 for Western Norway, 1864 for Jotunheimen and 1872 for Northern Norway. We account for average offsets in the overlapping period between SAT from the long-term meteorological stations and the regional SAT.

(2) We adjust regional SATs by subtracting offsets between the regional and local SATs from a nearby meteorological station or seNorge for valleys over the last few years.

(3) We compute the average monthly lapse rate between two meteorological stations, typically one at the bottom of the valley and one at or close to the mountain plateau over the last few years. The selected SAT data are listed in Supplementary Table ~~2~~S3.

(4) We compute monthly ~~temperature at~~SAT –along the ~~mountain top~~profiles using~~ the~~ monthly lapse rates.

The selected last few years used in this analysis are periods when temperature measurements in the rock walls are available. This allows for a comparison of SAT with GST ~~in the~~determined from rock wall loggers in months with minimal shortwave radiation, e.g. December, and gives more reliability. The aforementioned procedure allows for the reproduction of similar SAT trends at mountain plateaus as provided for valleys, hence removing ~~the~~ elevation dependency in the SAT trends present in the seNorge data. ~~We describe~~Appendix A describes 10~~-~~-year running mean surface air temperature (SAT10a) evolution for the highest elevations along each profile~~ in Appendix B. ~~. After generation of the SAT data sets, we account for the nival offsets and surface offsets arising from the shortwave solar radiation (See Subsections 3.3.2 and 3.3.3.) by modifying SAT along the profiles.

3.3.2 Nival offsets

We lack observations of snow cover dynamics and snow depths from the rock walls in Norway. In this study, we are mostly interested in the thermal insulation effect of snow cover and not snow depth itself, especially because our permafrost model lacks an explicit snow domain. In equilibrium permafrost models such as the TTOP-model (Smith and Riseborough, 2002), insulating snow effects are usually accounted for by using ~~nF~~freezing n-factors (nF) that link SATs and GSTs. We follow an easy-to-implement hypothesis that snow thickness and its insulating effect on the GST depend on the slope gradient. Hence, we assign various nF~~-factors~~ values along the profiles according to the computed slope gradient; however, some sediment/vegetation cover types have distinct values for nF (Table ~~3~~1). We assume that steep slopes, i.e. steeper than 60° are snow-free (discussed in Sect. 5.1.4). Furthermore, we detect 1 m deep sinks along the profiles using fillsinks from TopoToolbox 2 (Schwanghart and Scherler, 2014) and assume that these are areas where snow ~~might~~may accumulate and use the same nF as for the gentlest gradient (slope < 30°) ~~along profiles.~~in each profile. Additionally, we assign a special nF value of 0.25, as computed by Gisnås et al. (2017), for ~~the~~ broad-leaved forest (code 311) based on CORINE land cover 2018 (Aune-Lundberg and Strand, 2010). ~~The broad-leaved forest occurs at lower elevations along the profiles.~~

For the top block at Gámanjunni (slope gradient < 30°), we compute nF=0.~~5~~50 based on the SAT and GST measurements conducted by Eriksen (2018b). For the rock glacier at Ádjit, we found an nF value of 0.~~8~~80 (Eriksen, 2018a). Measurements from the three uppermost boreholes BH-1 (nF=0.78 in 2008–2019), PACE (nF=0.89 in 1999–2018) and BH-2 (nF=0.37 in 2008–2019) in ~~the~~ Jotunheimen yield an average rounded nF value of 0.70 that we apply for the blockfield locations. We note that nF for the blocky terrain (blockfields and rock glaciers) is not necessarily due to nival offsets and is rather caused by air convection (discussed in Sect. 5.1.1.).

3.3.3 Surface offsets

Our analysis of the measured 2 h rock wall temperature indicates that rock wall temperature in Norway is influenced by solar radiation as early as February in ~~the~~ Northern Norway and in all months of the year in ~~s~~Southern Norway. ~~Because of~~Due to their steep vertical slopes, incoming shortwave solar radiation ~~might~~may not necessarily be the largest during June, as expected for a horizontal surface at the latitudes in Norway. In the case of rock walls, ~~nT~~thawing n-factors (nT; Smith and Riseborough, 2002) ~~might thus~~may not be able to account for surface offsets (SOs) due to the shortwave solar radiation in the months when solar radiation is maximum and SAT is still negative, which ~~might~~may occur in the spring months. Additionally, reflected solar radiation from the surrounding terrain is likely an important factor during spring/early summer when snow cover ~~might~~may be present, or during ~~the~~a whole year in the rock walls above glaciers. Instead of using temperature transfer factors, we add measured average monthly SOs to SATs at the location of rock walls along profiles. Measured monthly SOs are computed as a difference between monthly mean ground surface (GST_{month}) and surface air (SAT_{month}) temperature:

$$SO_{month} = GST_{month} - SAT_{month}. \quad (1)$$

Note that we refer to both rock surface and soil surface temperatures as GSTs in this study. We apply the same SOs to all steep parts of slopes (>60°) along profiles and to all months during the entire modelling period. Table ~~4~~2 summarises the aspects along profiles and selected rock wall loggers to account for the monthly SOs. Supplementary Figure S1 shows more details about the applied loggers along profiles. In this study, SOs is usually referred to SOs arising mainly from solar radiation, unless other indicated.

3.4 Model initialisation, model ~~runs~~simulations and sensitivity tests

~~We~~Model simulations start ~~to run the model~~ around the end of LIA in Norway when the long-term SAT data from meteorological stations are available ~~for correlation~~ (1861/1864 for the profiles in ~~s~~Southern Norway, 1874 for the profiles in ~~the~~ Northern Norway). CryoGrid 2D is initialised in a two-step procedure: (1) by running a steady-state version of the model using the average GST for the first decade of the available data and the geothermal heat flux at the lower boundary, (2) spin-up of the model at monthly time steps around 50 times, which yields temperature difference between the consecutive ~~runs~~simulations at the order of 10^{-4} °C. After this initialisation procedure, we continue to run the model at monthly time steps. Accounting for additional at least 20 years of initialisation period, we present the results of the model ~~runs~~simulations since 1900. Zero heat flux condition is assumed along the vertical left and right boundaries. An average value of geothermal heat flux of 50 mW m^{-2}

(Slagstad et al., 2009) is applied at the lower boundary at all sites, except for the profiles in ~~the~~ Jotunheimen, where a value of 33 mW m^{-2} is used (Isaksen et al., 2001). Beneath modern glaciers or perennial snow, we apply GST of 0 °C corresponding to the temperate bed conditions, except for the shallower glaciers or ice patches along the Galdhøe profile in ~~the~~ Jotunheimen, where we apply cold basal conditions at -3 °C as measured in the Juvfonne ice patch (Ødegård et al., 2017). We note, however, that the assumed temperate bed conditions should be rather represented by polythermal bed conditions because the thinnest parts of glaciers have likely temperatures below the pressure melting point (Etzelmüller and Hagen, 2005).

We ~~conduct~~evaluate model sensitivity for all profiles by rerunning the model, including the initialisation steps~~, for several scenarios.~~. However, we note that some ~~runs~~simulations are to ~~test the~~ check the thermal influence of likely uncertainties in the model forcing or parameters ("uncertainty ~~in the runs,~~simulations"), and some are ~~control runs~~"test simulations" to investigate the thermal influence of e.g. ~~glacier cover~~nearby glaciers, sediments or SOs in the rock walls. ~~Sensitivity scenarios~~Uncertainty and test simulations are listed in Table ~~5.~~ 3.

4 Results

4.1 Surface offsets and logger data

Figure 3 shows the monthly SOs for ~~the majority of~~ rock wall loggers in Norway. The south-facing loggers usually have the maximum monthly SOs in April, whereas the rest of the loggers often have the maximum monthly SOs in May. There are a few exceptions, e.g. rock wall loggers at Mannen and Rombakstøtta indicate the maximum monthly offsets solely in June. ~~The observation-constrained modelling~~The calibration of GST forcing input using the measured SOs yields zero mean error and an RMSE below 1.40 °C for the monthly GSTs and significantly improves the correlation between the forcing data and the rock wall measurements (Supplementary Figures ~~S1-S20).~~S2-S21).

Supplementary Table S4 includes information about the measured GSTs at the study sites. Mean rock wall temperature at or below 0 °C over at least two consecutive years usually indicates permafrost; however due to lateral heat fluxes and the preservation of -long-term temperature signals at depth, permafrost may occur even if rock wall logger temperature is above 0 °C (Noetzli et al., 2007; Noetzli and Gruber, 2009). All loggers at Mannen and the W-facing logger at Ramnanosi suggest an unlikeliness of permafrost presence in these rock wall expositions over the last few years. The north-facing logger at Ramnanosi measured -mean rock wall temperature at 0.02 °C (Aug 2016–Jul 2020; 1370 m); hence, permafrost was likely in the north-facing parts of the slope, at least before the measurement period started. The north-facing logger in the Loen area indicates that permafrost is likely, whereas the west- and south-facing loggers have positive temperatures. In Jotunheimen, most rock wall loggers indicate that even cold permafrost exists in the Jotunheimen Mountains. In the Gámanjunni area, at least warm permafrost conditions can be expected in the rock walls. For Ádjit both loggers indicate permafrost, although the south-facing rock wall is close to non-permafrost conditions. All loggers at Rombakstøtta, except for the east-facing logger, indicate that at least warm permafrost may be present in the rock walls.

4.2 ~~Modelled~~ Distribution of modelled ground temperature

~~4.2.1 Western Norway~~

~~***Mannen***~~: ~~Most~~ We modelled GT at four sites in Western Norway, two sites in Jotunheimen and three sites in Northern Norway (Figure 4). These results are also presented in Videos 1-20.

4.2.1 The permafrost limits

Western Norway: The main simulations ~~indicate permafrost absence in~~ for the two profiles with the mountain peaks at an elevation below 1400 m **(**Mannen and Ramnanosi**)** suggest no permafrost in these mountains since 1900 (Figure 4; ~~Video 1). However, the coldest scenario ("T-~~Videos 1~~°C") reveals that permafrost pockets could have existed in the mountain before 2019 in moderately steep slopes below the uppermost rock face, where the monthly SOs arising from solar radiation were not assumed (Video 1). The modelled GTs above 1100 m are mainly~~-4). The simulations for the two profiles with higher mountain peaks **(**Hogrenningsnibba and Kvernhusfjellet**)** indicate that sporadic to discontinuous permafrost likely occurs in these mountains, even below glaciers and snow patches (Figure 4, Videos 5-8). The lower permafrost limits vary between 1300 m for the NNE-facing slope at Hogrenningsnibba to around 1600 m at the west-facing slope of Kvernhusfjellet over the 2010s.

Jotunheimen: For both profiles in Jotunheimen, sporadic to discontinuous permafrost is simulated down to an elevation of 1530–1590 m over the 2010s (Figure 4; Videos 9-14). Considering the simplified forcing for the gentle terrain in our modelling, a boundary between discontinuous and continuous permafrost can only be established assuming a particular isotherm, here -2 °C, as the lower limit for continuous permafrost. ~~0.5 and 1.5 °C, with a maximum range of GTs in the uncertainty runs between 0.~~In that case, continuous permafrost limit is at ~1780–1860 m for the gentle terrain over the 2010s.

Northern Norway: Modelled GT for Gámanjunni shows a colder NE-facing slope compared to the SW-facing slope, and the lower permafrost limits are approximately 100 m higher at the SW-facing slope, at an elevation of around 850 m over the 2010s (Figure 4; Videos 15-16). At Ádjit, the SW-facing rock wall is warmer than the NE-facing slope at Ádjit, even though the modelled permafrost limits are lower on the SW-facing slope than on the NE-facing one, at around 700 m over the 2010s, roughly where the active rock glacier has its front (Figure 4; Videos 17-18). The permafrost limits at Rombakstøtta are modelled slightly higher than at the other sites in Northern Norway (Figure 4; Videos 19-20), at approximately 900–950 m and 1000 m for the NNE- and SSW-facing slopes over the 2010s.

4.2.2 Ground heat flux direction

The heat flux direction is shown in Videos 2, 4, 6~~to 0.9 °C (Figure 4).~~, 8, 11, 14, 16, 18, 20. The main ground heat flux direction is ~~almost~~ often one-dimensional beneath larger plateaus (e.g. Ramnanosi, Mannen, Galdhøe). For the latter simulations, the main heat flux direction tilts slightly outwards in simulations without monthly SOs, where relatively colder zones are simulated below rock walls. Simulations with large SOs in the rock walls show that heat flux may be forced towards the colder plateaus if SOs are large enough (e.g. Veslpiggen, Ramnanosi). The main heat flux direction is more tilted towards colder zones for the mountains with more pronounced differences in GST between opposite mountainsides (e.g. Hogrenningsnibba, Kvernhusfjellet, Gámanjunni). The tilt between opposite mountainsides may sometimes even be horizontal beneath the mountain peaks with a shorter distance between two mountainsides and larger differences in GST (e.g. Ádjit, Hogrenningsnibba). If GST between the opposite mountainsides is similar (e.g. Rombakstøtta), the main heat flux direction will remain vertically one-dimensional~~ beneath~~. Glaciers may modify the main heat flux direction below the plateaus ~~and tilts outwards towards the colder slopes elsewhere (Video ~~(See Sect. 4.2~~). ~~.4).

~~***Hogrenningsnibba**: On the NNE-and SSW-facing slopes of Hogrenningsnibba, the lower permafrost limits remain respectively at about 1300 m and 1400–1450 m during the last 120 years (Figure 4; Video 3). The simulated GTs are slightly lower at the lower permafrost limit on the SSW-facing slope due to the less-conductive, 1-m thick colluvium layer (compare "Main" with "Bedrock" in Video 3). GTs are above -3 °C with the range of GTs in the uncertainty scenarios below 1 °C (Figure 4). In most scenarios, the main heat flux direction is towards the colder NNE-facing slope, except for the simulation with the glacier (Video 4).~~

~~***Kvernhusfjellet*: According to the GT field simulated for Kvernhusfjellet (Figure 4), warm sporadic to discontinuous permafrost occurs in the mountain, also below parts of the snow patch on the upper plateau and the glacier on the east-facing slope. In the west-facing slope, sporadic permafrost occurs down to an elevation of 1550 m in 1940, 1400 m in 1980, and degrades almost completely in 2020 with a deep permafrost limit at around 1620 m (Figure 4; Video 5). GTs are mostly above -1 °C with the modelled range of temperature in the uncertainty simulations of below 0.5 °C under the glaciated slope and 0.5–1 °C under the SW-facing slope (Figure 4). The warm-based glacier contributes to slightly higher GTs in the mountain (Video 5). Since the simulated permafrost is warm (>-2 °C), ignoring SOs results in a difference of several hundred metres in lower permafrost limit and changing the SAT forcing by adding 1 °C yields sporadic to no permafrost. In the "N logger" scenario, permafrost is modelled down to 1300 m in 2020, whereas in the warmer "S logger" scenario permafrost limit is at 1600 m in 2020. The main heat flux direction in the mountain is towards the coldest zones below the west-facing rock face (Video 6). In the warmest scenarios, the heat flow direction in the middle of the mountain is, however, almost one-dimensional vertically towards the plateau.** ~~

4.2.3 Steepness and SOs

Even though Kvernhusfjellet and Hogrenningsnibba lie close together, the permafrost limits are at a higher elevation at the W-E Kvernhusfjellet profile than at the SSW-NNE Hogrenningsnibba profile. This difference results from the extent of the steepest parts, where we applied SOs, and is particularly clear when comparing the "Main" simulations with the "Without monthly offsets" simulations (~~Videos 3,~~Figure 5~~),~~); i.e. ignoring SOs at the steeper Kvernhusfjellet leads to much lower GTs in the whole mountain than when ignoring SOs at ~~moderately steep Hogrenningsnibba.~~the moderately steep Hogrenningsnibba. In the "Without monthly offsets" simulation for Kvernhusfjellet, permafrost is modelled down to 1300 m over the 2010s, whereas in the warmer main simulation the permafrost limit is at 1600 m over the 2010s. Moreover, the ~~similar scenarios~~simulations with "Bedrock & Glacier at NNE" for Hogrenningsnibba and "S logger" for Kvernhusfjellet show how the differences in geometry influence permafrost distribution, e.g., the permafrost limit is modelled at 150 m lower elevation in the former ~~scenario.~~simulation (Videos 5 and 7). Furthermore, our results show that permafrost may underlie parts of the mountain where mean annual ground surface temperature (MAGST) is above 0 °C. For instance, the logger at Hogrenningsnibba indicates positive MAGST at the SSW-facing slope and permafrost underlies this slope in even the warmest simulation ("T+1 °C") due to permafrost extending there from the NNE-facing slope. The Kvernhusfjellet profile lacks a substantially colder slope, since there is a warm-based glacier on the E-facing slope, hence permafrost in the W-facing slope is unrelated to permafrost extending from a colder slope and is rather degrading permafrost.

Asymmetric lower permafrost limits at Gámanjunni are not related to the higher SOs applied to the SW-facing rock wall and are rather caused by the extent of steeper terrain in the profile. The NE-facing slope is rougher and consists of several smaller rock walls, whereas the SW-facing slope encompasses mainly one smoother rock wall, less than 50 m in height. The influence of geometry is especially clear in the "W logger" simulation (Figure 5), where we applied slightly colder forcing to the SW-facing rock walls and the results still show lower deeper GT in the NE-facing slope. The results for Gámanjunni show that in the simulations with SOs, the scree slope is often colder than the sun-exposed, SW-facing rock wall. The scree slope is also less coupled to atmospheric conditions due to snow cover and greater ice content, hence permafrost degradation occurs slower than in the rock wall, further amplifying the differences in GT between the sun-exposed rock face and scree slope during warmer periods. In the simulation "Without monthly offsets", the rock wall is always colder than the scree slope. ~~***Ramnanosi***: The main run for Ramnanosi using the west-facing RW logger suggests no permafrost in the mountain since 1900 (Figure 4; Video 7). For 2020, GTs are mostly below 2 °C at elevations above 1200 m with the GT range below 1.1 °C (Figure 4). The three coldest sensitivity scenarios, namely "Without monthly offsets", "T-1 °C" and "N logger" indicate that warm permafrost (>-2 °C) has been present in the rock wall above an elevation of 1200 m over the last 120 years (Video 7). Modelled permafrost is in a degrading state in 2020 and its temperature is above -0.5 °C in the coldest scenario. The main flux direction in Ramnanosi is usually towards the coldest zones somewhere in the upper parts between the rock wall and plateau in~~For the Ádjit profile, the SW-facing rock wall is much steeper than the NE-facing slope, which is the reverse of Gámanjunni geometry. The simulation "Without monthly offsets" (Figure 5) shows the SW-facing slope as colder than the NE-facing slope due to the extent of the rock walls.

Permafrost temperatures at Rombakstøtta are slightly higher in parts of the NNE-facing slope (>60°) than the SSW-facing slope (<60° steep), as we only applied monthly SOs on slopes steeper than 60°. In the simulation "Without monthly offsets" for Rombakstøtta, GTs are much lower on the NNE-facing rock wall than on the SSW-facing slope (Figure 5).

4.2.4 Thermal impact of glaciers

GTs are simulated to be higher beneath the warm-based glaciers at Veslpiggen, with no permafrost beneath the thickest parts of the glaciers (Figure 5). The ground below the thinner glacier sections is, nevertheless, underlain by permafrost. Removing glaciers below the Veslpiggen Plateau leads to major changes in the main heat flux direction from the tilted heat flux (between the E-facing slope towards the blockfield-covered plateau), to one-dimensional vertical heat flux in the "Without glaciers" simulation (Figure 5, Video 11). The modelled GT in the Galdhøe Plateau is much less thermally affected by glaciers than the Veslpiggen Plateau and is almost the same in the main simulation and the simulation without glaciers (Video 14), since there are no glaciers reaching as high up the mountainside as on the flanks below the Veslpiggen Plateau. The warm-based glacier also contributes to slightly higher GTs in Kvernhusfjellet (Video 7).

4.2.5 Model sensitivity: coldest and warmest simulations

Modelled GT is lowest in the simulations without SOs ("Without monthly offsets") or with 1 ºC lower SAT ("T-1 °C") for all profiles (Videos 1-20). The coldest simulations for Mannen and Ramnanosi reveal that warm permafrost (>-2 °C) or permafrost pockets could have existed in these mountains over colder periods or at the beginning of the 20th century (Videos 1 and 3). The simulations with less snow (“nF-0.1”) show almost as low GT as the “T-1 °C” simulations for some profiles (e.g. Veslpiggen, Galdhøe). For Ádjit and Gámanjunni, tested uncertainties in the water content affect the results much less than the uncertainty in the GST forcing and slightly less than the uncertainty in snow conditions.

Highest GT is most ~~scenarios (Video 8). For the colder scenarios, where rock walls have cold zones, heat flux is mainly directed towards them. In the “S logger” scenario with a much warmer rock face, heat flux is forced towards the colder zones parallel to the plateau surface, suggesting that plateaus may be colder than rock walls if SOs are large enough.~~

~~4.2.2 Jotunheimen~~

~~Figure 5 provides modelled maximum GT in the Jotunheimen profiles. For both profiles, sporadic to discontinuous permafrost is simulated down to an elevation of 1420–1520 m in 1980 and 1530–1590 m in 2020. Considering the simplified forcing for the gentle terrain in our modelling, a boundary between discontinuous and continuous permafrost can only be established assuming a particular isotherm, here -2 °C, as the lower limit for continuous permafrost. In that case, continuous permafrost starts at ~1780–1860 m in 2020 for the gentle terrain. For the highest plateaus (>2100 m), which are covered with blockfields, GT is modelled between -6 – -4 °C. The simulated span of the GT in the Jotunheimen with respect to the main run is similar to the runs for the Western Norway, with the deep GTs up to 1.0 °C different from the main run (Figure 5). The bedrock beneath glaciers have the least GT span since we considered the same temperatures at glacier beds in all sensitivity scenarios. Sensitivity~~often modelled in the simulations with “T+1 °C”, except for Jotunheimen. In Jotunheimen, the sensitivity simulations display highest GTs for “Blockfields nF = 0.4”, where snow conditions are changed substantially for the widespread blockfield-covered plateaus ~~in the Jotunheimen~~ (Videos 9, 10, 12, 13).

~~***Veslpiggen***: The assumed warm-based glaciers increase GTs at Veslpiggen and the ground below the thickest parts of the glaciers is modelled without permafrost. The ground below the thinner glacier parts is, nevertheless, underlain by permafrost. The assumed GST conditions~~ The assumed snow conditions at the blockfield locations at Veslpiggen have a large thermal influence on ~~the~~ deeper GTs in the rock walls. ~~In~~For the ~~NW-E~~ Veslpiggen ~~profile~~and Galdhøe profiles, the warmest ~~scenario~~simulation “Blockfields nF=0.4” indicates that the coldest permafrost areas below the ~~150 m high~~ NW- or W-facing rock walls, whereas in the main ~~scenario~~simulation coldest permafrost is modelled below the blockfield-covered ~~plateau (Video 9). Consequently, the main heat flux in the area has direction towards the coldest midsection below the rock wall in the scenario “Blockfields nF=0.4” (Video 11). Otherwise, the main heat flow is towards the coldest zone parallel to the surface topography of the plateau in the main scenario (Video 11). For the east-facing rock walls at Veslpiggen, GT in the rock walls frequently exceeds GT in the blockfields at a similar elevation due to the large SOs in this exposition, forcing the heat flux from the warmer rock walls towards the colder plateaus. Large SOs even in the NW-facing exposition and warm-based glaciers seem also to modify the GT in the Veslpiggen Plateau. The removal of glaciers leads to major changes in the main heat flux direction below the plateau from the tilted heat flux direction between the glaciated E-facing slope towards the colder blockfield-covered plateau in the main scenario to primarily vertically one-dimensional heat flux direction deeply in the mountain in the scenario “Without glaciers”.~~ plateaus (Video 9 and 12). SOs arising from solar radiation and SAT forcing are thus the most important factors for modelled GT within the tested values for most profiles; however, snow conditions may have a larger influence if the nF-factor is changed substantially for large areas.

4.2.6 Elevational distribution of GT at 20 m depth

We also analyse the distribution of GT in rock walls at 20 m depth, in relation to elevation for all simulations and profiles (Supplementary Figure S22). Simulations “Without monthly offsets” often yield the coldest midsection in a single rock wall, whereas most other simulations differ from these results, except for the simulations using data from the north-facing loggers for Kvernhusfjellet and Ramnanosi, which have small average annual SOs (~0.5 °C). Higher rock walls (> 50 m high, e.g. Veslpiggen) have the highest GTs in their midsection for simulations with large SOs (Figure 6). For the smaller rock walls (e.g. Gámanjunni, Kvernhusfjellet), GT at 20 m depth changes with elevation, depending on the distribution of the various terrain types in the vicinity of a single rock wall (Figure 6). GT increases with elevation if the terrain above a single rock wall is gentler than the terrain below this single rock wall, and the opposite is modelled if the terrain above is steeper than the terrain below. Thus, 20 m GT distribution in smaller rock walls is predominantly due to snow cover distribution in the rock wall vicinity. The thermal influence of snow cover on the plateau is also evident for larger rock walls below mountain plateaus (e.g. Rombakstøtta), where GT increases with elevation from the midpoint of a rock wall section (Figure 6). The uppermost east-facing rock wall at ~2300 m at Veslpiggen (“Veslpiggen E higher” in Figure 6) has glaciers below and blockfields above, and GT decreases with elevation due to the large thermal influence of the glaciers.

4.3 Ground temperature trends in rock walls

~~***Galdhøe***: The modelled GT in the Galdhøe Plateau is much less thermally affected by glaciers than the Veslpiggen Plateau and is almost the same in the main scenario and the scenario without glaciers (Video 12). The assumed forcing for the blockfields influences GT in the rock walls similar to the Veslpiggen Plateau. In the scenarios “Blockfields nF=0.4” and “Without monthly offsets” the main heat flux is directed towards the colder zones below the rock walls and even the east-facing rock wall is underlain by a relatively lower GT than the surrounding ground (Video 14). Most other scenarios mainly show a slightly tilted one-dimensional heat flow direction towards coldest permafrost below the blockfield-covered plateau. GT below blockfields is modelled colder than below till, which can be seen at one section along the Galdhøe profile, where we applied the till stratigraphy and nF-factor of 0.4 (Compare with Figure 2).~~

~~4.2.3 Northern Norway~~

~~***Gámanjunni***: Modelled maximum GT for Gámanjunni shows colder northeast-facing slope compared with the southwest-facing slope, and the lower permafrost limits are approximately 100 m higher at the southwest-facing slope, at an elevation of around 850 m in 2020 (Figure 6). We note, however, that this asymmetry is not related to the higher SOs applied to the SW-facing rock wall, and is rather caused by the extent of the steeper terrain in the profile. The NE-facing slope is rougher and consists of several smaller rock walls, whereas the SW-facing slope encompasses mainly one smoother rock wall, less than 50 m in height. The influence of geometry is especially clear in the “W logger” scenario (Video 15), where we applied slightly colder forcing to the SW-facing rock walls and the results still show lower deeper GT in the NE-facing slope. The modelled permafrost temperatures in the main simulation are between -2 and 0 °C, barring the upper parts of the NE-facing rock wall~~

~~where permafrost colder than in -2 °C was modelled in the colder years. The sensitivity test maximum range in the modelled maximum GT is mostly <1 °C, except for e.g. the lowest part of the unstable slope at Gámanjunni in some years (Figure 6). Furthermore, the simulations indicate that the uncertainty in the water content is less important than uncertainties in the temperature forcing or snow conditions (Video 15). The main heat flux direction in the mountain is often modelled towards the coldest zone below the NE-facing slope, whose depth is deepening over the last few years (Video 16). In addition, the results show that in the simulations with SOs, the scree slope is often colder than the sun-exposed, SW-facing rock wall. The scree slope is also less coupled to atmospheric conditions due to snow cover and greater ice contents, hence permafrost degradation occurs slower than in the rock wall, further amplifying the differences in GT between the sun-exposed rock face and scree slope during the warmer periods. In the simulation "Without monthly offsets", the rock wall is always colder than the scree slope.~~

~~***Ádjit***: At Ádjit, the modelled permafrost limits are lower on the southwest-facing slope than on the northeast-facing one, at around 650 m in 1980 and 700 m in 2020, roughly where the active rock glacier has its front (Figure 6). The south-facing rock wall is warmer than the north-east-facing slope, where in the colder periods, cold permafrost (< -2 °C) was modelled in the upper parts (Video 17). The maximum range of GT is generally below 1 °C; however, some parts close to or inside the rock glacier have a slightly higher GT span of up to 1.2 °C (Figure 6). For this profile, the SW-facing rock wall is much steeper than the moderately steep NE-facing slope above 1000 m elevation, which is the reverse of Gámanjunni geometry. The simulation "Without monthly offsets" (Video 17) shows the SW-facing slope as colder than the NE-facing slope due to the extent of the rock walls. Furthermore, tested uncertainties in the moisture content affect the results much less than the uncertainty in the GST forcing and slightly less than the uncertainty in the snow conditions. In the main scenario, the main heat flux direction is towards the colder zones below the NE-facing slope (Video 18). The colder zones move rapidly; hence, the tilt of the heat flux direction from the SW-facing rock wall undergoes some changes and is horizontal in the middle of the rock wall in 2020.~~

~~***Rombakstøtta***: Permafrost limits at Rombakstøtta are modelled slightly higher than at the other sites in the Northern Norway (Figure 6), at approximately 900–950 m and 1000 m for the NNE- and SSW-facing slopes in both 1980 and 2020. Only warm permafrost with temperatures above -2 °C is modelled in the main scenario, with the span of GT of less than 1.1 °C (Figure 6). Permafrost temperatures are slightly higher in some parts of the NNE-facing slope because we only applied monthly SOs due to solar radiation on slopes steeper than 60° and the SSW-facing slope is mainly <60° steep. In the scenario "Without monthly offsets" GTs are much lower on the NNE-facing rock wall than on the SSW-facing slope (Video 19). The main heat flux direction in the main scenario is towards the cold zone somewhere in the upper sections in the middle of the mountain, suggesting that the forcing between the steeper NNE-rock wall and the SSW-slope is somewhat similar (Video 20). This balance is disturbed in the scenario "Without monthly offsets", where a colder zone is modelled below the NNE-facing rock wall.~~

~~4.3 Ground temperature trends in rock walls~~

~~4.3.1 Western Norway~~

~~GTs at 20 m depth increased less than 0.2 °C decade^{-1} at Mannen site between the 1900s and the 1930s, changed less than 0.05 °C decade^{-1} between the 1930s and the 1980s, and increased again between the 1980s and the 2010s with a rate of 0.1–0.2 °C decade^{-1} (Figure 7). For Hogrenningsnibba slight GT increase is modelled between the~~

~~1900s and the 1930s (Figure 7). 20 m GT remained similar between the 1930s and the 1980s. Between the 1980s and the 2010s, 20 m GT increased around 0.1–0.2 °C decade^{-1} and the warming rates were larger than over the previous decades. Kvernhusfjellet has similar cooling and warming trends as Hogrenningsnibba; however, with slightly higher rates below the steepest parts (Figure 7). Figure 7 also shows that the steepest parts of the profile are most responsive to both cooling and warming. Unlike the other sites in the Western Norway, Ramnanosi had a decreasing trend in SAT10a at the beginning of the 20th century (Figure B1); hence, also GT decreased slightly between the 1900s and the 1930s (Figure 7). 20 m GT at Ramnanosi had only small differences between the 1930s and the 1980s and increased by 0.05–0.25 °C decade^{-1} since the 1980s (Figure 7).~~

~~4.3.2 Jotunheimen~~

~~At the highest elevations in the Jotunheimen, GT at 20 m increased between the 1900s and the 1930s by less than 0.1 °C decade^{-1}, then remained similar between the 1930s and the 1980s, and raised by up to 0.35 °C decade^{-1} between the 1980s and the 2010s (Figure 8). Steep slopes~~Modelled GT trends since the 1900s are shown in Figure 7. The steepest parts of the profiles are the most responsive to both warming~~; however,~~ and cooling trends in GST. However, modelled GT in the blockfields ~~on the highest plateaus~~in Jotunheimen is also strongly coupled with SAT in our simulations, since we applied a high nF-factor~~ (0.7~~. Furthermore, 2D effects largely influence modelled GT trends in the uppermost parts of the narrow mountain peaks (Ádjit, Rombakstøtta).

~~4.3.3 Northern Norway~~

~~Gámanjunni and Ádjit~~

The 1900s-1930s: Modelled GT at 20 m depth increased by less than 0.1 °C decade^{-1} at the sites in Southern Norway, except for Ramnanosi, which had a negative trend in SAT10a at the beginning of the 20th century (Figure A1). The sites in Northern Norway had the largest SAT10s rise at the beginning of the 20th century ~~since 1900~~ (Figure ~~B1~~A1), therefore simulated GT increase is larger between the 1900s and ~~the~~ 1930s than between the 1980s and ~~the~~ 2010s ~~(Figure 9). Between the~~.

The 1930s-1980s: Modelled GTs at 20 m depth remained similar (< 0.05 °C decade^{-1}) between the 1930s and ~~the 1980s,~~1980s for the sites in Southern Norway. Modelled GT in Northern Norway slightly decreased at depths below 20 m and increased at depths deeper than 20 m in some areas due to a rise in atmospheric temperature in the early 20th century.

The ~~rock walls are~~**1980s-2010s**: Simulated GTs at 20 m depth increased between the ~~most sensitive terrain type to GST trends. Ádjit has similar trends to Gámanjunni; however~~1980s and 2010s with ~~larger rates, especially in the uppermost parts where 2D effects largely influence GT temperature~~a rate of 0.1–0.35 °C decade^{-1} (Figure ~~9).~~7). The 1980s-2010s ground warming reaches deeper than the 1900s-1930s ground warming. Rombakstøtta has similar cooling and warming trends to the other sites in ~~the~~ Northern Norway; however, increases of both SAT10a and simulated GT are ~~larger~~higher since the 1980s (Figure ~~9~~7).

~~4.4 Ground temperature at 20 m depth~~

~~4.4.1 Elevation distribution~~

~~Modelled GT at 20 m depth in the rock walls is often coldest in the scenarios “Without monthly offsets” or “T-1 °C” (Figure 10). Scenarios “Without monthly offsets” yield usually coldest midsection in a single rock wall, whereas most other scenarios differ from these results, except for the simulations using data from the north-facing loggers for Kvernhusfjellet and Ramnanosi, which have small average annual SOs (~0.5 °C). Highest GT at 20 m is most often modelled in the runs with “T+1 °C”, hence SOs arising from solar radiation and SAT forcing are the most important factors for the modelled GT within the tested values. In the following, we mention the remaining thermal controls on modelled GT in the rock walls.~~

~~For the smaller NNE- or NE-facing rock walls at Hogrenningsnibba, Mannen, Ádjit, Gámanjunni, and the lower (< 1550 m) smaller west-facing rock walls at Kvernhusfjellet, 20 m GT increases or decreases with elevation depending on the distribution of the various terrain types in the vicinity of a single rock wall. GT increases with elevation if terrain above a single rock wall is gentler than terrain below this single rock wall, and the opposite is modelled if the terrain above is steeper than terrain below. Thus, 20 m GT distribution in such rock walls is predominantly due to snow cover distribution in the rock wall vicinity. The larger NE-facing rock walls at Rombakstøtta have in general decreasing GT with elevation; however, the mentioned small rock wall pattern is superimposed on the latter pattern, e.g. the thermal influence of snow cover on the plateau, possibly with heat flux from the SSW-facing rock wall, is evident in the topmost rock wall. The SSW-facing rock walls at Hogrenningsnibba and Rombakstøtta also fit this pattern for small rock walls. For the west-facing Ramnanosi, GT is highest in the lower part of the rock wall, because the assumed no SOs arising from solar radiation and little snow on the plateau lead to lower GT in the upper part of the rock wall.~~

~~The SE-facing rock walls at Ádjit and Gámanjunni have somewhat different GT patterns. Ádjit has pronounced higher GT in the middle of the rock wall and it seems that the SOs in the middle section dominate other thermal influences. The small rock wall at Gámanjunni has a pattern of larger rock walls, i.e. the middle part of the rock wall is either coldest (“Without monthly offsets”) or warmest, indicating that the thermal influence of snow is smaller.~~

~~The east-facing rock walls in the Jotunheimen have also various GT distributions at 20 m, depending on the rock wall size. Larger rock walls (> 50 m high) have the highest GTs in their midsection in most scenarios, except for the scenario “Without surface offsets”, where the midsection is coldest, pointing to the large thermal influence of SOs. The smaller, lower east-facing rock walls at Galdhøe have less steep terrain below than above them, hence GT decreases with elevation. The small east-facing rock walls at an elevation of ~2200 m at Veslpiggen are below blockfield-covered plateaus, therefore temperature decreases with elevation in most scenarios, except where more snow was applied on the plateau. The uppermost east-facing rock wall at ~2300 m at Veslpiggen has glaciers below and blockfields on the plateau, and GT decreases with elevation due to the large thermal influence of the glaciers. The lower west-facing rock wall at Galdhøe is thermally influenced by the colder, moderately steep terrain below and warmer gentler terrain above. The GT distribution in the upper west-facing rock walls in the Jotunheimen is governed by the snow conditions on the blockfield-covered plateau, and GT decreases in general with elevation in the scenarios with less snow on the plateau.~~

~~**4.4.2 Warming rates**~~

Over the last four decades, SAT at the rock wall elevations along the profiles increased by 0.25–0.4 °C decade^{-1} with the largest warming rates in ~~the~~ Jotunheimen and at Rombakstøtta (Figure ~~11~~8 A, C, E, G). ~~As mentioned earlier, we~~ We reconstructed the same SAT~~10a~~ trends along ~~the profiles~~each profile elevation-wise, ~~so there is no elevation trend in the results, although we cannot exclude such~~ whereas modelled trends~~. We show the SAT10a pattern here only to compare it with the modelled GT and we note that they might be inaccurate.~~

~~Trends~~ of GT at 20 m depth have a more complex pattern elevation-wise (Figure ~~11~~8 B, D, F, H); however, the largest simulated values are still in ~~the~~ Jotunheimen and at Rombakstøtta. The simulation results show that GT at 20 m depth increased on average by 0.2 °C decade^{-1}~~.~~ in the rock walls. The Jotunheimen area has the largest modelled mean 20 m GT increase (0.25 °C decade^{-1}), likely because we allowed blockfield-covered plateaus to be relatively strongly coupled with SAT, so two-dimensional warming is more effective in rock walls below plateaus. Ádjit has larger warming rates ~~compared with~~than Gámanjunni, especially at ~~the~~ higher elevations, pointing to the increasing importance of the two-dimensionality since the former has a sharper peak. ~~The Jotunheimen has the largest mean 20 m GT increase (0.25 °C decade^{-1}), likely because we allowed the blockfield-covered plateaus to be relatively strongly coupled with SAT, so the two-dimensional warming is more effective in rock walls below plateaus. In general at all sites, within~~ In general, modelled warming rates seem to increase towards the uppermost part of a single rock wall~~, warming rates seem to increase towards the uppermost part of the rock wall.~~ section. We simulated similar patterns in the previous simulations using the seNorge data set when SAT increase rates sometimes decreased with elevation. It is expected that the 2D effects will increase with elevation in a single rock wall just based on the topography of the study sites. ~~model runs using the seNorge data set when SAT increase rates sometimes decreased with elevation. It is expected that the 2D effects will increase with elevation in a single rock wall just based on the topography of the study sites.~~ For a 2D profile, the distance from ~~surfaces above~~ surface above a rock wall to a 20 m depth in a rock wall below, is shorter than the distance from surface below a rock wall to a 20 m depth in a rock wall ~~below is shorter than the distance from surfaces below a rock wall to a 20 m depth in a rock wall above.~~above. Generally, ground warming rates at 20 m depth seem to be independent of ~~elevation (Figure 11 F) and slightly increase with latitude (Figure 11 H). The latitude dependency is nevertheless the combination of the sharp peak Ádjit and the larger SAT increase at Rombakstøtta, hence we note that there are only a few profiles included in this study and further studies are required to investigate SAT, GST and GT trends in rock walls in Norway.~~latitude (Figure 8 H) and slightly increase with elevation (Figure 8 F).

~~Furthermore, we show sensitivity~~Sensitivity of the modelled GT rise at 20 m depth ~~in~~between the 1980s and 2010s (Supplementary Figure ~~12. For~~S23) shows that for most ~~rock walls~~simulations warming rates increase with elevation ~~as shown earlier~~. There are, nevertheless, a few exceptions:

(1) Warming rates may decrease with elevation for rock walls that are ~~slightly less steep~~ convex in the upper parts~~.~~, due to the assumed snow accumulation in the less steep parts.

(2) For parts of rock walls where permafrost thawed at 20 m depth between the 1980s and ~~the~~ 2010s, warming rate is larger~~.~~ (some simulations for Ádjit, Hogrenningsnibba, Ramnanosi, Rombakstøtta). Even small latent heat effects in permafrost slightly retard warming, and this effect disappears when permafrost is absent. ~~For instance, the "N logger" scenario for Ramnanosi shows the largest rates of warming in the lower rock wall, where GT is below 0 °C in the 1980s and above 0 °C in the 2010s. For the upper rock~~

~~wall, permafrost is still modelled in some years in the 2010s. The “nF-0.10” and “T+1°C” scenarios for Ádjit, together with the “T+1°C” scenario for Hogrenningsnibba and Rombakstøtta similarly show higher warming rates in portion of the rock walls where permafrost degraded between the compared decades.~~ However, warming retardation due to the latent heat effects depends on the ice content, and results from the assumed 5 % vol. ice content for fully frozen ground, thus for lower ice contents, latent heat effects are smaller.

Glaciers reduce ground warming in nearby steep rock faces, e.g. the east-facing rock wall in ~~the~~ Jotunheimen has higher modelled GT increase in the ~~scenario~~simulation “Without glaciers~~”.~~.” (Supplementary Figure S23). Otherwise, the assumed snow conditions have ~~largest~~the greatest influence on ~~the~~simulated warming rates, i.e. any snow accumulation in rock walls leads to lower warming rates. Snow cover in the rock wall vicinity also influences ~~the~~ modelled warming rates, e.g. rock walls below plateaus or rock ledges in ~~the~~ Jotunheimen have smaller warming rates if more snow is applied above them.

5 Discussion

5.1 Limitations and strengths

5.1.1 Subsurface heat transfer

The CryoGrid 2D model is based entirely on thermal conduction ~~that~~, which is believed to be the dominant heat transfer process in the ground (Williams and Smith, 1989). However, non-conductive thermal processes along with discontinuities and within the cracks, such as air convection or advection by moving water, ~~might~~may contribute to the subsurface thermal regime (e.g. Draebing et al., 2014). ~~Draebing et al., 2014).~~ Many discontinuities may exist in the bedrock and may be further widened by frost weathering processes, allowing for ~~generating~~the generation of pathways for ~~the~~ advective heat transfer to occur. The exact configuration of bedrock discontinuities ~~allowing for including~~is unavailable, making it unfeasible to include them in our modelling ~~is unavailable.~~. A study by Hasler et al. (2011a) in the Swiss Alps showed that while heat advection by percolating water has a negligible thermal impact, air ventilation likely causes thermal offsets similar to the offsets in coarse sediments, and values of up to 3 °C are reported. Since some cracks exist on the plateau above Mannen (Saintot et al., 2012) and Ramnanosi, air ventilation could lower GT in the area; however, since thick snow cover accumulates on the Mannen Plateau, plugging of the cracks with snow could prevent air ventilation (e.g. Blikra and Christensen, 2014). Another study by Moore et al. (2011) analysed ~~measured~~ deep GT profiles and attributed their disturbed profiles to localised convection cells in the fractures, whereas seasonal water infiltration had a minor influence on GTs. Nevertheless, several studies still emphasise the importance of advective heat input for GTs in permafrost-underlain terrain (e.g. Krautblatter and Hauck, 2007; Hasler et al., 2011b). A study by Magnin et al. (2017a) showed, however, that non-conductive thermal processes are only relevant in the upper 6 m below the ground surface. It is also noteworthy that conductive heat transfer in discontinuities filled with ice would alter GTs, i.e. ice infills in permafrost could act as ~~significant~~major heat sinks; ~~however~~yet, we cannot find any study that supports this hypothesis except for an open question in Gruber (2005). If ice/water-filled fractures inside the bedrock exist, this would locally delay permafrost thawing/formation due to latent heat effects.

Air convection is likely responsible for the observed negative thermal anomalies in ~~the~~ coarse-sediment landforms, such as blockfields (Heggem et al., 2005), rock glaciers (Wicky and Hauck, 2020) and talus slopes (Lambiel and Pieracci, 2008; Wicky and Hauck, 2017). Studies by Juliussen and Humlum (2008) and Gruber and Hoelze (2008) show examples of how ~~the~~ conductive heat transfer could account for the negative thermal anomalies in the blockfields. Even though views of these authors on the governing mechanisms could be implemented in our model, ~~responsible~~the thermal processes responsible are yet to be proven. In our study, negative thermal anomalies in the blockfields and rock glaciers are at least partly accounted for through the larger nF-factors than in the other sediment cover types.

Furthermore, the CryoGrid 2D model considers the 2D heat diffusion, which is an advance compared with the 1D case; nevertheless, heat transfer processes in complex terrain may occur three-dimensionally (Noetzli et al., 2007; Noetzli and Gruber, 2009). Myhra et al. (2017) argued that even though this is ~~the~~a clear limitation of the CryoGrid 2D model, applying it to the Norwegian mountains with flat plateaus and long valleys could be adequate. We note that our transects are only approximately suitable for two-dimensional heat conduction; yet they still follow the general characteristics of the slope and are representative of their surroundings. Magnin et al. (2017a) employed a similar 2D model to ours and validated their data against rock wall boreholes. The authors claimed that the 3D effects were likely of little importance for GT and the 2D modelling approach was sufficient for sharp topography in the European Alps. ~~Nevertheless~~Despite these findings, our 2D approach could potentially underestimate the GT trends in areas where GST signal penetrates from more than two sides, as modelled in Noetzli and Gruber (2009).

5.1.2 Model forcing

The CryoGrid 2D model was forced using lapse-rate adjusted SATs, together with the measured average monthly SOs in steep rock faces. ~~The~~While the number of meteorological stations is low in the mountains in Norway~~;~~ ~~nevertheless~~, they still are well correlated with the rock wall logger data after adjustments for the monthly SOs. There are some uncertainties in lapse rates and the reconstructed long~~–~~-time forcing is especially uncertain. Moreover, we had to use the SeNorge data set for some sites, which is based on the spatial interpolation between the in~~–~~-situ data (Lussana et al., 2018).

Furthermore, we only force the model directly with GST, instead of including a surface energy balance, as for instance in Noetzli et al. (2007). We applied the same SOs to each year, based on the average offsets between GST and SAT, which could otherwise be modelled using surface energy balance. However, we lack data to be able to implement such an approach at the time scales used in this study. Snow cover and solar radiation are believed to be the main controlling factors for GST in the rock walls (Haberkorn et al., 2015) and snow cover governs the distribution of GST in the gentle terrain in Norway (Farbrot et al., 2011; Gisnås et al., 2014), hence our methods account for the most important SOs measured in Norway. Magnin et al. (2017a) showed that a similar approach, i.e. without energy balance and without consideration of snow accumulation in rock walls, was appropriate to reproduce ~~rock wall~~ temperature below steep flanks of sharp mountain peaks at depths > 6 or > 8 m by comparing the modelled temperature ~~with~~to the measured temperature profiles in boreholes. For shallower depths, additional effects of non-conductive heat transfer and local snow accumulations, that were ignored in the modelling, caused substantial temperature differences.

Our analysis of the 2 h temperature suggests that solar radiation is ~~very probably~~highly likely to be the main controlling factor for SOs in~~ the~~ Norwegian rock walls, as also shown in Magnin et al. (2019). Large increases in maximum daily temperature can be seen in the rock wall temperature series, pointing to solar radiation as the dominant source of energy that modifies GSTs. ~~The north~~North-facing slopes in Norway can receive enough shortwave radiation to have mean annual SOs of around 0.5–1.5 °C (Figure 3), hence ignoring SOs would lead to much lower GTs even for this exposition. Similar ranges of average SOs were measured in the small cliffs in the north-facing loggers in ~~the~~ Northern Norway (Frauenfelder et al., 2018). Furthermore, we note that we did not apply non-nival SOs to moderately steep slopes (< 60° gradient), since we doubt that the observed non-nival SOs are as large as in the monitored slopes. For instance, Hasler et al. (2011a) suggested that late-lying snow ~~reduces~~lowers GST in moderately steep slopes, due to ~~a~~the reduction ~~in~~of the incoming shortwave radiation.

5.1.3 Snow distribution

One of the CryoGrid 2D model limitations is the lack of a snow domain; hence, we apply nF-factors for the gentle and medium-steep terrain. Preferably, snow depth should be rather described dynamically, both temporally and spatially, including snow redistribution by avalanching and wind. However, research concerning snow distribution ~~is~~on steep rock walls in Norway is lacking, so there are large uncertainties in snow depth and its timing. ~~The studies that~~Studies we reviewed from elsewhere had some contrasting results about snow distribution in the steep rock walls: 1) some studies point to that steep slopes above a certain threshold (e.g. more than 45º, 50º, 60º or 70º) cannot accumulate permanent snow cover due to avalanching or wind drift (Blöschl et al., 1991; Kirnbauer et al., 1991; Blöschl and Kirnbauer, 1992; Winstral et al., 2002; Machguth et al., 2006), 2) other studies, often using airborne or terrestrial laser scanning, show that almost any slope gradient can accumulate snow (Wirz et al., 2011; Sommer et al., 2015). The latter group of studies, nevertheless, recognises that snow cover is limited in steeper terrain and accumulates less snow than gentler terrain. Furthermore, the studies use various parameters as the most crucial to explain snow distribution in steep terrain, e.g.~~, :~~: 1) summer slope angle (Blöschl and Kirnbauer, 1992; Sommer et al., 2015), 2)~~ ~~ terrain-wind-interaction (Winstral et al., 2002; Wirz et al., 2011), 3) elevation and terrain roughness, which possibly correlates with the summer slope angle (Lehning et al., 2011). We note, however, that we used a high~~-~~-resolution DEM of at least 1 m resolution to construct each profile, and 1 m DEM was considered precise enough to detect rock ledges in the Swiss Alps, where snow can accumulate (Haberkorn et al., 2017), and such areas have snow cover in our study. Snow distribution in rock walls in Norway remains to be quantified, e.g. using LIDAR-scanning, and its governing factors recognised.

5.1.4 Thermal influence of snow

Snow cover could either ~~warm~~insulate or cool the ground. The overall effect of snow cover on GT is complex because it depends on~~ e.g.:~~ snow thickness, depth, duration, timing, melting processes within a snowpack, snow structure (Zhang, 2005~~) or~~), sun exposure (Magnin et al., 2017b), MAAT, substrate, the thickness of the active layer and ground moisture (Throop et al., 2012). Snow cover affects GT in both steep and gentle terrain in multiple ways:

(1) As an additional buffer layer with low thermal conductivity, snow insulates the ground, given that SAT is lower than GT and snow cover is sufficiently thick, e.g. at least 0.6 m in the gentle terrain (Luetschg et al., 2008) or even 0.2 m in the rock walls (Haberkorn et al., 2015). This is likely the most important net thermal impact of

snow on the GTs in Norway. Observed differences between GST and SAT are positive at most permafrost sites in Norway (Farbrot et al., 2011) and as shown in this study (Figure 3~~)~~), all measured mean annual SOs in the rock walls are positive, hence the overall annual cooling of the ground surface~~ annually~~ due to snow cover is not observed in Norway. We note that the installed rock wall loggers in Norway should measure only snow-free rock walls by design (Magnin et al., 2019), hence, the available measurements are insufficient to preclude cooling due to snow cover.

We assumed that rock walls are snow-free, because our analysis of the measured rock wall temperature in Norway indicates only minor thermal influence of snow, as also mentioned in Magnin et al. (2019). We note, however, that the computed mean monthly SOs (Figure 3) also account~~ also~~ for thermal effects of snow cover if there are any, hence rock walls are not sensu stricto snow-free in this study. For instance, W- and N-facing loggers at Gámanjunni ha~~r~~ve approximately 1 °C higher temperature than the south-facing logger (Figure 3) in December and January, which is likely due to snow cover. The rock wall loggers at Rombakstøtta are probably the most influenced by snow from all loggers in Norway, e.g. the W-facing logger is colder than the N-facing logger in May (Figure 3), and both E- and W-facing loggers ~~show ~~sometimes show much smaller standard deviation of daily temperatures compared with the N-facing logger, which is likely the least snow-influenced logger in this area.

(2) Snow cover increases albedo of the surface and thus reduces absorbed short-wave radiation, ~~i.e.~~meaning late-lying snow ~~will cool~~would delay or reduce the ~~rock wall in~~spring warming of the ~~sunny conditions because sun rays cannot reach it~~ground (e.g. Hasler et al., 2011a; Magnin et al., 2017b). This cooling effect was concluded to be a major cooling mechanism on the thinly snow-covered rock walls in the Mont Blanc Massif (Magnin et al., 2015). However, this cooling hypothesis was concluded to be of little importance in the study by Haberkorn et al. (2017), who show that sunny snow-covered rock walls are always warmer than snow-free rock walls due to reduced ground heat loss in winter, i.e. point (1) above.

(3) High emissivity of snow increases the outgoing longwave radiation; however, its high absorptivity has the opposite effect, hence the~~i~~rmal impact of emissivity and absorptivity on snow temperature is influenced by atmospheric conditions (Zhang, 2005).

(4) Snow requires large energy inputs to melt, hence GT will be lower than SAT during snowmelt; however, this usually lasts for a short time and ~~might~~may be unimportant on ~~yearly~~annual time scales (Zhang, 2005). However, meltwater percolating inside ~~the ~~cracks can refreeze and act as an additional heat source or favour~~ an~~ accelerated melting of the cleft ice (Hasler et al., 2011b).

(5) During autumn, ~~a ~~thin snow cover could lead to an enhanced conductive heat flux from the ground due to~~ the~~ large thermal gradients between the cooled snow surface and warmer upper ground layers (Keller and Gubler, 1993; Luetschg et al., 2008). Furthermore, in the low-snow years, GT at the top of permafrost is relatively constant during freezeback and may be higher than GST that is coupled to SAT, leading to positive thermal offsets (Palmer et al., 2012). ~~2008).~~ In addition, temporary ground cooling was observed at several sites across Switzerland during one or two winters in 2015-2017, when snow cover arrived very late and was thinner than usual (PERMOS, 2019; Noetzli et al., 2020). The latter cooling effect was not recorded at steep bedrock sites, where GT is usually insensitive or less sensitive to snow cover changes (PERMOS, 2019; Noetzli et al., 2020).

(6) Deposition of snow ~~might~~may reduce ventilation effects in clefts (Hasler et al., 2011a).

(7) If snow accumulates under ~~the~~ rock walls or ~~in the~~on rock ledges, the incoming short-wave radiation may be reflected diffusively towards snow-free parts of the rock wall, hence warming it. The latter effect is less investigated in ~~the~~ permafrost studies, although its importance was emphasised in the surface energy balance modelling of the high-arctic rock walls in Svalbard in Schmidt et al. (2021) and mentioned in Fiddes et al. (2015). We speculate that the reflected shortwave from ~~the~~ surrounding snow-covered surfaces may be important in some rock wall aspects in Norway~~. Measured~~, because measured rock wall temperatures ~~in rock walls during winter show temperature increase, seen in the~~ at 2 ~~h temperature measurements as~~ hour intervals often show a distinct daily temperature distribution due to ~~the~~ shortwave solar radiation~~, –~~ during late winter or spring. Such a temperature increase is even measured in February in ~~the~~ Northern Norway ~~that we consider is connected with snow accumulation in the surrounding terrain.~~. A similar temperature increase is not observed at the same magnitude during autumn, when snow is ~~present~~ less ~~often~~common. We recognise, however, that this seasonality could be related to cloud cover, issues with lapse rate or cooling effects of thin snow cover during autumn. Additionally, rock walls just above glaciers, e.g. in ~~the~~ Jotunheimen, ~~might be~~may likely be affected by reflected solar radiation from the glaciers all year round, and measurements from the east-facing rock walls just above the glaciers show particularly large SOs (Figure 3). Hasler et al. (2011a) also ~~mention~~states that ~~the~~ south- and east-facing rock faces above glaciers in the Swiss Alps experience extreme solar radiation. Nevertheless, the observed SOs in ~~the~~ Jotunheimen could be a result of the dark ~~surface~~colouration of the rocks in this area, which have a lower albedo compared with the bedrock at the other sites presented in this study.

5.2 Comparison ~~with~~to borehole data, geophysical surveys and other studies

~~Since we used the rock wall loggers as data for calibration of the forcing input and they only represent near-surface temperatures, we only compare them with our modelling results qualitatively in this section, i.e. by assuming that the mean temperature in a rock wall logger of 0 °C indicates permafrost. We additionally compare our results with the statistical modelling presented in Magnin et al. (2019) for the period 1981–2010 (Figure C1), and these results agree quite well with the modelled GT. We note, however, that this reference data should not be thought of as validation data for deeper GTs and merely represent surface conditions, because: (1) Neither the rock wall temperatures nor the statistical modelling account for the temperature offsets deeper in the ground, e.g. measurements conducted by Hasler et al. (2011a) in the European Alps were even 3 °C lower at depth than mean annual rock surface temperatures, hence the existing surface information might be insufficient, (2) as discussed in Noetzli et al. (2007) and Noetzli and Gruber (2009), permafrost may occur below the slopes where surface information indicates permafrost-free ground, because of lateral heat fluxes and/or the preservation of long-term temperature signals at greater depths.~~

~~5.2.1 Western Norway~~

~~Mean temperatures measured in the rock wall loggers at Mannen are 1.27 °C (Aug 2015–Jul 2018; 1290 m) and 2.55 °C (Aug 2015–Jul 2020; 1290 m) for the north- and east-facing loggers, respectively. Mean measured rock wall temperature in the west-facing logger at Ramnanosi is 1.55 °C (Aug 2016–Jul 2020; 1370 m). Hence, all loggers at Mannen and the W-facing logger at Ramnanosi suggest an unlikeliness of permafrost presence in these rock wall expositions over the last few years. The north-facing logger at Ramnanosi measured the mean rock wall temperature of 0.02 °C (Aug 2016–Jul 2020; 1370 m); hence,~~

~~**permafrost was likely in the north-facing parts of the slope at least before the measurement period started.**~~**5.2.1 Western Norway**

At Mannen, both the geophysical surveys presented in Etzelmüller et al. (2022) and our thermal modelling suggest that the existence of discontinuous permafrost is unlikely. The geophysical data indicate that sporadic permafrost can occur in the Mannen area; however, high resistivity values (> 20 kΩm) measured in this area could also reflect very good water drainage conditions, due to highly fractured bedrock or even ion-poor pore water (Dalsegg and Rønning, 2012).

~~Since some cracks exist on the plateau above Mannen (Saintot et al., 2012) and Ramnanosi, air ventilation could lower GT in the area; however, since thick snow cover accumulates on the Mannen Plateau, plugging of the cracks with snow could prevent air ventilation. The modelled GT for Mannen differs slightly from the results shown in Etzelmüller et al. (2021), where the seNorge data were used as forcing and SOs were ignored.~~

~~Measured mean temperature in the rock wall loggers in the Loen area was -1.77 °C (1709 m), 1.40 °C (1648 m) and 1.76 °C (1662 m) for the period Aug 2015 Aug 2018 for the north-, south- and west-facing loggers, respectively. The north-facing logger indicates that permafrost is likely, hence it agrees well with the modelled GT in this exposition. The west- and south-facing loggers have positive temperatures; however, it does not preclude that permafrost cannot exist in the mountain, because the modelled GTs are higher in the uppermost parts than in the middle parts along the rock wall, due to the influence of the thick snow on the plateaus. Furthermore, modelled permafrost in Kvernhusfjellet is clearly degrading over the last few years and possibly the same is the case for the SSW-facing slope at Hogrenningsnibba.~~

5.2.2 The Jotunheimen Mountains

~~In the Jotunheimen mean measured RW temperature is -1.77 °C (Sep 2010 Jul 2020; 2320 m), -2.15 °C (Sep 2010 Jul 2020; 2204 m), -2.23 °C (Sep 2010 Jul 2020; 2226 m), -3.55 °C (Sep 2010 Sep 2018; 2179 m) for the east-facing higher ("Eh"), east-facing lower ("El"), south-facing, and west-facing loggers, respectively. Most loggers indicate that even cold permafrost exists in the Jotunheimen Mountains, hence they agree quite well with the modelling results. We also compared~~Results from thermal simulations, both the modelled GTs and deeper warming rates, are in good agreement with the available borehole data ~~and the results agree quite well (not shown in this study~~in the Jotunheimen Mountains (Supplementary Figure S24 and Supplementary Table S5), although there are variations in snow conditions between the boreholes, hence we compared the measurements ~~with the various sensitivity scenarios.~~ to various snow sensitivity simulations. For the BH5 borehole in Jotunheimen (Figure 1D) and nearby gentle slopes, geophysical surveys performed in 1999 and 2010, together with numerical modelling, indicated the degradation of permafrost over the intervening decade (Isaksen et al. 2011). We compared the modelled subsurface thermal fields for Galdhøe to the geophysical surveys from 1999 and 2010, and our results show a similar pattern of possible permafrost degradation in this marginal permafrost area (Supplementary Figure S25). The results are especially similar for the sensitivity simulation with less snow ("nF+0.1").

5.2.3 Northern Norway

~~In the Gámanjunni area, RW loggers measured -0.08 °C (1220 m), -1.31 °C (1243 m), -1.62 °C (1183 m) in the south-, north- and west-facing loggers in the period Aug 2015–Sep 2020. Hence, at least warm permafrost conditions can be expected in the uppermost parts along the profile, as our model reproduces. The results shown in Etzelmüller et al. (2021) for Gámanjunni show somewhat different subsurface GT field, because the seNorge data were used there as forcing and SOs were unaccounted for.~~

~~For Ádjit measured RW temperatures are -0.01 °C (1245 m) and -1.80 °C (1230 m) for the south- and north-facing loggers in the period Aug 2015–Sep 2020. Both loggers indicate permafrost, although the south-facing rock wall is close to non-permafrost conditions. However, permafrost is still possible deep in the mountain, as modelled in our simulations, where the 2D effects modify the subsurface thermal field.~~ Three-dimensional GT modelling of Polvartinden Mountain, around 30 km northeast of Ádjit, which suggested the lower permafrost limits at 600–650 m over the last few years (Frauenfelder et al., 2018), is in agreement with our results. ~~which agrees well with our results~~ ~~Rombakstøtta loggers have mean RW temperature of 0.10 °C (1228 m), -0.71 °C (1224 m), -0.96 °C (1208 m) for the east-, north- and west-facing loggers. All loggers for the east-facing logger at Rombakstøtta indicate that at least warm permafrost might be present in the rock walls, which agrees well with the modelled GTs.~~ Furthermore, the local permafrost limit at an elevation of around 700 m, derived from various temperature measurements at the Jettan rockslide (Blikra and Christensen, 2014), 12 km NW of Gámanjunni, is in accordance with our modelled permafrost limit for less sun-exposed slopes. The results shown in Etzelmüller et al. (2022) for Gámanjunni show a somewhat different subsurface GT field, due to different model forcing. However, geophysical surveys reproduce the main patterns of the modelled subsurface thermal field at Gámanjunni presented in our study, and in Etzelmüller et al. (2022). The geophysical surveys at Gámanjunni indicate: (1) the thermal influence of the NW and SW facing rock walls, (2) higher resistivity (i.e. cooler conditions) in the scree below the SW-facing rock wall, (3) a warmer subsurface below the snow-covered plateau. In comparison with Etzelmüller et al. (2022), our thermal fields show (1) and (2) agree even better with the geophysical surveys, because we accounted for the additional surface offsets in the SW-facing rock wall. The conductive thermal field is slightly perturbed by the non-conductive heat transfer mechanisms in larger fractures. Etzelmüller et al. (2022) argued that comparison of the modelled ground temperature and geophysical surveys is useless at smaller scales, due to high resistivity variations in rough terrain, influenced by crack and fractures, strong topographic variations and local water infiltration.

5.3 Thermal regime in steep slopes

Due to the strong coupling of GST and SAT in rock walls, rock walls ~~might~~may have lower GT compared with the surrounding terrain, and permafrost aggradation ~~might occur in them~~ may much faster in them than in ~~the~~ other types of terrain in the decreasing SAT conditions, as ~~e.g.~~ shown in the previous modelling study by Myhra et al. (2017). However, sun-exposed large rock walls ~~might~~may allow more heat to enter the mountain. One example is Kvernhusfjellet, where the lower limit of permafrost is at 1620 m over the last few years, which is higher than at the moderately steep Hogrenningsnibba, where the permafrost limit ~~is~~has been at 1450 m ~~over the last few years~~. In Norway, permafrost research on moderately steep terrain is yet to be conducted, since there are large uncertainties in both snow distribution and SOs in moderately steep terrain in Norway. However, our results

~~are in agreement~~agree with the conclusions in Magnin et al. (2019) that the permafrost limits ~~might~~may be higher in the sun-exposed rock walls than in the less steep terrain.

We constructed meshes for various topographies and extended the previously presented 2D modelling for Norway (Myhra et al., 2017), mainly by including SOs. While~~ the~~ previous results mostly showed the midsection along a single rock wall as the coldest, our simulations show the midsection, or more precisely the lower portions of the midsection, sometimes as the warmest along the rock wall (at 20 m depth), barring the north-facing rock walls. The sensitivity ~~scenarios~~simulations where we skipped SOs show the same results as in Myhra et al. (2017) with the much colder midsections. Because the rock wall data from Norway indicated average ~~yearly~~annual SOs of at least 0.5 °C, the colder midsections in the north-facing slopes are less pronounced in the main ~~scenarios~~simulations, when compared with the ~~scenarios~~simulations without SOs. Our results also show that scree slopes ~~might~~may be warmer than rock walls if SOs are large enough, e.g. 3 °C. The latter is in discordance with the study by Myhra et al. (2019), where rock walls had a cooling effect on scree slopes; however, we note that they still agree for rock walls with minimal SOs. The simulated subsurface thermal fields are more similar to the results from 3D modelling ~~from~~in the European Alps (Noetzli and Gruber, 2009~~).~~), especially for Hogrenningsnibba, which has the most similar geometry to the one presented in th~~e~~at study~~ from the European Alps~~. Our simulations show quite similar distribution of the isotherms to the ones from the European Alps, except that the isotherms inside Hogrenningsnibba are less inclined. This is expected since the difference in rock surface temperature~~ difference~~ between the north- and south-facing slopes is smaller than in the European Alps, as discussed in Magnin et al. (2019). Slope steepness is, however, also an important factor influencing the subsurface thermal field. Ádjit is the ~~steepest slope~~narrowest ridge presented in this study and although the measured mean annual GST difference between the north- and south-facing slopes is below 2 °C, almost horizontal heat flux direction between ~~them~~the opposite mountainsides is often modelled. This suggests an increasing sensitivity of the subsurface thermal fields to small differences in forcing for the steep and narrow terrain. For instance, the modelled subsurface thermal field for the nearby less~~-~~ steep and less narrow Polvartinden, indicates almost horizontal isotherms (Frauenfelder et al., 2018). We note, however, that the differences in SOs for various aspects presented in the latter study ~~are smaller, around 1 °C.~~were smaller, around 1 °C. The modelled GT in the Hogrenningsnibba profile also indicates that permafrost may underlie a warmer mountainside with positive MAGSTs, due to permafrost occurrence in a colder mountainside, as shown in the studies of Noetzli et al. (2007) and Noetzli and Gruber (2009).

The importance of multi-dimensionality for the rates of GT rise was previously investigated in the studies by Noetzli et al. (2007) and Noetzli and Gruber (2009), where it was shown that surface warming penetrates steeper topography from several sides, thus leading to a faster pace of ground warming compared with flatter topography. Our study also suggests ~~also~~ that multi-dimensionality in mountain ridges is an important factor, although we only investigated a 2D case. The simulated GT increase rates increase with elevation, when terrain is in many cases also more exposed to surface warming penetration. The modelled warming rate of on average 0.25 °C decade^{-1} in rock walls in ~~the~~ Jotunheimen over the 1980s-2010s is slightly higher than the warming rate of 0.2 °C decade^{-1} measured at 20 m depth in the deep borehole at Juvvasshøe since 1999 (Smith et al., 2021). GT in this borehole is highly coupled with SAT, and the borehole has nF-factor of around 0.9.

5.4 Geomorphological implications

Our study focuses on rock wall permafrost evolution in Norway since the end of the Little Ice Age. The results indicate a substantial increase of GT at 20 m depth since the 1980s at all sites in Norway. Although mechanical aspects of GT increase are not considered in our modelling, the ground thermal regime itself has an important influence on geomorphological processes in periglacial regions (e.g. Berthling and Etzelmüller, 2011) and ultimately landscape development (e.g. Egholm et al., 2015). The ground thermal regime and its temporal development in steep slopes certainly influence the weakening of rock bonds, widening of cracks and the potential for frost weathering processes. Several authors have linked permafrost degradation and destabilisation of slopes (e.g. Davies et al., 2000; Davies et al., 2001; Gruber and Haeberli, 2007; Krautblatter et al., 2013). Conductive warming of ice-filled fractures, which are believed to stabilise permafrost-underlain mountains (e.g. Dramis et al., 1995), may result in: (1) loss of joint bonding and reduction of shear strength of the joint due to water release through ice melting, (2) shear strength changes due to mechanical ice properties that are a function of the normal stress and temperature (Davies et al., 2001). Furthermore, advective heat transport by percolating meltwater may result in rapid, local degradation of rock wall permafrost, which can trigger rockfalls even in cold permafrost areas (Hasler et al., 2011b). Krautblatter et al. (2013) noticed, in addition, that rock-mechanical properties themselves depend on rock temperature; hence, thawing can lead to a significant drop in rock strength. Frost weathering processes caused by ice segregation and/or volumetric expansion of in situ water are believed to contribute to the generation of weakness planes or widening fractures in frost-affected rocks (Gruber and Haeberli, 2007; Krautblatter et al., 2013). It is uncertain how the modelled GT distribution and GT increase may affect slope stability. Our results suggest that GT increase increases with elevation within a single rock wall section, hence this may indicate that instability risk is larger with elevation for a single rock wall section; however, GT may be highest in the middle of the rock wall, hence this part may be more susceptible to permafrost degradation in the sun-exposed rock walls. Furthermore, shaded rock walls may act as "refrigerators" in the landscape due to low snow cover within the rock walls and small amounts of solar radiation (e.g. Myhra et al., 2017). Thus, these landscape areas are locations for steep thermal gradients on the transition of snow-free steep rock walls and snow-covered more gentle terrain or glaciers/snow-field covered areas. This is exemplified in other studies and formerly addressed by Myhra et al. (2019) for the upper parts of talus slopes or rock glaciers below shaded rock walls, for cirques (Sanders et al., 2012) and below coastal cliffs in Arctic settings (Ødegård and Sollid, 1993; Wangensteen et al., 2007; Schmidt et al., 2021). All these settings influence frost weathering, as these strong thermal gradients favour frost segregation and frost cracking (Hales and Roering, 2007). Similar processes are also discussed for snow patches in relation to nivation processes (Berrisford, 1991). Thus, especially the constant change of ground thermal regime associated with rock walls and their vicinity are hot spots in material production and further geomorphological transport processes.

6 Conclusions

From this study, the following conclusions could be drawn:

(1) ~~Discontinuous permafrost~~Permafrost is likely ~~occurs~~discontinuous along most of the modelled profiles, except for Mannen and Ramnanosi. ~~Nevertheless~~However, convective heat transfer along discontinuities at both Mannen and Ramnanosi could lower GT; hence, both sites could be underlain

by sporadic permafrost. Rock walls at the highest elevations in the Jotunheimen Mountains are in the continuous permafrost zone.

(2) Rock walls in ~~the~~ Northern Norway experienced larger GT variations after LIA than rock walls in ~~s~~Southern Norway, since both the 1930s atmospheric warming and the 1970s–80s cooling were more pronounced in the north. All simulations show increasing GT since the 1980s. Rock walls in Norway are warming ~~at the rates of~~by 0.2 °C decade^{-1} on average at 20 m depth over the last three decades.

(3) Many of the modelled sites lie close to the lower boundary of mountain permafrost, hence the modelled GT is sensitive to the changes in the forcing. Within the tested forcing, uncertainties in the SAT le~~a~~d~~ed~~ to the largest changes in the modelled GT. Neglecting SOs ~~might~~may lead to much lower GT in the rock walls, even in Norway.

(4) The rock wall exposition and its size ~~seem~~appear to be important modifying factors for ~~the~~ permafrost distribution in the mountains. High rock walls, higher than 50 m, or several small rock walls (<50 m high) allow effective ground cooling and lead to lower permafrost limits in the mountain if SOs are not too large (e.g. Gámanjunni). High rock walls or several small rock walls ~~might~~may also allow more heat to enter a mountain and frequently sun-exposed rock walls may even have higher permafrost limits than moderately steep terrain (e.g. ~~Kvernhusfjellet). GST forcing in smaller rock walls influences GT more locally, e.g. if they have large SOs, the thaw depth is deeper.~~Kvernhusfjellet).

(5) The elevational distribution of GT at 20 m depth is influenced by the assumed snow conditions above and below rock walls~~. This effect~~, this is especially pronounced for smaller rock walls. Larger rock walls and sometimes even smaller rock walls ~~might~~may have coldest or warmest midsection depending on SOs. The north-facing rock walls have usually small SOs, hence their midsection is coldest. The rock walls with large SOs have warmest midsection.

(6) ~~Multi-~~The main ground heat flux direction is often one dimensional ~~thermal effects~~ inside the mountains ~~are smaller~~ in Norway ~~than in the European Alps. This is the combined result of the (1) differences in~~, especially below mountain ~~geometry, which in Norway are usually mountain peaks, arêtes of smaller relief than in the Alps~~plateaus or ~~deep valleys, (2)~~ mountains with minimal difference in GST ~~differences in rock walls~~forcing between the ~~various expositions are not as pronounced as in the Alps. The steepest mountains~~ opposite mountainsides (e.g. Rombakstøtta). The narrow ridges in Norway are, however, sensitive to even small differences in GSTs between ~~the various expositions.~~opposite mountain faces (e.g. Ádjit).

(7) Ground heat flux is modified in rock walls in ~~the~~ Jotunheimen by blockfields and ~~large~~ glaciers. GST in blockfields may be relatively strongly coupled with SAT, leading to lower GT and higher rates of GT increase (at 20 m depth) in rock walls close to blockfields. ~~Large glaciers~~Glaciers decrease GT increase in ~~the~~ nearby parts of rock walls; however, in view of their potential future retreat, warming rates ~~might~~may increase in the closest parts of rock walls.

(8) In rock walls with large SOs, plateaus above or talus below ~~might~~may be colder than the rock wall, forcing ground heat flux towards colder plateaus or talus slopes.

~~(9) North-facing rock walls could even be warmer than moderately steep south-facing rock walls. Nevertheless, this effect requires further studies to be confirmed.~~

Appendices

~~**Appendix A. Thermal conductivity.**~~

~~**Table A1. Thermal conductivity for the mineral fraction.**~~

~~**Mountain, municipality**~~	~~**Thermal conductivity [W m^{-1} K^{-1}]**~~
~~**Mannen, Rauma**~~	~~**2.5**~~
~~**Hogrenningsnibba, Stryn**~~	~~**2.3**~~
~~**Kvernhusfjellet, Stryn**~~	~~**2.3**~~
~~**Ramnanosi, Aurland**~~	~~**3.1**~~
~~**Veslpiggen, Lom**~~	~~**2.7**~~
~~**Galdhøe, Lom**~~	~~**2.7**~~
~~**Gámanjunni 3, Kåfjord**~~	~~**2.9**~~
~~**Ádjit, Storfjord**~~	~~**2.9**~~
~~**Rombakstøtta, Narvik**~~	~~**2.9**~~

Appendix ~~B~~A. Surface air temperature trends

Atmospheric temperature has in general had ~~an increasing~~a positive trend in Norway since the end of the LIA~~.~~, with the largest changes occurring over the last 40 years. Figure ~~B1~~A1 shows the 10~~-~~-year running mean surface air temperature (SAT10a) evolution for the highest elevations along each profile. In the first decade of the 20th century, SAT10a were -0.59 to -1.75 °C lower than over the last 10~~-~~year period (2011–2020).

The warming during the early 20th century was largest in ~~the~~ Northern Norway, which experienced at least 1 °C warming between the 1900s and ~~the~~ 1930s, whereas ~~the~~ Western Norway had around 0.4–0.7 °C warming in the same period. Ramnanosi is the site with the largest cooling trend at the beginning of the 20th century. ~~The~~ Jotunheimen had only small cooling between these decades. SAT10a was 0.5–0.7 °C lower in ~~the~~ Northern and Western Norway, respectively, between the 1930s and ~~the~~ 1980s. In ~~the~~ Jotunheimen, SAT10a increased between the 1930s and ~~the~~ 1980s by around 0.4 °C, although we note that there was a slight cooling in the area in the early 1980s; however, it vanishes when the results are presented as a mean value for the whole 1980s. SAT10a increased by 0.86–1.16 °C at all study sites after the 1970s–1980s cooling. The recent warming is ~~the~~ largest in ~~the~~ Jotunheimen and at Rombakstøtta.

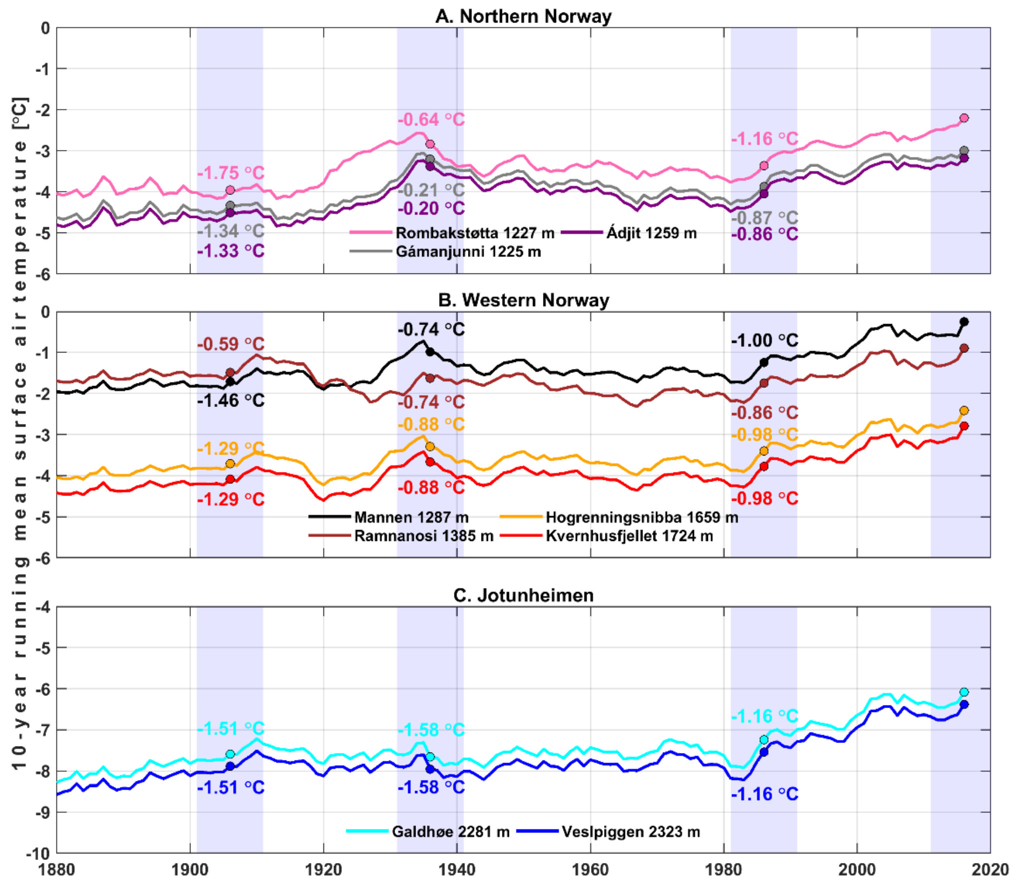

Figure ~~B1~~A1. 10-year running mean surface air temperature (SAT_{10a}) for peak elevations along each of the constructed profile in ~~the~~ Northern and Western Norway, together with Jotunheimen. Numbers along the plot lines are mean decadal temperature offsets in the 1900s, 1930s and 1980s relative to the 2010s. Data from Hanssen-Bauer et al. (2006), Lussana (2020) and meteorological stations.

~~**Appendix C. Model comparison.**~~

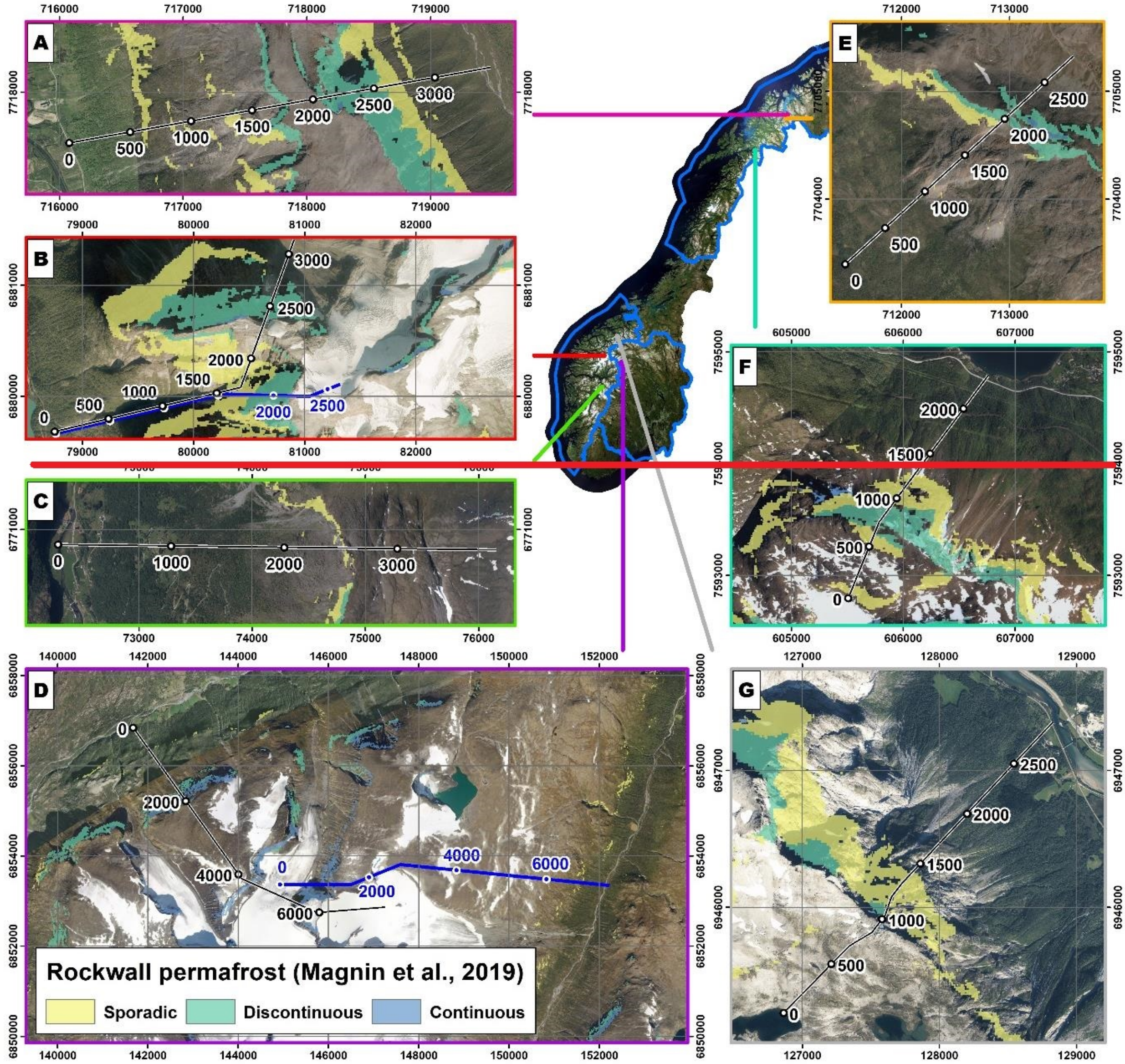

~~**Figure C1. Rock wall permafrost distribution according to Magnin et al. (2019) for: A) Gámanjunni 3, Kåfjord, B) Hogrenningsnibba (the northernmost profile/the black line) and Kvernhusfjellet (the southernmost profile/the blue line), Stryn, C) Ramnanosi, Aurland, D) Veslpiggen (the southernmost profile/the black line) and Galdhøe (the northernmost profile/the blue line), the Jotunheimen Mountains, E) Ádjit, Storfjord, F) Rombakstøtta, Narvik, and G) Mannen, Rauma. Numbers along the profiles indicate distance in metres. Map background credits: © Statens kartverk, Geovekst og kommunene. Coordinates in UTM zone 33N are shown.**~~

Data availability

Data are temporarily available through the University of Oslo's OneDrive cloud storage and will be later uploaded to Zenodo: https://uio-my.sharepoint.com/:u:/g/personal/justync_uio_no/EULI5I7AKY1NtTmAw-SBSuwBWZh0bY2gCW_S6Wf4HVM-Yw?e=CiQ2gW (size ~38 GB).

Author contribution

JC performed the simulations and prepared the manuscript with contributions from all co-authors. BE prepared the first version of the forcing data and supervised the study. JC, BE and SW contributed to the conceptualisation of this study and developed the methods. KI prepared the regional SAT data sets and contributed to the analysis of the SAT trends. FM contributed to the discussion on the thermal regime in steep slopes.

Competing interests

The authors declare that they have no conflict of interest.

Funding

This study was funded through Justyna Czekirda's doctoral research fellow position at the Department of Geosciences, University of Oslo, Norway. Additional funding was provided by the project 'CryoWALL – Permafrost slopes in Norway' (243784/CLE) funded by the Research Council of Norway.

Acknowledgments

This study is based on rock wall loggers installed by Tobias Hipp and Bas Altena within CRYOLINK project in 2011, together with rock wall loggers installed later during the project 'CryoWALL – Permafrost slopes in Norway' (243784/CLE). Both projects were funded by the Research Council of Norway. Installation and data retrieval from the loggers were actively supported by the Geological Survey of Norway (NGU) and the Norwegian Water and Energy Directorate (NVE). Particular thanks are due to Reginald L. Hermanns (NGU) and Lars Harald Blikra (NVE). Paula Hilger, Thorben Dunse (both the University College of Western Norway), Ove Brynhildsvoll, Trond Eiken, Jaroslav Obu, Bas Altena, Juditha Aga, Harald Wathne Hestad and Erling Thokle Hovden (all University of Oslo) helped with retrieving rock wall logger data. Ole Einar Tveito from the Norwegian Meteorological Institute assisted in preparing climatic data. Kristin Sæterdal Myhra (the University College of Western Norway) provided the CryoGrid 2D code, while ice thickness data for the selected glaciers in Norway ~~were~~was provided by Liss Marie Andreassen (NVE). Thomas Barnes (University of Oslo) proofread the manuscript. We want to thank the mentioned institutions and individuals.

References

Allen, S. K., Gruber, S., and Owens, I. F.: Exploring Steep Bedrock Permafrost and its Relationship with Recent Slope Failures in the Southern Alps of New Zealand, Permafrost Periglac, 20, 345-356, https://doi.org/10.1002/ppp.658, 2009.

Andreassen, L. M., Huss, M., Melvold, K., Elvehøy, H., and Winsvold, S. H.: Ice thickness measurements and volume estimates for glaciers in Norway, J Glaciol, 61, 763-775, https://doi.org/10.3189/2015JoG14J161, 2015.

Aune-Lundberg, L. and Strand, G.-H.: CORINE Land Cover classes. Examination of the content of CLC classes in Norway, Norwegian Forest and Landscape Institute, Ås, 2010.

Berrisford, M. S.: Evidence for enhanced mechanical weathering associated with seasonally late-lying and perennial snow patches, Jotunheimen, Norway, Permafrost Periglac, 2, 331-340, https://doi.org/https://doi.org/10.1002/ppp.3430020408, 1991.

Berthling, I. and Etzelmüller, B.: The concept of cryo-conditioning in landscape evolution, Quaternary Research, 75, 378-384, https://doi.org/10.1016/j.yqres.2010.12.011, 2011.
Blikra, L. H. and Christiansen, H. H.: A field-based model of permafrost-controlled rockslide deformation in northern Norway, Geomorphology, 208, 34-49, https://doi.org/10.1016/j.geomorph.2013.11.014, 2014.
Blikra, L. H., Longva, O., Braathen, A., Anda, E., Dehls, J., and Stalsberg, K.: Rock slope failures in Norwegian fjord areas: examples, spatial distribution and temporal pattern, in: Landslides from massive rock slope failure, Springer, 475-496, 2006.
Blöschl, G. and Kirnbauer, R.: An analysis of snow cover patterns in a small alpine catchment, Hydrological Processes, 6, 99-109, https://doi.org/10.1002/hyp.3360060109, 1992.
Blöschl, G., Kirnbauer, R., and Gutknecht, D.: Distributed Snowmelt Simulations in an Alpine Catchment: 1. Model Evaluation on the Basis of Snow Cover Patterns, Water Resources Research, 27, 3171-3179, https://doi.org/10.1029/91WR02250, 1991.
Boeckli, L., Brenning, A., Gruber, S., and Noetzli, J.: A statistical approach to modelling permafrost distribution in the European Alps or similar mountain ranges, The Cryosphere, 6, 125-140, https://doi.org/10.5194/tc-6-125-2012, 2012.
Boyd, R., Mikalsen, T., Minsaas, O., and Zwaan, K. B.: Storfjord 1633 IV 1:50.000, Berggrunnsgeologisk kart, foreløpig utgave (EN Bedrock-geologic map, provisional version), Norges geologiske undersøkelse (EN Geological Survey of Norway), 1985.
Böhme, M., Hermanns, R. L., Gosse, J., Hilger, P., Eiken, T., Lauknes, T. R., and Dehls, J. F.: Comparison of monitoring data with paleo-slip rates: Cosmogenic nuclide dating detects acceleration of a rockslide, Geology, 47, 339-342, https://doi.org/10.1130/G45684.1, 2019.
Böhme, M., Bunkholt, H. S. S., Oppikofer, T., Dehls, J. F., Hermanns, R. L., Eriksen, H. Ø., Lauknes, T. R., and Eiken, T.: Using 2D InSAR, dGNSS and structural field data to understand the deformation mechanism of the unstable rock slope Gamanjunni 3, northern Norway, in: Proceedings of the 12th International Symposium on Landslides, Napoli, Italy, 12-19 June 2016, 443-449, https://doi.org/10.1201/b21520-45, 2016a.
Böhme, M., Bunkholt, H. S. S., Dehls, J. F., Oppikofer, T., Hermanns, R., Dalsegg, E., Kristensen, L., Lauknes, T. R., and Eriksen, H. Ø.: Geologisk modell og fare-og risikoklassifisering av det ustabile fjellpartiet Gamanjunni 3 i Manndalen, Troms, NGU Rapport, 64, 2016b.
Böhme, M., Hermanns, R. L., Fischer, L., Oppikofer, T., Bunkholt, H., Derron, M. H., Carrea, D., Jaboyedoff, M., and Eiken, T.: Detailed assessment of the deep-seated gravitational deformation at Stampa above Flåm, Norway, Landslides and Engineered Slopes: Protecting Society through Improved Understanding, Taylor & Francis Group, London, 647-652, 2012.
Böhme, M., Hermanns, R. L., Oppikofer, T., Fischer, L., Bunkholt, H. S. S., Eiken, T., Pedrazzini, A., Derron, M.-H., Jaboyedoff, M., Blikra, L. H., and Nilsen, B.: Analyzing complex rock slope deformation at Stampa, western Norway, by integrating geomorphology, kinematics and numerical modeling, Engineering Geology, 154, 116-130, https://doi.org/10.1016/j.enggeo.2012.11.016, 2013.
~~Christiansen, H. H., Etzelmüller, B., Isaksen, K., Juliussen, H., Farbrot, H., Humlum, O., Johansson, M., Ingeman-Nielsen, T., Kristensen, L., Hjort, J., Holmlund, P., Sannel, A. B. K., Sigsgaard, C., Åkerman, H. J., Foged, N., Blikra, L. H., Pernosky, M. A., and Ødegård, R. S.: The thermal state of permafrost in the nordic area during the international polar year 2007-2009, Permafrost Periglac, 21, 156-181, https://doi.org/10.1002/ppp.687, 2010.~~
Dabrowski, M., Krotkiewski, M., and Schmid, D. W.: MILAMIN: MATLAB-based finite element method solver for large problems, Geochem Geophy Geosy, 9, https://doi.org/10.1029/2007gc001719, 2008.
Dalsegg, E. and Rønning, J. S.: Geofysiske målinger på Mannen i Rauma kommune, Møre og Romsdal (in Norwegian), Geological Survey of Norway, 2012.024, 2012.
Davies, M. C. R., Hamza, O., and Harris, C.: The effect of rise in mean annual temperature on the stability of rock slopes containing ice-filled discontinuities, Permafrost Periglac, 12, 137-144, https://doi.org/10.1002/ppp.378, 2001.
Davies, M. C. R., Hamza, O., Lumsden, B. W., and Harris, C.: Laboratory measurement of the shear strength of ice-filled rock joints, Ann Glaciol, 31, 463-467, https://doi.org/10.3189/172756400781819897, 2000.
Draebing, D., Krautblatter, M., and Dikau, R.: Interaction of thermal and mechanical processes in steep permafrost rock walls: A conceptual approach, Geomorphology, 226, 226-235, https://doi.org/10.1016/j.geomorph.2014.08.009, 2014.
Dramis, F., Govi, M., Guglielmin, M., and Mortara, G.: Mountain Permafrost and Slope Instability in the Italian Alps - the Val-Pola Landslide, Permafrost Periglac, 6, 73-81, https://doi.org/10.1002/ppp.3430060108, 1995.
Egholm, D. L., Andersen, J. L., Knudsen, M. F., Jansen, J. D., and Nielsen, S. B.: The periglacial engine of mountain erosion – Part 2: Modelling large-scale landscape evolution, Earth Surf. Dynam., 3, 463-482, https://doi.org/10.5194/esurf-3-463-2015, 2015.
Eriksen, H. Ø.: Instrumentation and temperature data (2014–2017) for the Ádjet Mountain in Skibotn, Troms [~~dataset~~data set], https://doi.org/10.6084/m9.figshare.6225056.v3, 2018a.

Eriksen, H. Ø.: Instrumentation and temperature data (2013–2017), Gámanjunni 3 Rockslide and Rock Glacier, Manndalen, Troms [~~dataset~~data set], https://doi.org/10.6084/m9.figshare.6254750.v1, 2018b.

Eriksen, H. Ø., Rouyet, L., Lauknes, T. R., Berthling, I., Isaksen, K., Hindberg, H., Larsen, Y., and Corner, G. D.: Recent Acceleration of a Rock Glacier Complex, Ádjet, Norway, Documented by 62 Years of Remote Sensing Observations, Geophys Res Lett, 45, 8314-8323, https://doi.org/10.1029/2018GL077605, 2018.

Etzelmüller, B. and Hagen, J. O.: Glacier-permafrost interaction in Arctic and alpine mountain environments with examples from southern Norway and Svalbard, Geological Society, London, Special Publications, 242, 11-27, https://doi.org/10.1144/gsl.Sp.2005.242.01.02, 2005.

Etzelmüller, B., Berthling, I., and Sollid, J. L.: The distribution of permafrost in Southern Norway; a GIS approach, in: Proceedings of the Seventh International Conference on Permafrost, Yellowknife, Canada, 23-27 June 1998, 251-258, 1998.

Etzelmüller, B., Berthling, I., and Sollid, J. L.: Aspects and concepts on the geomorphological significance of Holocene permafrost in southern Norway, Geomorphology, 52, 87-104, https://doi.org/10.1016/S0169-555X(02)00250-7, 2003.

Etzelmüller, B., Guglielmin, M., Hauck, C., Hilbich, C., Hoelzle, M., Isaksen, K., Noetzli, J., Oliva, M., and Ramos, M.: Twenty years of European mountain permafrost dynamics—the PACE legacy, Environmental Research Letters, 15, 104070, https://doi.org/10.1088/1748-9326/abae9d, 2020.

Etzelmüller, B., Czekirda, J., Magnin, F., Duvillard, P. A., ~~Malet, E.,~~ Ravanel, L., Malet, E., Aspaas, A., Kristensen, L., Skrede, I., Majala, G. D., Jacobs, B., Leinauer, J., Hauck, C., Hilbich, C., Böhme, M., Hermanns, R., Eriksen, H. Ø., Lauknes, T. R., Krautblatter, M., and Westermann, S.: Permafrost in monitored unstable rock slopes in Norway – ~~N~~new insights from ~~rock wall~~ temperature ~~monitoring~~and surface velocity measurements, geophysical surveying, and ~~numerical~~ground temperature modelling, Earth Surf. Dynam~~.~~ ~~Discuss., 2021, 1-55~~., 10, 97-129, https://doi.org/10.5194/esurf-~~2021-~~10~~, 2021.~~
-97-2022, 2022. Farbrot, H., Isaksen, K., and Etzelmüller, B.: Present and past distribution of mountain permafrost in Gaissane Mountains, Northern Norway, in: Proceedings of the Ninth International Conference on Permafrost, Fairbanks, Alaska, 29 June - 3 July 2008, 427-432, 2008.

Farbrot, H., Isaksen, K., Etzelmüller, B., and Gisnås, K.: Ground Thermal Regime and Permafrost Distribution under a Changing Climate in Northern Norway, Permafrost Periglac, 24, 20-38, https://doi.org/10.1002/ppp.1763, 2013.

Farbrot, H., Hipp, T. F., Etzelmüller, B., Isaksen, K., Ødegård, R. S., Schuler, T. V., and Humlum, O.: Air and Ground Temperature Variations Observed along Elevation and Continentality Gradients in Southern Norway, Permafrost Periglac, 22, 343-360, https://doi.org/10.1002/ppp.733, 2011.

Fiddes, J., Endrizzi, S., and Gruber, S.: Large-area land surface simulations in heterogeneous terrain driven by global data sets: application to mountain permafrost, The Cryosphere, 9, 411-426, https://doi.org/10.5194/tc-9-411-2015, 2015.

Fischer, L., Kääb, A., Huggel, C., and Noetzli, J.: Geology, glacier retreat and permafrost degradation as controlling factors of slope instabilities in a high-mountain rock wall: the Monte Rosa east face, Nat Hazard Earth Sys, 6, 761-772, https://doi.org/10.5194/nhess-6-761-2006, 2006.

Fischer, L., Purves, R. S., Huggel, C., Noetzli, J., and Haeberli, W.: On the influence of topographic, geological and cryospheric factors on rock avalanches and rockfalls in high-mountain areas, Nat Hazard Earth Sys, 12, 241-254, https://doi.org/10.5194/nhess-12-241-2012, 2012.

Frauenfelder, R., Isaksen, K., Lato, M. J., and Noetzli, J.: Ground thermal and geomechanical conditions in a permafrost-affected high-latitude rock avalanche site (Polvartinden, northern Norway), Cryosphere, 12, 1531-1550, https://doi.org/10.5194/tc-12-1531-2018, 2018.

Gauer, P., Kristensen, K., Ragulina, G., Frauenfelder, R., and Jaedicke, C.: Skredfarekartlegging i Narvik kommune (EN Landslide hazard mapping in Narvik municipality), Norges vassdrags- og energidirektorat (EN The Norwegian Water Resources and Energy Directorate), 20-2016, 2016.

Gisnås, K., Westermann, S., Schuler, T. V., Litherland, T., Isaksen, K., Boike, J., and Etzelmüller, B.: A statistical approach to represent small-scale variability of permafrost temperatures due to snow cover, The Cryosphere, 8, 2063-2074, https://doi.org/10.5194/tc-8-2063-2014, 2014.

Gisnås, K., Etzelmüller, B., Lussana, C., Hjort, J., Sannel, A. B. K., Isaksen, K., Westermann, S., Kuhry, P., Christiansen, H. H., Frampton, A., and Akerman, J.: Permafrost Map for Norway, Sweden and Finland, Permafrost Periglac, 28, 359-378, https://doi.org/10.1002/ppp.1922, 2017.

Goehring, B. M., Brook, E. J., Linge, H., Raisbeck, G. M., and Yiou, F.: Beryllium-10 exposure ages of erratic boulders in southern Norway and implications for the history of the Fennoscandian Ice Sheet, Quaternary science reviews, 27, 320-336, https://doi.org/10.1016/j.quascirev.2007.11.004, 2008.

Gruber, S.: Mountain permafrost: Transient spatial modelling, model verification and the use of remote sensing, Dr. sc. nat. dissertation, University of Zurich, Switzerland, 2005.

Gruber, S. and Haeberli, W.: Permafrost in steep bedrock slopes and its temperature-related destabilization following climate change, J Geophys Res-Earth, 112, https://doi.org/10.1029/2006jf000547, 2007.

Gruber, S. and Hoelze, M.: The cooling effect of coarse blocks revisited: a modeling study of a purely conductive mechanism, in: Proceedings of the Ninth International Conference on Permafrost, Fairbanks, Alaska, 29 June - 3 July 2008, 557-561, 2008.

Gruber, S., Hoelzle, M., and Haeberli, W.: Permafrost thaw and destabilization of Alpine rock walls in the hot summer of 2003, Geophys Res Lett, 31, https://doi.org/10.1029/2004gl020051, 2004.

Haberkorn, A., Phillips, M., Kenner, R., Rhyner, H., Bavay, M., Galos, S. P., and Hoelzle, M.: Thermal regime of rock and its relation to snow cover in steep alpine rock walls: Gemsstock, Central Swiss Alps, Geografiska Annaler: Series A, Physical Geography, 97, 579-597, https://doi.org/10.1111/geoa.12101, 2015.

Haberkorn, A., Wever, N., Hoelzle, M., Phillips, M., Kenner, R., Bavay, M., and Lehning, M.: Distributed snow and rock temperature modelling in steep rock walls using Alpine3D, The Cryosphere, 11, 585-607, https://doi.org/10.5194/tc-11-585-2017, 2017.

Haeberli, W., Huggel, C., Kaab, A., Zgraggen-Oswald, S., Polkvoj, A., Galushkin, I., Zotikov, I., and Osokin, N.: The Kolka-Karmadon rock/ice slide of 20 September 2002: an extraordinary event of historical dimensions in North Ossetia, Russian Caucasus, J Glaciol, 50, 533-546, https://doi.org/10.3189/172756504781829710, 2004.

Hales, T. C. and Roering, J. J.: Climatic controls on frost cracking and implications for the evolution of bedrock landscapes, Journal of Geophysical Research: Earth Surface, 112, https://doi.org/10.1029/2006JF000616, 2007.

Hanssen-Bauer, I., Tveito, O., and Szewczyk-Bartnicka, H.: Comparison of grid-based and station-based regional temperature and precipitation series, Met.no Report, 4/2006, 2006.

Harris, C., Haeberli, W., Vonder Mühll, D., and King, L.: Permafrost monitoring in the high mountains of Europe: the PACE Project in its global context, Permafrost Periglac, 12, 3-11, https://doi.org/10.1002/ppp.377, 2001.

Hasler, A., Gruber, S., and Haeberli, W.: Temperature variability and offset in steep alpine rock and ice faces, The Cryosphere, 5, 977-988, https://doi.org/10.5194/tc-5-977-2011, 2011a.

Hasler, A., Gruber, S., Font, M., and Dubois, A.: Advective Heat Transport in Frozen Rock Clefts: Conceptual Model, Laboratory Experiments and Numerical Simulation, Permafrost Periglac, 22, 378-389, https://doi.org/10.1002/ppp.737, 2011b.

Heggem, E. S. F., Juliussen, H., and Etzelmüller, B.: Mountain permafrost in Central-Eastern Norway, Norsk Geografisk Tidsskrift - Norwegian Journal of Geography, 59, 94-108, https://doi.org/10.1080/00291950510038377, 2005.

Hilger, P., Hermanns, R. L., Czekirda, J., Myhra, K. S., Gosse, J. C., and Etzelmüller, B.: Permafrost as a first order control on long-term rock-slope deformation in (Sub-) Arctic Norway, Quaternary Science Reviews, 251, 106718, https://doi.org/10.1016/j.quascirev.2020.106718, 2021.

Hipp, T., Etzelmüller, B., and Westermann, S.: Permafrost in Alpine Rock Faces from Jotunheimen and Hurrungane, Southern Norway, Permafrost Periglac, 25, 1-13, https://doi.org/10.1002/ppp.1799, 2014.

Hipp, T., Etzelmüller, B., Farbrot, H., Schuler, T. V., and Westermann, S.: Modelling borehole temperatures in Southern Norway – insights into permafrost dynamics during the 20th and 21st century, The Cryosphere, 6, 553-571, https://doi.org/10.5194/tc-6-553-2012, 2012.

Huggel, C., Salzmann, N., Allen, S., Caplan-Auerbach, J., Fischer, L., Haeberli, W., Larsen, C., Schneider, D., and Wessels, R.: Recent and future warm extreme events and high-mountain slope stability, Philos T R Soc A, 368, 2435-2459, https://doi.org/10.1098/rsta.2010.0078, 2010.

Isaksen, K., Holmlund, P., Sollid, J. L., and Harris, C.: Three deep Alpine-permafrost boreholes in Svalbard and Scandinavia, Permafrost Periglac, 12, 13-25, https://doi.org/10.1002/ppp.380, 2001.

Isaksen, K., Sollid, J. L., Holmlund, P., and Harris, C.: Recent warming of mountain permafrost in Svalbard and Scandinavia, Journal of Geophysical Research: Earth Surface, 112, https://doi.org/10.1029/2006JF000522, 2007.

Isaksen, K., ~~Farbrot, H., Blikra, L. H., Johansen, B., Sollid, J. L., and Eiken, T.: Five year ground surface temperature measurements in Finnmark, Northern Norway, in: Proceedings of the Ninth International Conference on Permafrost, Fairbanks, Alaska, 29 June - 3 July 2008, 789-794, 2008.~~

~~Isaksen, K.,~~ Ødegård, R. S., Etzelmüller, B., Hilbich, C., Hauck, C., Farbrot, H., Eiken, T., Hygen, H. O., and Hipp, T. F.: Degrading Mountain Permafrost in Southern Norway: Spatial and Temporal Variability of Mean Ground Temperatures, 1999–2009, Permafrost Periglac, 22, 361-377, https://doi.org/10.1002/ppp.728, 2011.

Juliussen, H. and Humlum, O.: Preservation of block fields beneath Pleistocene ice sheets on Sølen and Elgåhogna, central-eastern Norway, Zeitschrift für Geomorphologie, 51, 113-138, https://doi.org/10.1127/0372-8854/2007/0051S2-0113, 2007.

Juliussen, H. and Humlum, O.: Thermal regime of openwork block fields on the mountains Elgåhogna and Sølen, central-eastern Norway, Permafrost Periglac, 19, 1-18, https://doi.org/10.1002/ppp.607, 2008.

Karlsen, T. A.: Narvik, berggrunnskart (EN bedrock map) 1413 IV, 1: 50.000, foreløpig utgave (EN Provisional version), Norges geologiske undersøkelse (EN Geological Survey of Norway), 1991.

Keller, F. and Gubler, H.: Interaction between snowcover and high mountain permafrost Murtel/Corvatsch, Swiss Alps, in: Proceedings of the Sixth International Conference on Permafrost, Beijing, China, 5-9 July 1993, 332-337, 1993.

Kirnbauer, R., Blöschl, G., Waldhäusl, P., and Hochstöger, F.: An analysis of snow cover patterns as derived from oblique aerial photographs, in: Proc. Vienna Symp.—Snow, Hydrology and Forests in High Alpine Areas, Vienna, Austria, 11-24 August 1991, 91-99, 1991.

Kleman, J., Stroeven, A. P., and Lundqvist, J.: Patterns of Quaternary ice sheet erosion and deposition in Fennoscandia and a theoretical framework for explanation, Geomorphology, 97, 73-90, https://doi.org/10.1016/j.geomorph.2007.02.049, 2008.

Krautblatter, M. and Hauck, C.: Electrical resistivity tomography monitoring of permafrost in solid rock walls, Journal of Geophysical Research: Earth Surface, 112, https://doi.org/10.1029/2006JF000546, 2007.

Krautblatter, M., Funk, D., and Günzel, F. K.: Why permafrost rocks become unstable: a rock-ice-mechanical model in time and space, Earth Surf Proc Land, 38, 876-887, https://doi.org/10.1002/esp.3374, 2013.

Kristensen, L., Czekirda, J., Penna, I., Etzelmüller, B., Nicolet, P., Pullarello, J. S., Blikra, L. H., Skrede, I., Oldani, S., and Abellan, A.: Movements, failure and climatic control of the Veslemannen rockslide, Western Norway, Landslides, 1-18, https://doi.org/10.1007/s10346-020-01609-x, 2021.

Lambiel, C. and Pieracci, K.: Permafrost distribution in talus slopes located within the alpine periglacial belt, Swiss Alps, Permafrost Periglac, 19, 293-304, https://doi.org/10.1002/ppp.624, 2008.

Lebrouc, V., Schwartz, S., Baillet, L., Jongmans, D., and Gamond, J. F.: Modeling permafrost extension in a rock slope since the Last Glacial Maximum: Application to the large Sechilienne landslide (French Alps), Geomorphology, 198, 189-200, https://doi.org/10.1016/j.geomorph.2013.06.001, 2013.

Lehning, M., Grünewald, T., and Schirmer, M.: Mountain snow distribution governed by an altitudinal gradient and terrain roughness, Geophys Res Lett, 38, https://doi.org/10.1029/2011GL048927, 2011.

Lilleøren, K. S., Etzelmüller, B., Schuler, T. V., Gisnås, K., and Humlum, O.: The relative age of mountain permafrost — estimation of Holocene permafrost limits in Norway, Global and Planetary Change, 92-93, 209-223, https://doi.org/10.1016/j.gloplacha.2012.05.016, 2012.

Luetschg, M., Lehning, M., and Haeberli, W.: A sensitivity study of factors influencing warm/thin permafrost in the Swiss Alps, J Glaciol, 54, 696-704, https://doi.org/10.3189/002214308786570881, 2008.

Lussana, C.: seNorge_2018 daily total precipitation amount 1957-2017, version 18.12 [~~dataset~~data set], https://doi.org/10.5281/zenodo.2082320, 2018.

Lussana, C.: seNorge observational gridded datasets. seNorge_2018, version 20.05 [~~dataset~~data set], 2020.

Lussana, C., Tveito, O. E., and Uboldi, F.: Three-dimensional spatial interpolation of 2 m temperature over Norway, Quarterly Journal of the Royal Meteorological Society, 144, 344-364, https://doi.org/https://doi.org/10.1002/qj.3208, 2018.

Lutro, O. and Tveten, E.: Geologisk kart over Norge, berggrunnskart (EN Geological map over Norway, bedrock map) ÅRDAL M 1: 250.000, Norges geologiske undersøkelse (EN Geological Survey of Norway), 1996.

Lutro, O. and Tveten, E.: Berggrunnskart (EN Bedrock map) GALDHØPIGGEN 1518 II, M 1: 50.000, Norges geologiske undersøkelse (EN Geological Survey of Norway), 2012.

Machguth, H., Paul, F., Hoelzle, M., and Haeberli, W.: Distributed glacier mass-balance modelling as an important component of modern multi-level glacier monitoring, Annals of glaciology, 43, 335-343, https://doi.org/10.3189/172756406781812285, 2006.

Magnin, F., Deline, P., Ravanel, L., Noetzli, J., and Pogliotti, P.: Thermal characteristics of permafrost in the steep alpine rock walls of the Aiguille du Midi (Mont Blanc Massif, 3842 m a.s.l), The Cryosphere, 9, 109-121, https://doi.org/10.5194/tc-9-109-2015, 2015.

Magnin, F., Etzelmüller, B., Westermann, S., Isaksen, K., Hilger, P., and Hermanns, R. L.: Permafrost distribution in steep rock slopes in Norway: measurements, statistical modelling and implications for geomorphological processes, Earth Surf Dynam, 7, 1019-1040, https://doi.org/10.5194/esurf-7-1019-2019, 2019.

Magnin, F., Josnin, J. Y., Ravanel, L., Pergaud, J., Pohl, B., and Deline, P.: Modelling rock wall permafrost degradation in the Mont Blanc massif from the LIA to the end of the 21st century, The Cryosphere, 11, 1813-1834, https://doi.org/10.5194/tc-11-1813-2017, 2017a.

Magnin, F., Westermann, S., Pogliotti, P., Ravanel, L., Deline, P., and Malet, E.: Snow control on active layer thickness in steep alpine rock walls (Aiguille du Midi, 3842 m asl, Mont Blanc massif), Catena, 149, 648-662, https://doi.org/10.1016/j.catena.2016.06.006, 2017b.

Moore, J. R., Gischig, V., Katterbach, M., and Loew, S.: Air circulation in deep fractures and the temperature field of an alpine rock slope, Earth Surf Proc Land, 36, 1985-1996, https://doi.org/10.1002/esp.2217, 2011.

Morken, O. A.: Integrated analysis of past, and potential future rock slope failures of various size from Rombakstøtta, Nordland, Master's Thesis, NTNU, Norway, 2017.

Myhra, K. S., Westermann, S., and Etzelmüller, B.: Modelled Distribution and Temporal Evolution of Permafrost in Steep Rock Walls Along a Latitudinal Transect in Norway by CryoGrid 2D, Permafrost Periglac, 28, 172-182, https://doi.org/10.1002/ppp.1884, 2017.

Myhra, K. S., Westermann, S., and Etzelmüller, B.: Modeling Conductive Heat Flow Between Steep Rock Walls and Talus Slopes – Thermal Processes and Geomorphological Implications, Frontiers in Earth Science, 7, https://doi.org/10.3389/feart.2019.00192, 2019.

Noetzli, J., Christiansen, H., Deline, P., Gugliemin, M., Isaksen, K., Romanovsky, V., Smith, S., Zhao, L., and Streletskiy, D.: Permafrost thermal state, in: State of the Climate in 2019, Bulletin of the American Meteorological Society 101 (8), 20-22, https://doi.org/10.1175/BAMS-D-20-0104.1, 2020.

Noetzli, J. and Gruber, S.: Transient thermal effects in Alpine permafrost, The Cryosphere, 3, 85-99, https://doi.org/10.5194/tc-3-85-2009, 2009.

Noetzli, J., Gruber, S., Kohl, T., Salzmann, N., and Haeberli, W.: Three-dimensional distribution and evolution of permafrost temperatures in idealized high-mountain topography, J Geophys Res-Earth, 112, https://doi.org/10.1029/2006jf000545, 2007.

Nopper, H.: Geomorphological study of the rock-slope failure at Adjet, Storfjord, Troms, Master's Thesis, UiT, Norway, 2015.

Olsen, L., Sveian, H., Ottesen, D., and Rise, L.: Quaternary glacial, interglacial and interstadial deposits of Norway and adjacent onshore and offshore areas, Quaternary Geology of Norway, Geological Survey of Norway Special Publication, 13, 79-144, 2013.

Ødegård, R. S. and Sollid, J. L.: Coastal cliff temperatures related to the potential for cryogenic weathering processes, western Spitsbergen, Svalbard, Polar Research, 12, 95-106, https://doi.org/10.3402/polar.v12i1.6705, 1993.

Ødegård, R. S., Sollid, J. L., and Liestøl, O.: Ground temperature measurements in mountain permafrost, Jotunheimen, southern Norway, Permafrost Periglac, 3, 231-234, https://doi.org/10.1002/ppp.3430030310, 1992.

Ødegård, R. S., Nesje, A., Isaksen, K., Andreassen, L. M., Eiken, T., Schwikowski, M., and Uglietti, C.: Climate change threatens archaeologically significant ice patches: insights into their age, internal structure, mass balance and climate sensitivity, The Cryosphere, 11, 17-32, https://doi.org/10.5194/tc-11-17-2017, 2017.

Palmer, M. J., Burn, C. R., and Kokelj, S. V.: Factors influencing permafrost temperatures across tree line in the uplands east of the Mackenzie Delta, 2004–2010, Canadian Journal of Earth Sciences, 49, 877-894, https://doi.org/10.1139/e2012-002, 2012.

PERMOS: Permafrost in Switzerland 2014/2015 to 2017/2018. Noetzli, J., Pellet, C., and Staub, B. (eds.), Glaciological Report (Permafrost) No. 16-19 of the Cryospheric Commission of the Swiss Academy of Sciences, https://doi.org/10.13093/permos-rep-2019-16-19, 2019.

Quenardel, J. M. and Zwaan, K. B.: Berggrunnskart (EN Bedrock map) MANNDALEN 1633 I - M 1:50.000. Foreløpig utgave (EN Provisional version), Norges geologiske undersøkelse (EN Geological Survey of Norway), 2008.

Ravanel, L. and Deline, P.: Climate influence on rockfalls in high-Alpine steep rockwalls: The north side of the Aiguilles de Chamonix (Mont Blanc massif) since the end of the 'Little Ice Age', Holocene, 21, 357-365, https://doi.org/10.1177/0959683610374887, 2011.

Ravanel, L., Magnin, F., and Deline, P.: Impacts of the 2003 and 2015 summer heatwaves on permafrost-affected rock-walls in the Mont Blanc massif, Sci Total Environ, 609, 132-143, https://doi.org/https://doi.org/10.1016/j.scitotenv.2017.07.055, 2017.

Ravanel, L., Allignol, F., Deline, P., Gruber, S., and Ravello, M.: Rock falls in the Mont Blanc Massif in 2007 and 2008, Landslides, 7, 493-501, https://doi.org/10.1007/s10346-010-0206-z, 2010.

Saintot, A., Oppikofer, T., Derron, M.-H., and Henderson, I.: Large gravitational rock slope deformation in Romsdalen valley (Western Norway), Revista de la Asociación Geológica Argentina, 69, 354-371, 2012.

Sanders, J. W., Cuffey, K. M., Moore, J. R., MacGregor, K. R., and Kavanaugh, J. L.: Periglacial weathering and headwall erosion in cirque glacier bergschrunds, Geology, 40, 779-782, https://doi.org/10.1130/g33330.1, 2012.

Schmidt, J. U., Etzelmüller, B., Schuler, T. V., Magnin, F., Boike, J., Langer, M., and Westermann, S.: Surface temperatures and their influence on the permafrost thermal regime in high-Arctic rock walls on Svalbard, The Cryosphere, 15, 2491-2509, https://doi.org/10.5194/tc-15-2491-2021, 2021.

Schwanghart, W. and Scherler, D.: Short Communication: TopoToolbox 2 – MATLAB-based software for topographic analysis and modeling in Earth surface sciences, Earth Surf. Dynam., 2, 1-7, https://doi.org/10.5194/esurf-2-1-2014, 2014.

Slagstad, T., Balling, N., Elvebakk, H., Midttømme, K., Olesen, O., Olsen, L., and Pascal, C.: Heat-flow measurements in Late Palaeoproterozoic to Permian geological provinces in south and central Norway and a new heat-flow map of Fennoscandia and the Norwegian–Greenland Sea, Tectonophysics, 473, 341-361, https://doi.org/10.1016/j.tecto.2009.03.007, 2009.

Smith, M. W. and Riseborough, D. W.: Climate and the limits of permafrost: a zonal analysis, Permafrost Periglac, 13, 1-15, https://doi.org/10.1002/ppp.410, 2002.

Smith, S. L., Romanovsky, V. E., Isaksen, K., Nyland, K. E., Kholodov, A. L., Shiklomanov, N. I., Streletskiy, D. A., Farquharson, L. M., Drozdov, D. S., Malkova, G. V., and Christiansen, H. H.: Permafrost, in: State of the Climate in 2020, Bulletin of the American Meteorological Society 102 (8), 290-292, https://doi.org/10.1175/BAMS-D-21-0086.1, 2021.

Sollid, J. L. and Sørbel, L.: Distribution of Glacial Landforms in Southern Norway in Relation to the Thermal Regime of the Last Continental Ice Sheet, Geografiska Annaler: Series A, Physical Geography, 76, 25-35, https://doi.org/10.1080/04353676.1994.11880403, 1994.

Sollid, J. L., Holmlund, P., Isaksen, K., and Harris, C.: Deep permafrost boreholes in western Svalbard, northern Sweden and southern Norway, Norsk Geografisk Tidsskrift - Norwegian Journal of Geography, 54, 186-191, https://doi.org/10.1080/002919500448567, 2000.

Sollid, J. L., Isaksen, K., Eiken, T., and Ødegård, R. S.: The transition zone of mountain permafrost on Dovrefjell, southern Norway, in: Proceedings of the Eigth International Conference on Permafrost, Zürich, Switzerland, 21-25 July 2003, 1085-1090, 2003.

Sommer, C. G., Lehning, M., and Mott, R.: Snow in a Very Steep Rock Face: Accumulation and Redistribution During and After a Snowfall Event, Frontiers in Earth Science, 3, https://doi.org/10.3389/feart.2015.00073, 2015.

Steiger, C., Etzelmüller, B., Westermann, S., and Myhra, K. S.: Modelling the permafrost distribution in steep rock walls in Norway, Norwegian Journal of Geology/Norsk Geologisk Forening, 96, https://doi.org/10.17850/njg96-4-04, 2016.

Throop, J., Lewkowicz, A. G., and Smith, S. L.: Climate and ground temperature relations at sites across the continuous and discontinuous permafrost zones, northern Canada1This article is one of a series of papers published in this CJES Special Issue on the theme of Fundamental and applied research on permafrost in Canada.2Earth Science Sector (ESS) Contribution 20110128, Canadian Journal of Earth Sciences, 49, 865-876, https://doi.org/10.1139/e11-075, 2012.

Tveito, O., Førland, E., Heino, R., Hanssen-Bauer, I., Alexandersson, H., Dahlström, B., Drebs, A., Kern-Hansen, C., Jónsson, T., and Vaarby Laursen, E.: Nordic temperature maps, DNMI 09/00, 2000.

Wangensteen, B., Eiken, T., Ødegård, R. S., and Ludvig Sollid, J.: Measuring coastal cliff retreat in the Kongsfjorden area, Svalbard, using terrestrial photogrammetry, Polar Research, 26, 14-21, https://doi.org/10.1111/j.1751-8369.2007.00002.x, 2007.

Westermann, S., Schuler, T. V., Gisnås, K., and Etzelmüller, B.: Transient thermal modeling of permafrost conditions in Southern Norway, Cryosphere, 7, 719-739, https://doi.org/10.5194/tc-7-719-2013, 2013.

Wicky, J. and Hauck, C.: Numerical modelling of convective heat transport by air flow in permafrost talus slopes, The Cryosphere, 11, 1311-1325, https://doi.org/10.5194/tc-11-1311-2017, 2017.

Wicky, J. and Hauck, C.: Air Convection in the Active Layer of Rock Glaciers, Frontiers in Earth Science, 8, https://doi.org/10.3389/feart.2020.00335, 2020.

Williams, P. J. and Smith, M. W.: The frozen earth: fundamentals of geocryology, Cambridge University Press, Cambridge, UK, https://doi.org/10.1017/CBO9780511564437, 1989.

Winstral, A., Elder, K., and Davis, R. E.: Spatial Snow Modeling of Wind-Redistributed Snow Using Terrain-Based Parameters, Journal of Hydrometeorology, 3, 524-538, https://doi.org/10.1175/1525-7541(2002)003<0524:Ssmowr>2.0.Co;2, 2002.

Wirz, V., Schirmer, M., Gruber, S., and Lehning, M.: Spatio-temporal measurements and analysis of snow depth in a rock face, The Cryosphere, 5, 893-905, https://doi.org/10.5194/tc-5-893-2011, 2011.

Zhang, T.: Influence of the seasonal snow cover on the ground thermal regime: An overview, Reviews of Geophysics, 43, https://doi.org/10.1029/2004RG000157, 2005.

~~Ødegård, R. S., Sollid, J. L., and Liestøl, O.: Ground temperature measurements in mountain permafrost, Jotunheimen, southern Norway, Permafrost Periglac, 3, 231-234, https://doi.org/10.1002/ppp.3430030310, 1992.~~

~~Ødegård, R. S., Nesje, A., Isaksen, K., Andreassen, L. M., Eiken, T., Schwikowski, M., and Uglietti, C.: Climate change threatens archaeologically significant ice patches: insights into their age, internal structure, mass balance and climate sensitivity, The Cryosphere, 11, 17-32, https://doi.org/10.5194/tc-11-17-2017, 2017.~~

Figures

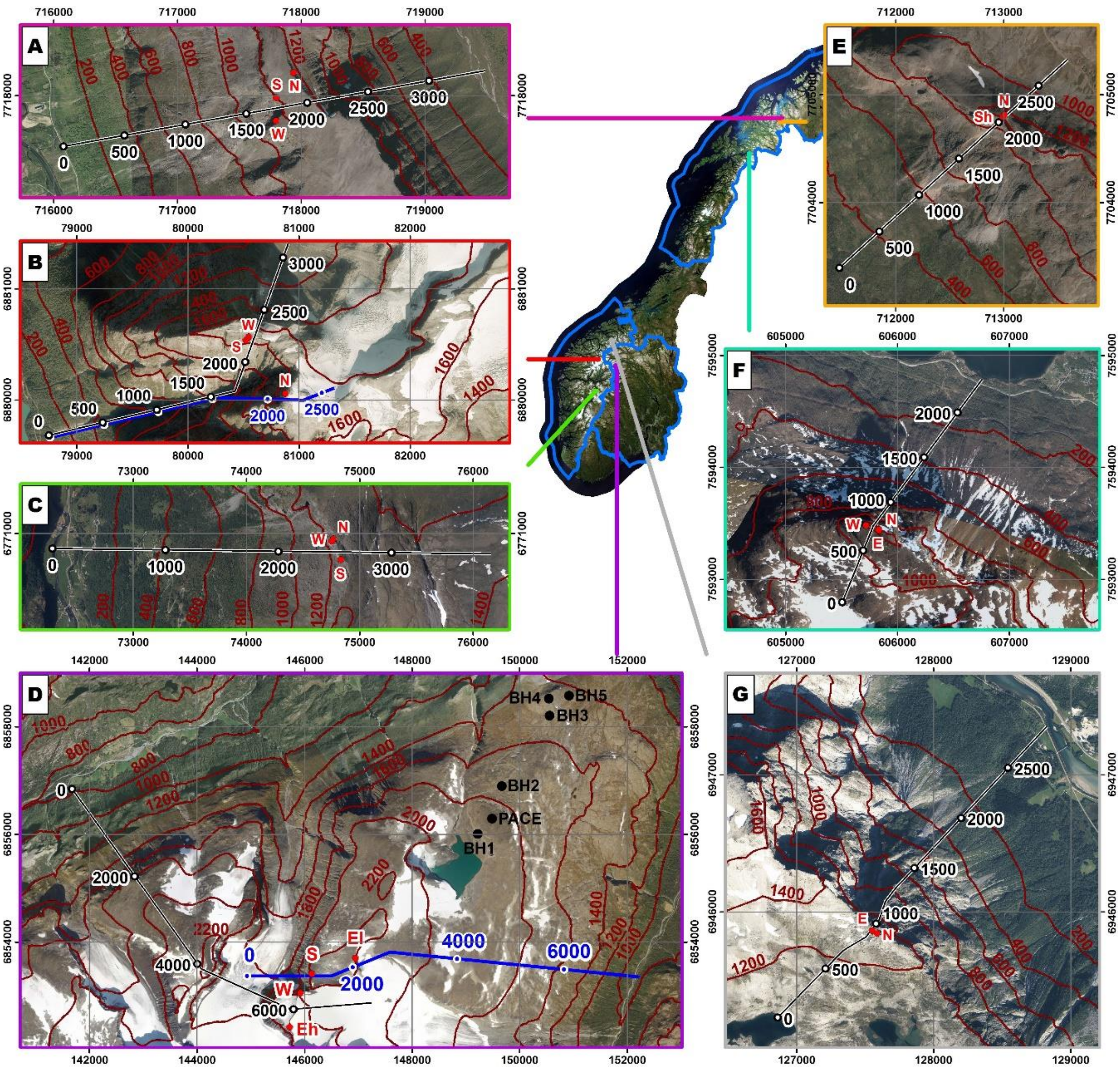

Figure 1. Transects for the two-dimensional modelling. A) Gámanjunni 3, Kåfjord, B) Hogrenningsnibba (the northernmost profile/the black line) and Kvernhusfjellet (the southernmost profile/the blue line), Stryn, C) Ramnanosi, Aurland, D) Veslpiggen (the southernmost profile/the black line) and Galdhøe (the northernmost profile/the blue line), the Jotunheimen Mountains, E) Ádjit, Storfjord, F) Rombakstøtta, Narvik, and G) Mannen, Rauma. Red points with letters depict rock wall loggers in the various expositions: N=north-facing logger, S=south-facing logger, E=east-facing logger, W=west-facing logger, suffix "l"=at a lower elevation, suffix "h"=at a higher elevation. Black circles show borehole locations. Numbers along the profiles indicate distance in metres. Three geographical regions of Western ~~Norway~~, Eastern and Northern Norway are outlined by the blue lines. Map background credits: © Statens kartverk, Geovekst og kommunene. Coordinates in UTM zone 33N are shown.

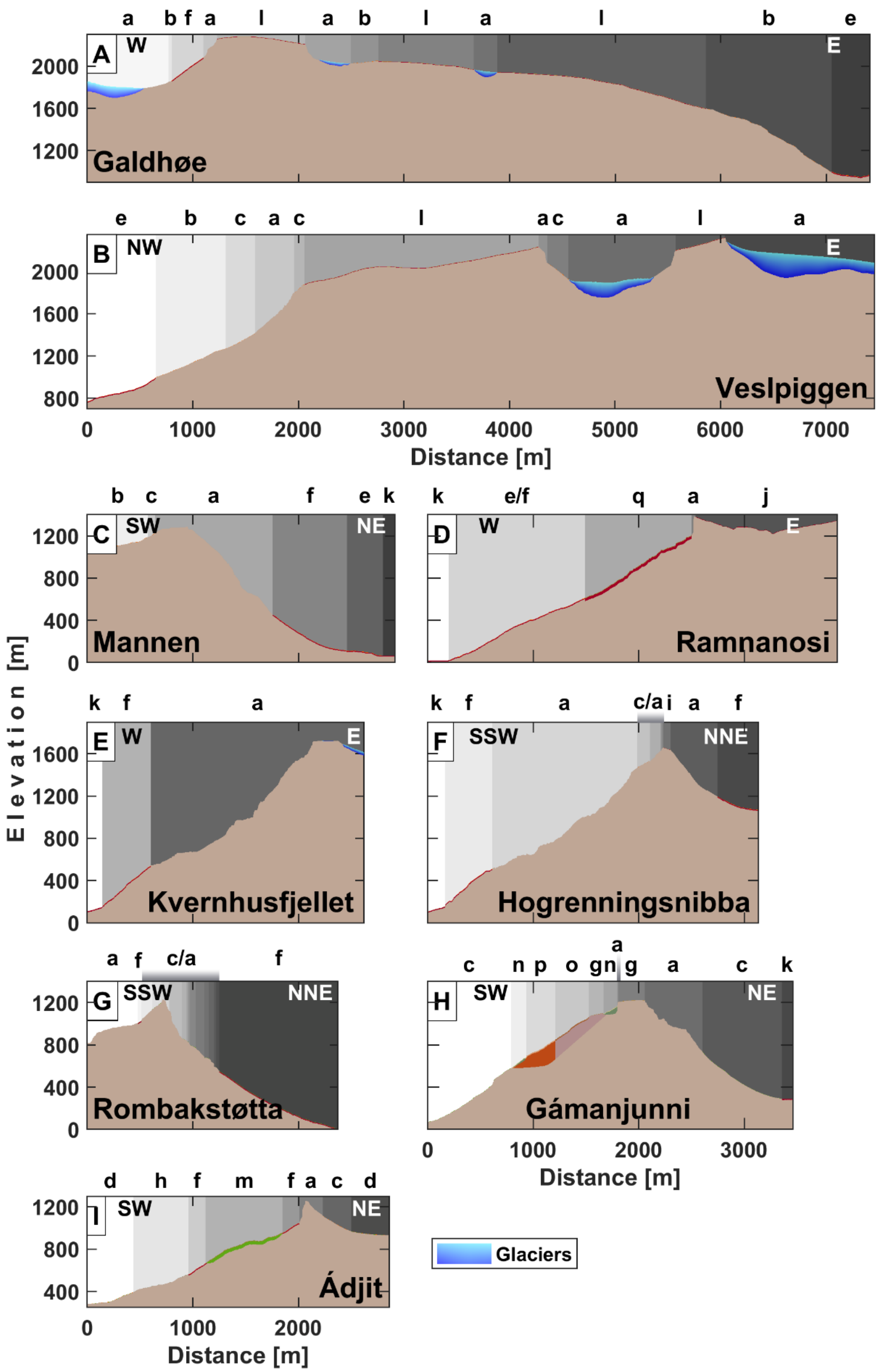

Figure 2. **Slope geometry and stratigraphy~~: A) Galdhøe, B) Veslpiggen, C) Mannen, D) Gámanjunni 3, E) Kvernhusfjellet, F) Hogrenningsnibba, G) Rombakstøtta, H) Ramnanosi, I) Ádjit.~~. The small case letters are stratigraphy codes described in detail in Supplementary Table ~~2~~S1. The label "c/a" indicates alternating stratigraphy of bedrock and thin colluvium. Blue patches depict glaciers or perennial snow. Note that the meshes extend down to 6000 m below sea level and the parts below valley bottoms are not shown.**

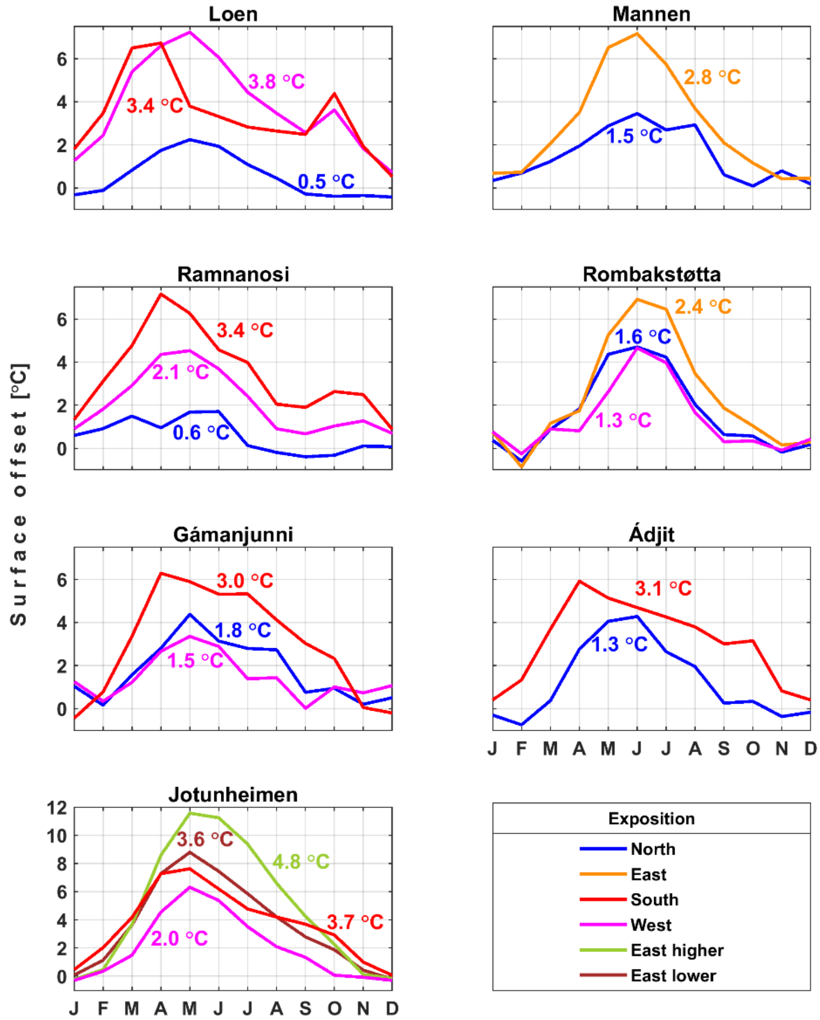

Figure 3. Monthly surface offsets between air and rock wall temperature for each site and logger exposition. Numbers along the plot lines are average values. X-axis contains initials for months. Note that Jotunheimen has different y-axis than the other subplots. For Ádjit only the upper south-facing ("Sh" in Figure 1~~.~~) logger is shown. Suffix "l"=at a lower elevation, suffix "h"=at a higher elevation.

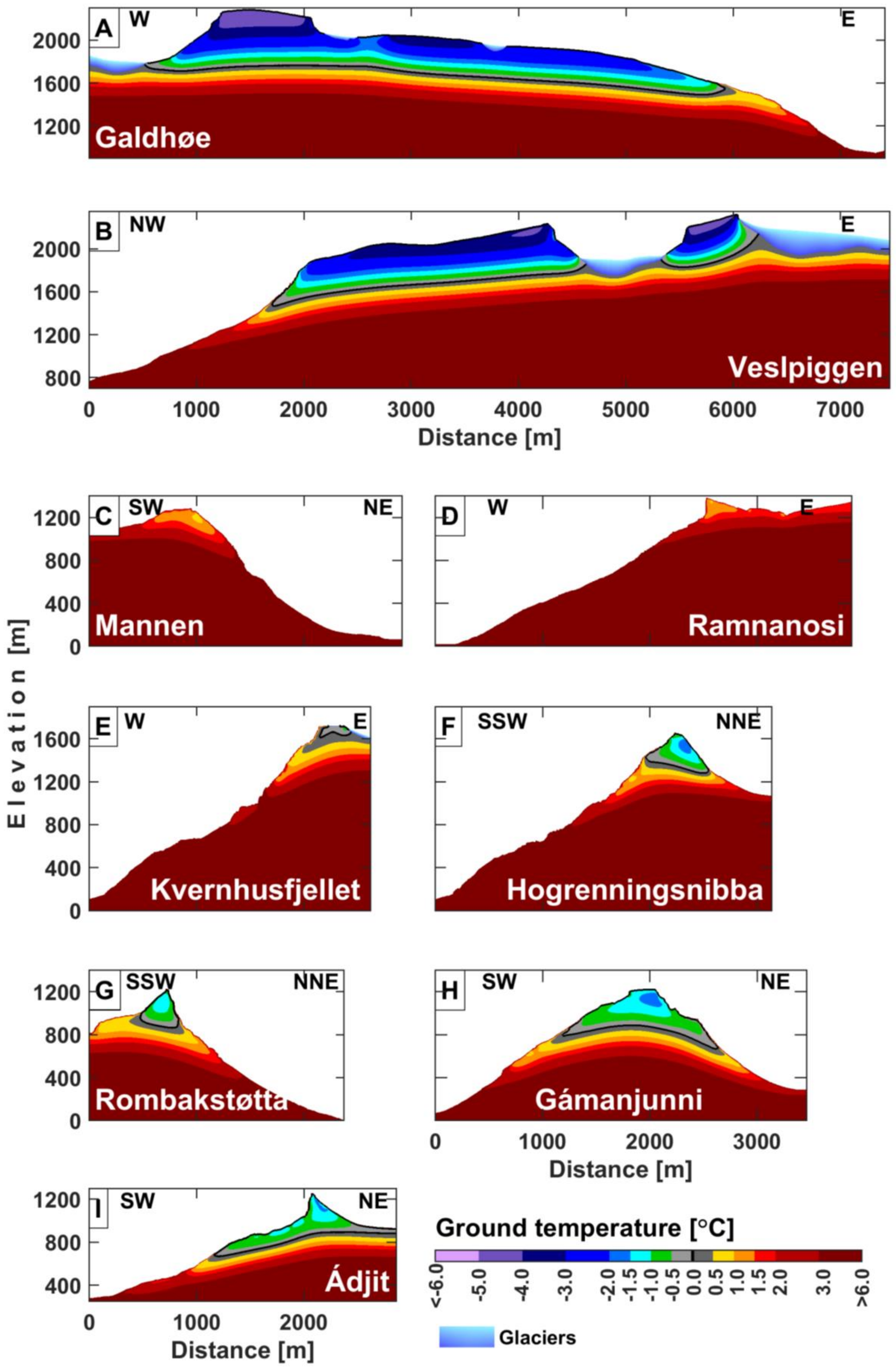

Figure 4. ~~**Modelled**~~**Average annual maximum GT over the 2010s.**

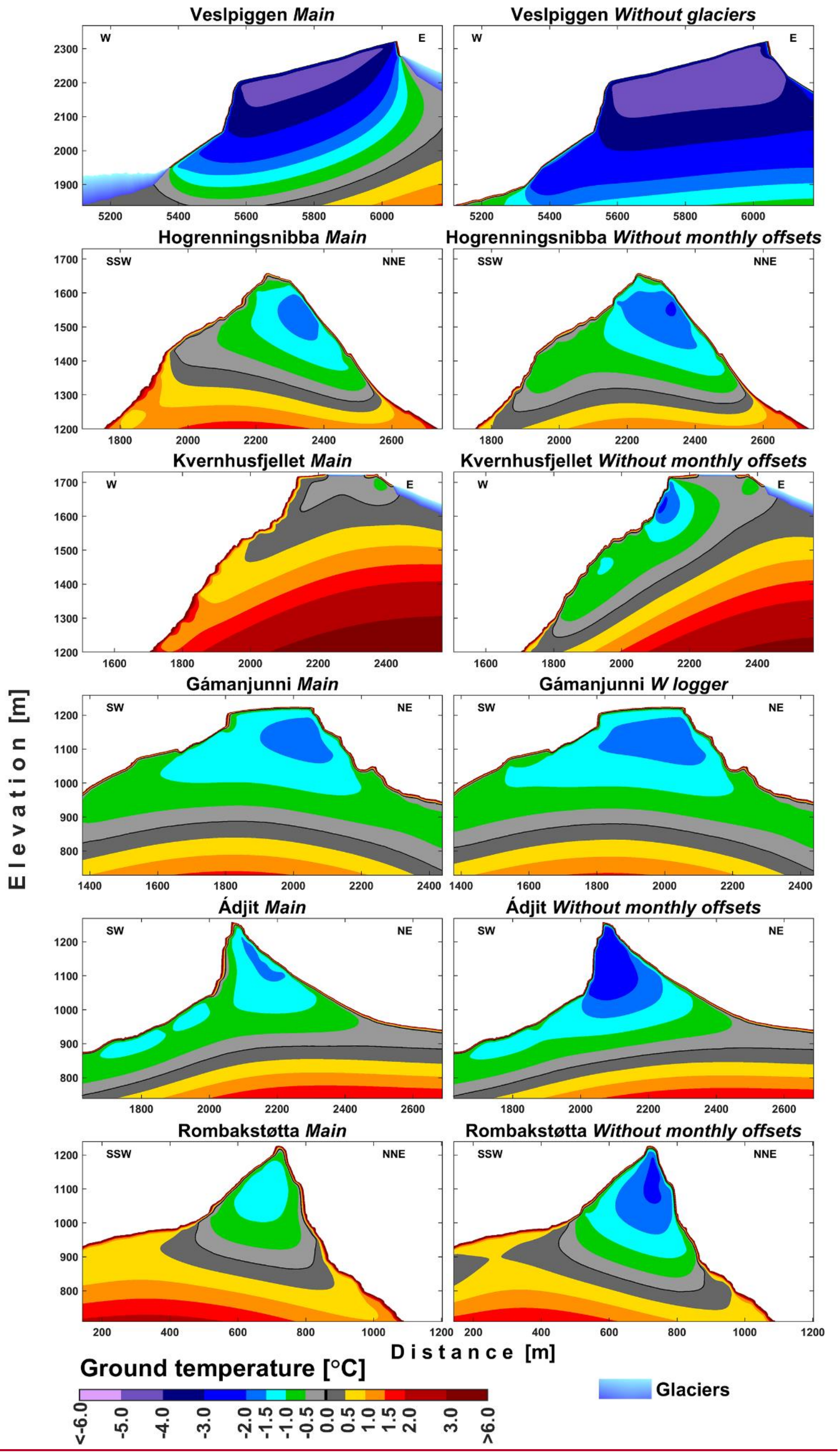

Figure 5. ~~and sensitivity test maximum range in the modelled~~Average annual maximum GT over the 2010s for ~~the profiles in the Western Norway in 1980 and 2020. Maximum absolute differences in comparison to the main run are shown based on the uncertainty~~various simulations. ~~Map background credits: © Statens kartverk, Geovekst, kommuner og OSM – Geodata AS.~~

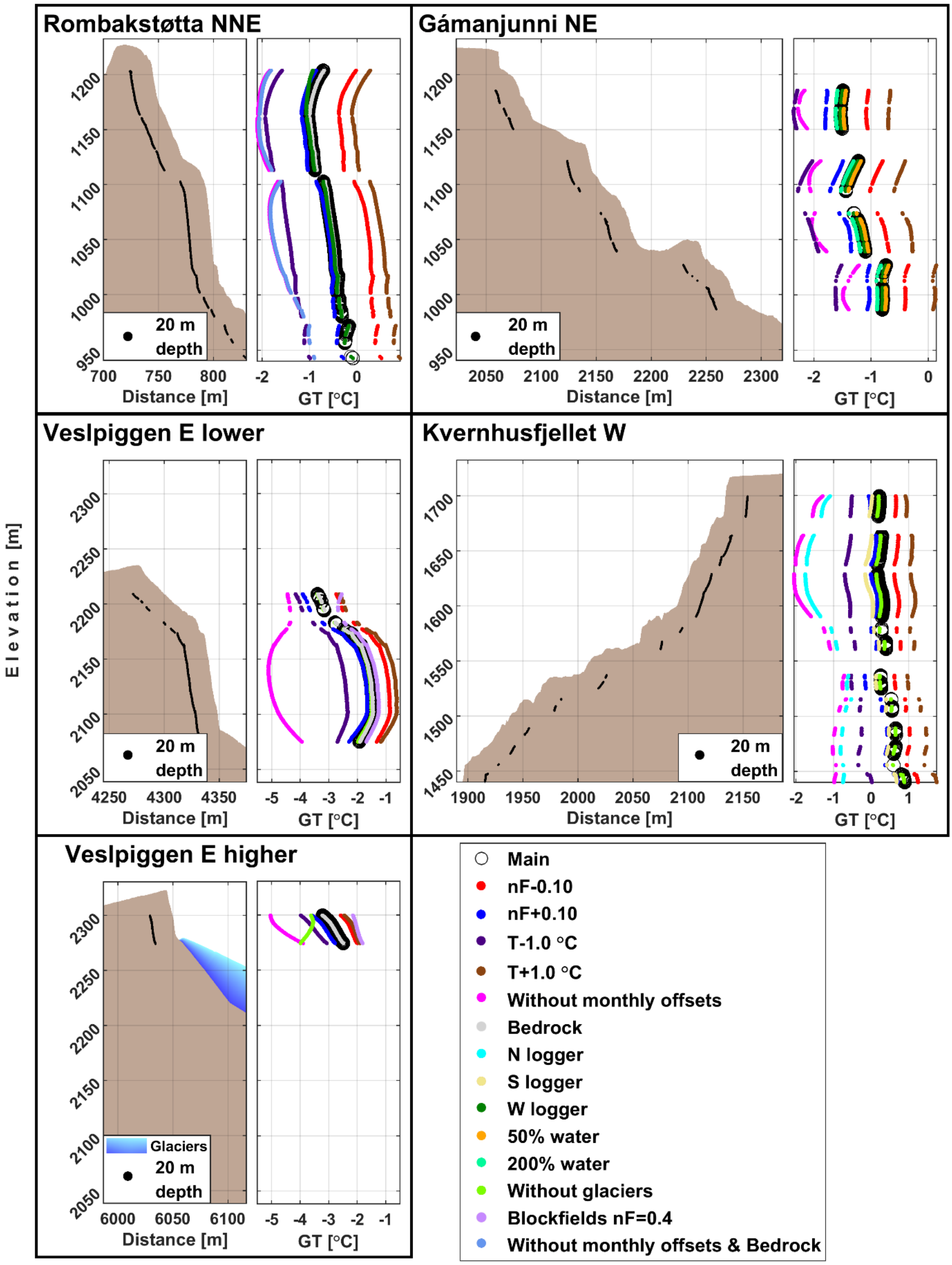

Figure 6. GT in rock walls at 20 m depth for various profiles over the 2010s. Right subplots show GT in nodes depicted in left subplots.

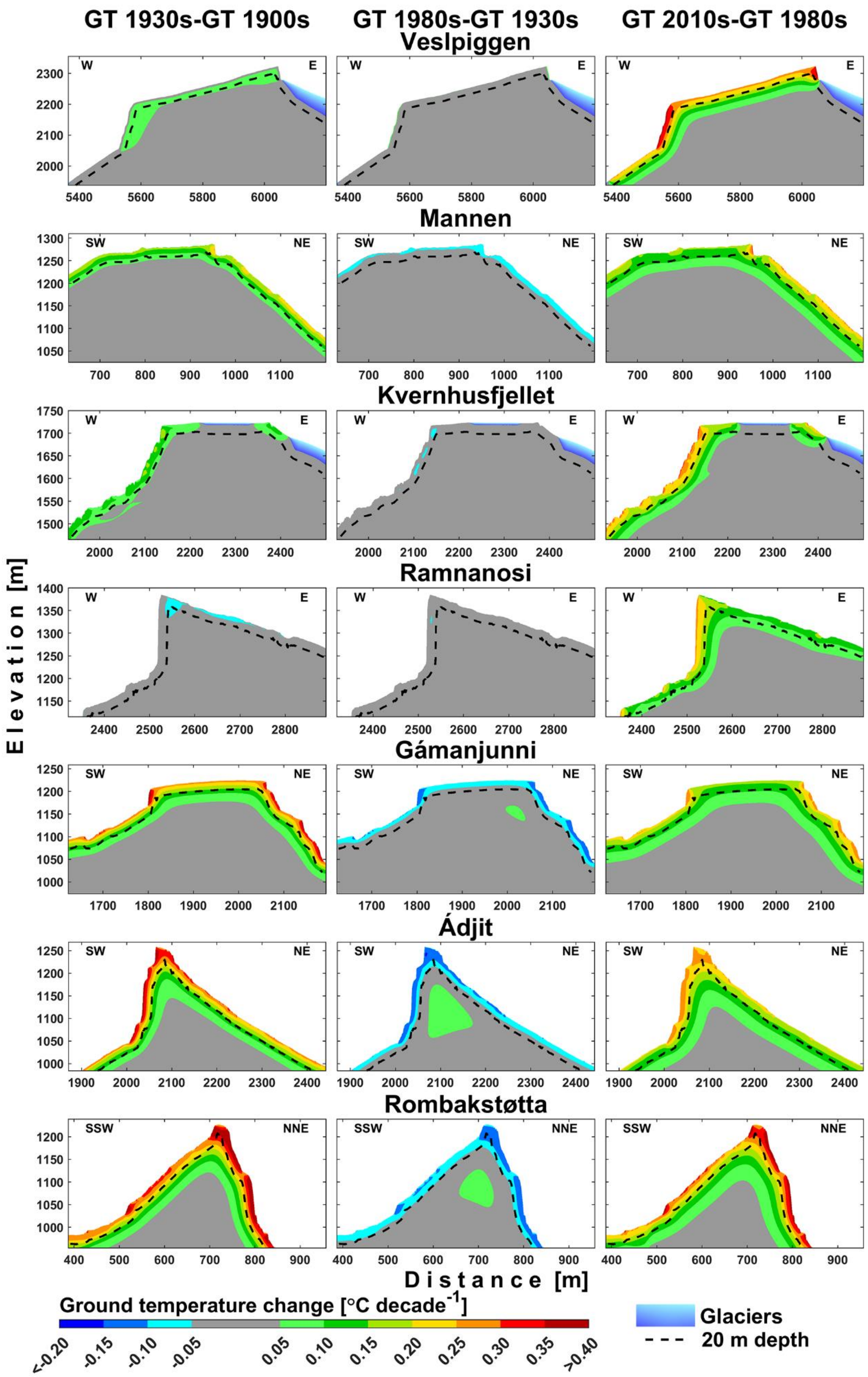

Figure 7. Rate of change in 10 year mean GT for the various profiles between the following decades: (1) the 1900s and 1930s, (2) the 1930s and 1980s, (3) the 1980s and 2010s. 20 m depth is delineated by the black dashed lines.

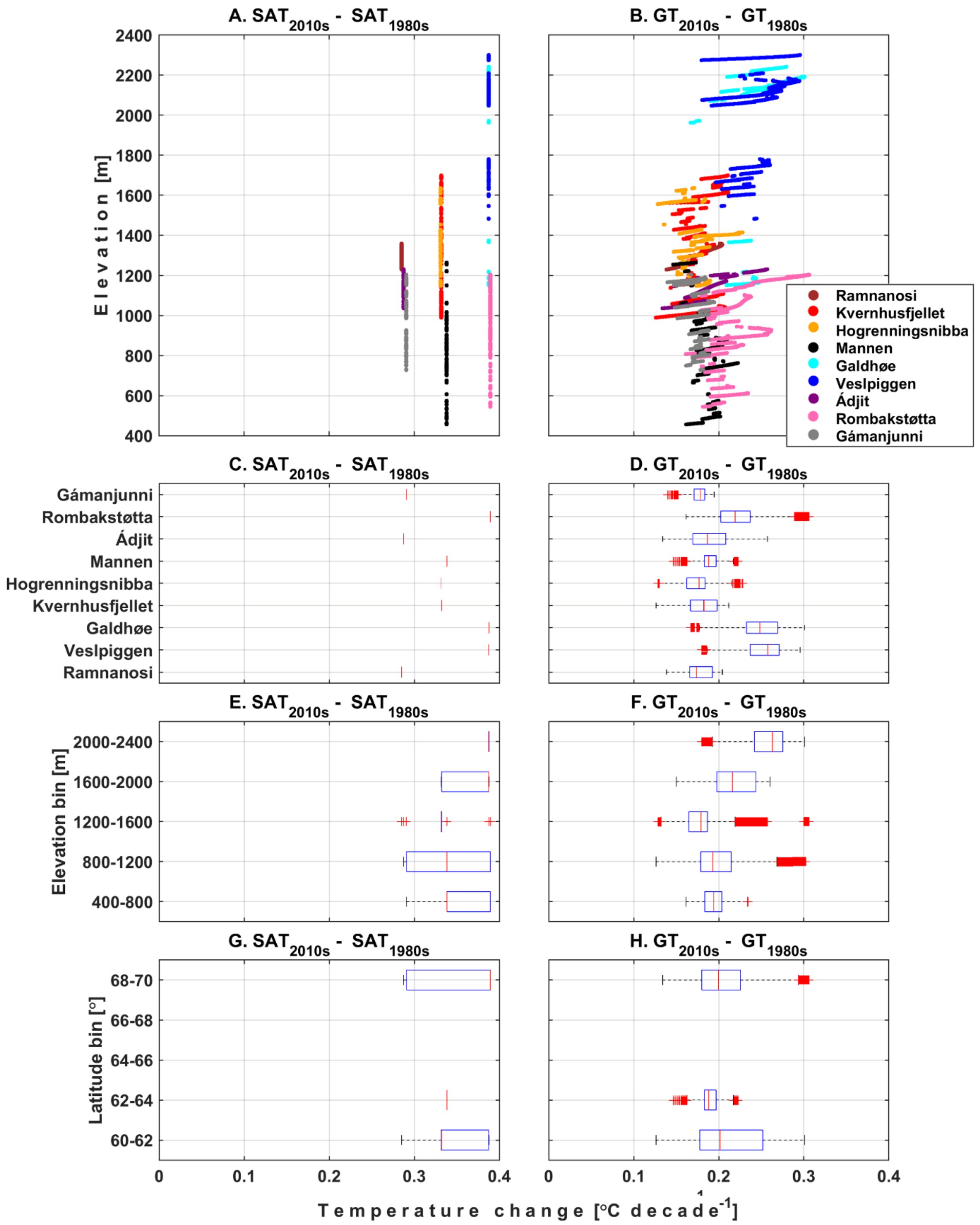

Figure 8. Rates of SAT and GT change at 20 m depth between the 1980s and 2010s for all nodes below steep rock slopes (slope gradient > 60°). Lower subplots: Boxplots with SAT and GT rise between the 1980s and 2010s for: (C-D) every profile, (E-F) 400 m elevation bins and (G-H) 2-degree latitude bins.

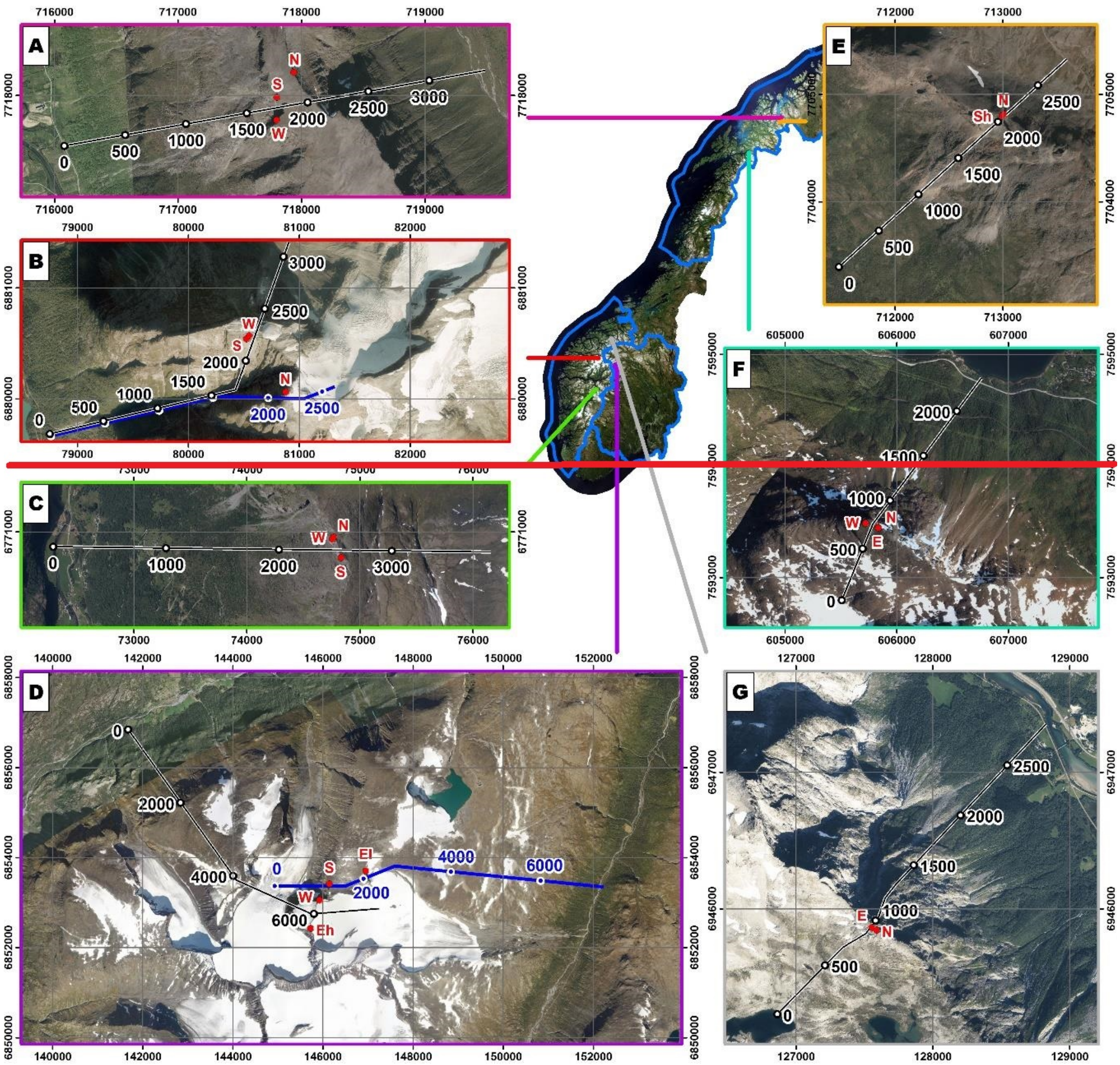

A
B
C
D
E
F
G
N
S
W
Sh
E
Eh
El

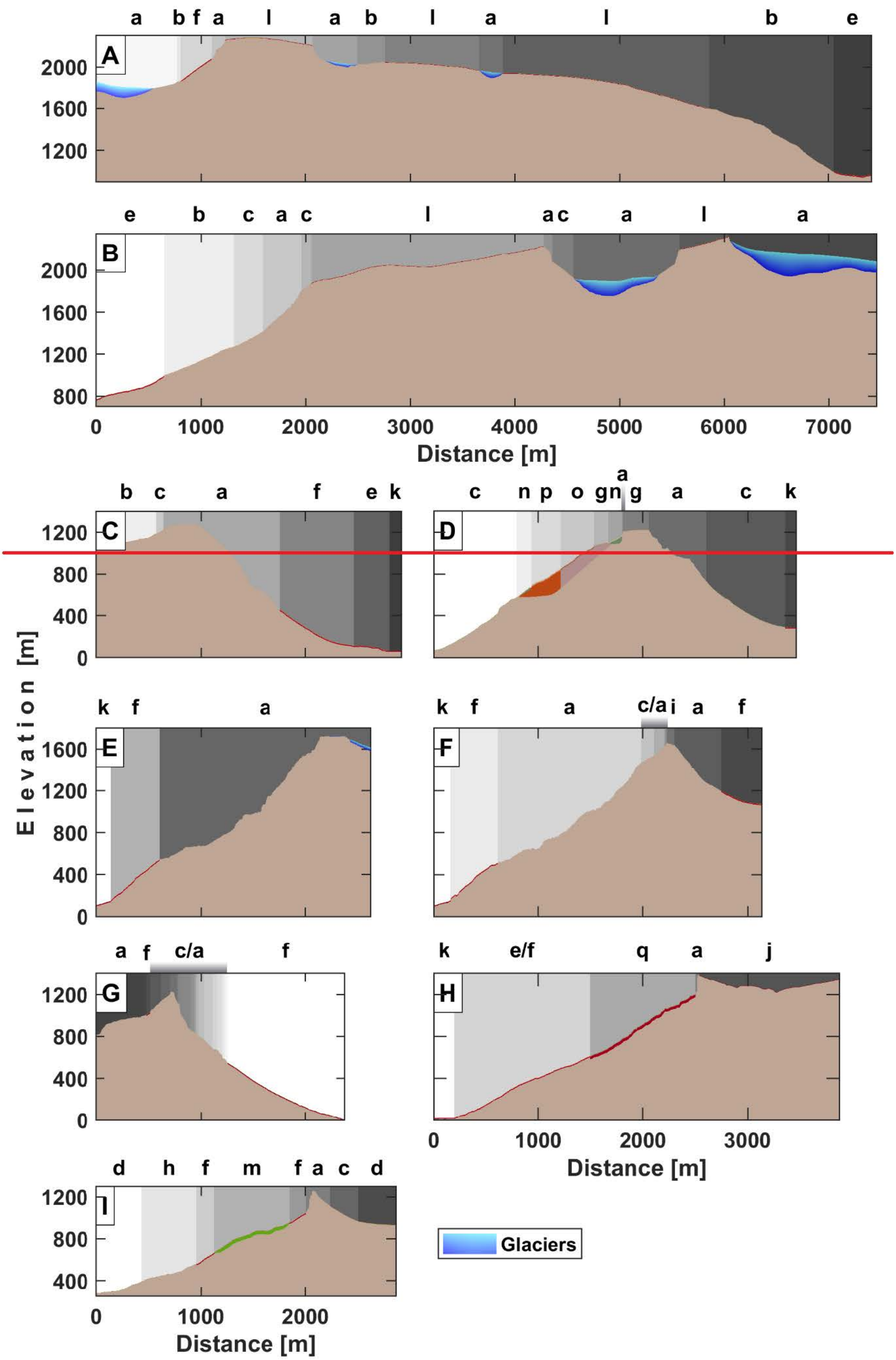

a b f a l a b l a l b e
A
2000
1600
1200
e b c a c l a c a l a
B
2000
1600
1200
800
0 1000 2000 3000 4000 5000 6000 7000
Distance [m]
b c a f e k
C
1200
800
400
0
c n p o g n a g a c k
D
Elevation [m]
k f a
E
1600
1200
800
400
0
k f a c/a i a f
F
a f c/a f
G
1200
800
400
0
k e/f q a j
H
0 1000 2000 3000
Distance [m]
d h f m f a c d
I
1200
800
400
0 1000 2000
Distance [m]
Glaciers

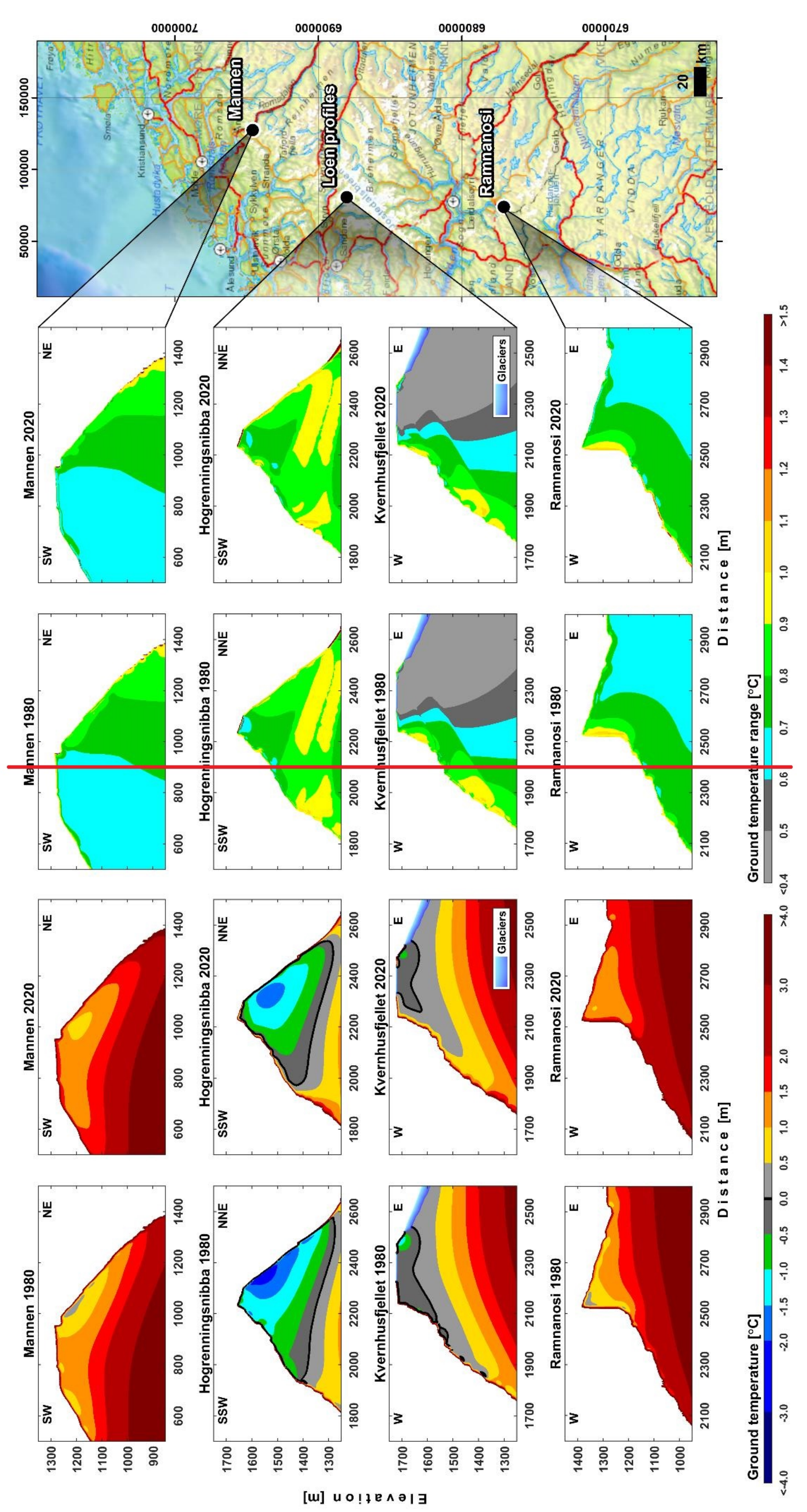

Mannen 1980
Mannen 2020
Hogrenningsnibba 1980
Hogrenningsnibba 2020
Kvernhusfjellet 1980
Kvernhusfjellet 2020
Ramnanosi 1980
Ramnanosi 2020
SW
NE
SSW
NNE
W
E
Glaciers
Elevation [m]
Distance [m]
Ground temperature [°C]
Ground temperature range [°C]
Mannen
Loen profiles
Ramnanosi
20 km

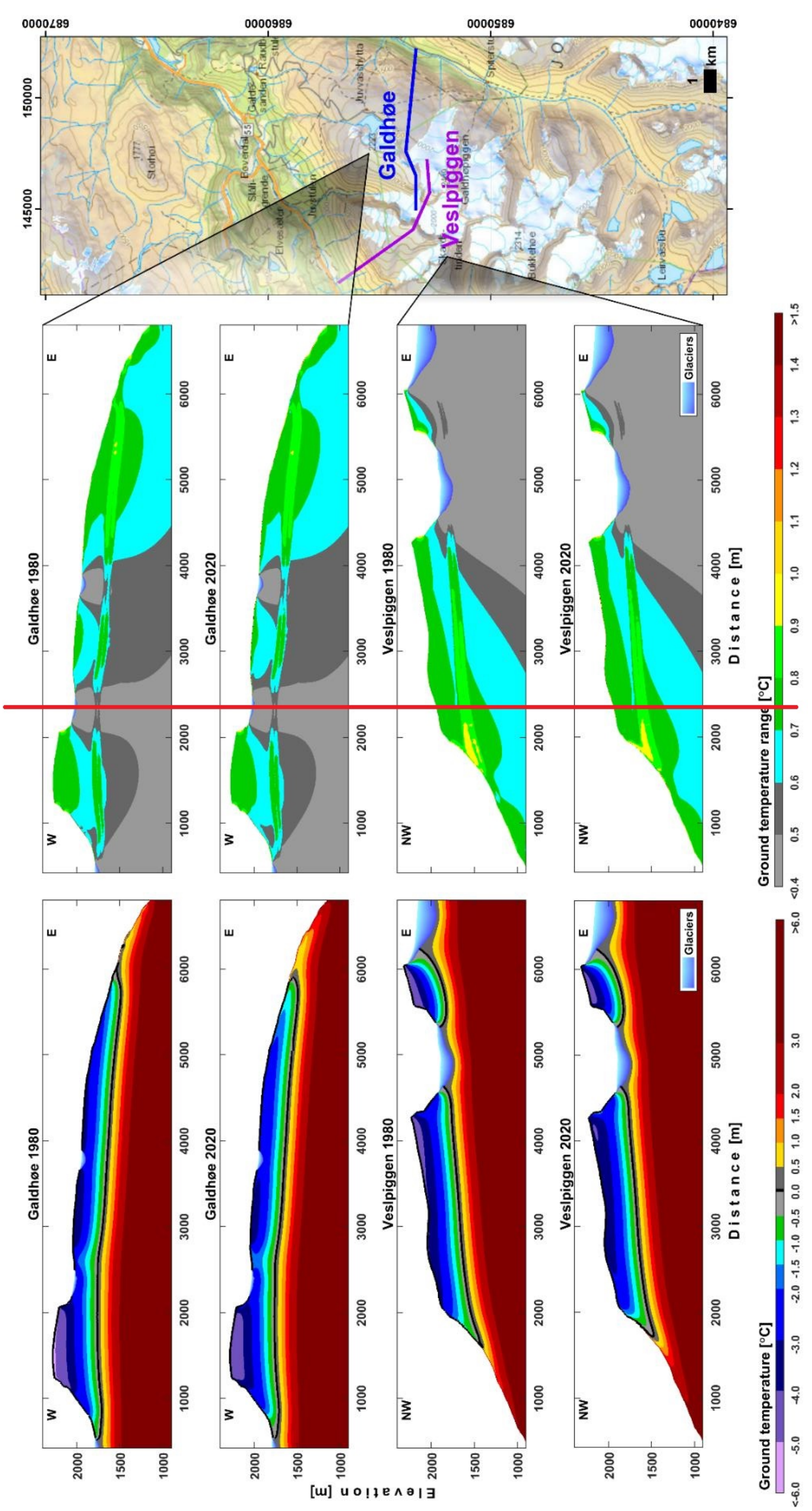

~~**Figure 5. Modelled maximum GT and sensitivity test maximum range in the modelled maximum GT for the profiles in the Jotunheimen in 1980 and 2020. Maximum absolute differences in comparison to the main run are shown based on the uncertainty simulations.** Map background credits: © Statens kartverk, Geovekst, kommuner og OSM – Geodata AS.~~

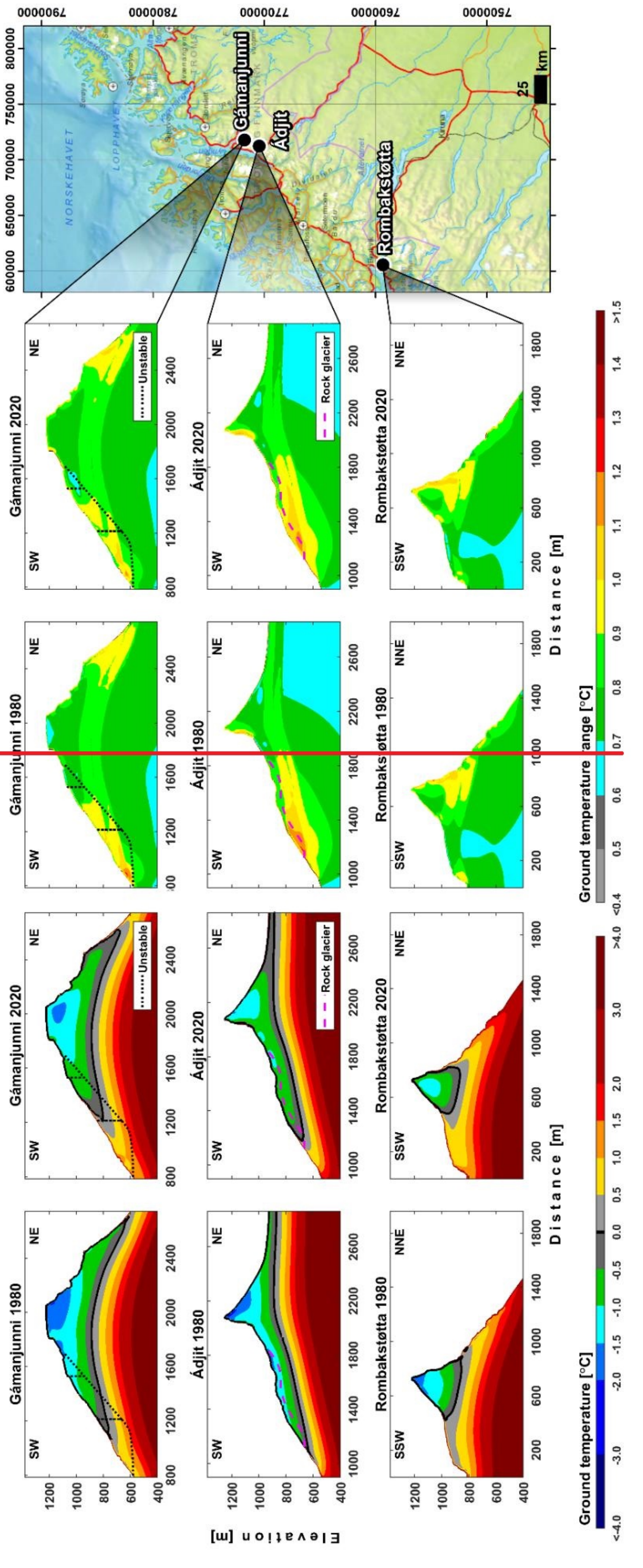

~~**Figure 6. Modelled maximum GT and sensitivity test maximum range in the modelled maximum GT for the profiles in the Northern Norway in 1980 and 2020. Maximum absolute differences in comparison to the main run are shown based on the uncertainty simulations.** Map background credits: © Statens kartverk, Geovekst, kommuner og OSM – Geodata AS.~~

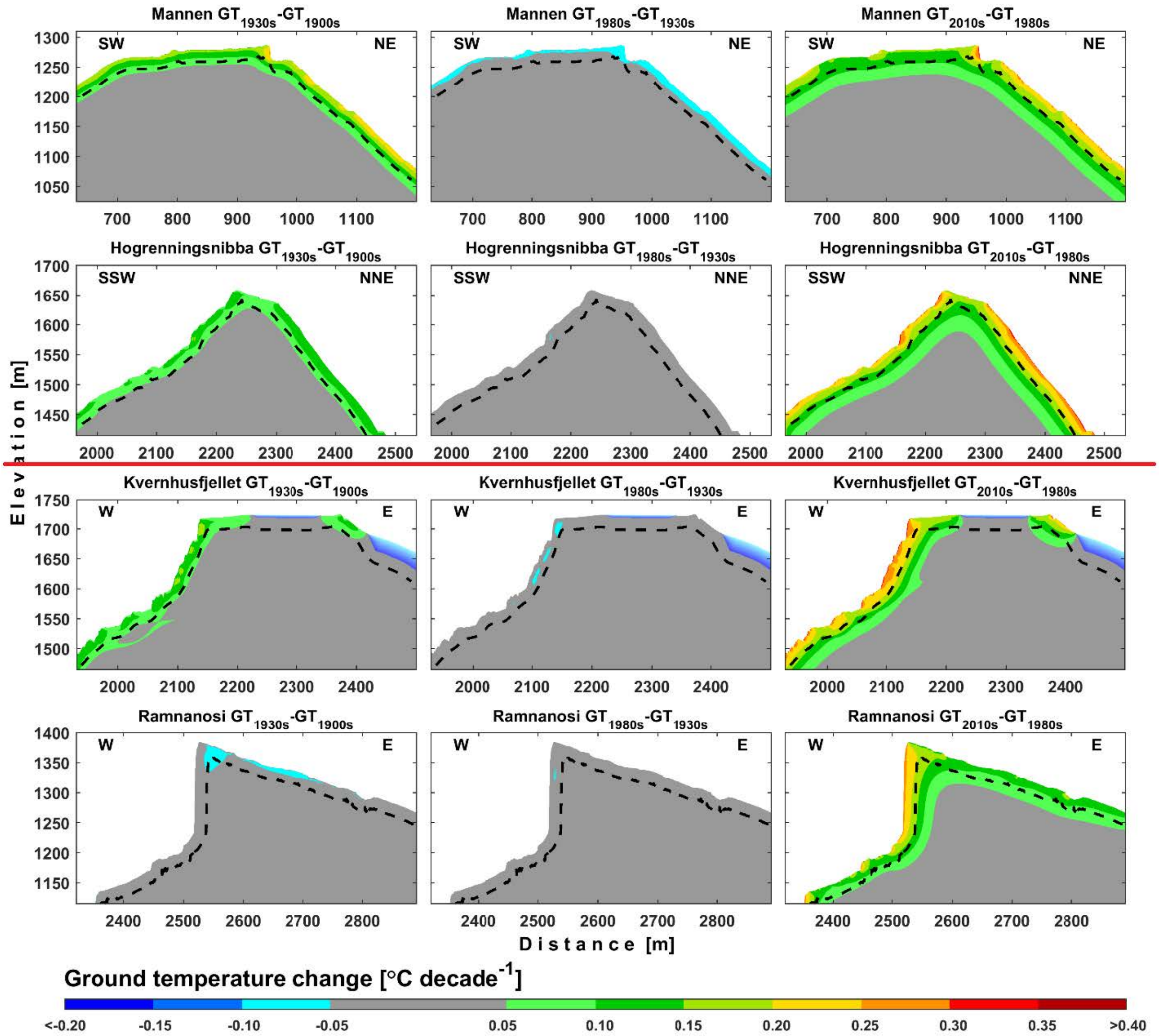

25 ~~**Figure 7. Rate of change in 10 year mean GT for the profiles in the Western Norway between the following decades: (1) the 1900s and the 1930s, (2) the 1930s and the 1980s, (3) the 1980s and the 2010s. 20 m depth is delineated by the black dashed lines.**~~

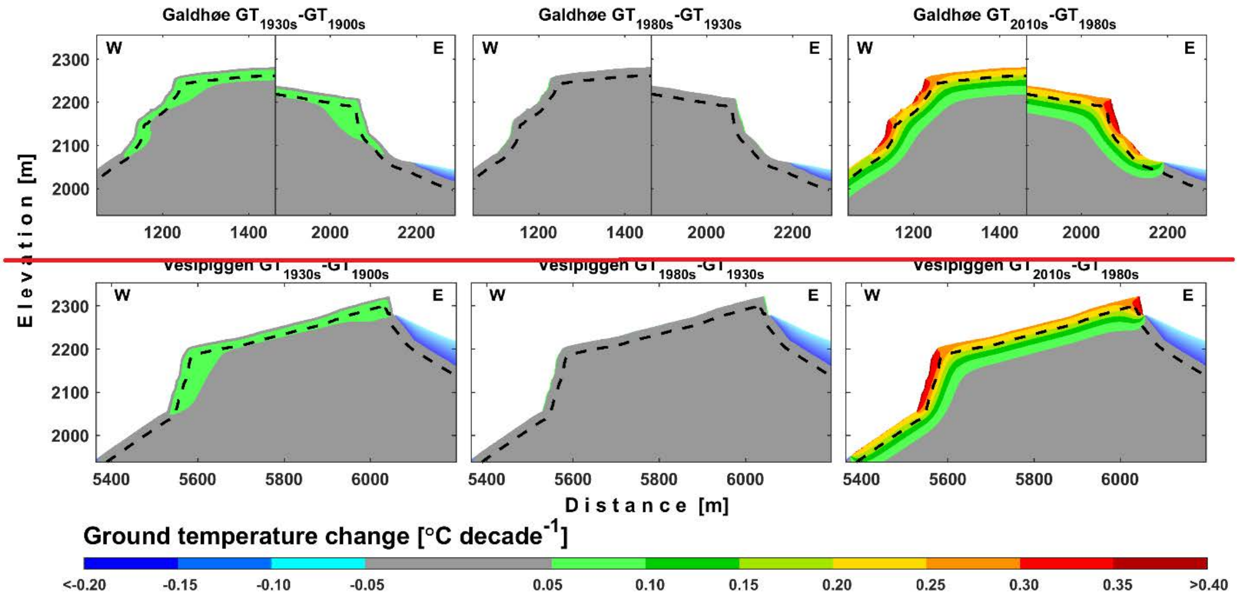

~~**Figure 8. Rate of change in 10 year mean GT for the profiles in the Jotunheimen between the following decades: (1) the 1900s and the 1930s, (2) the 1930s and the 1980s, (3) the 1980s and the 2010s. 20 m depth is delineated by the black dashed lines.**~~

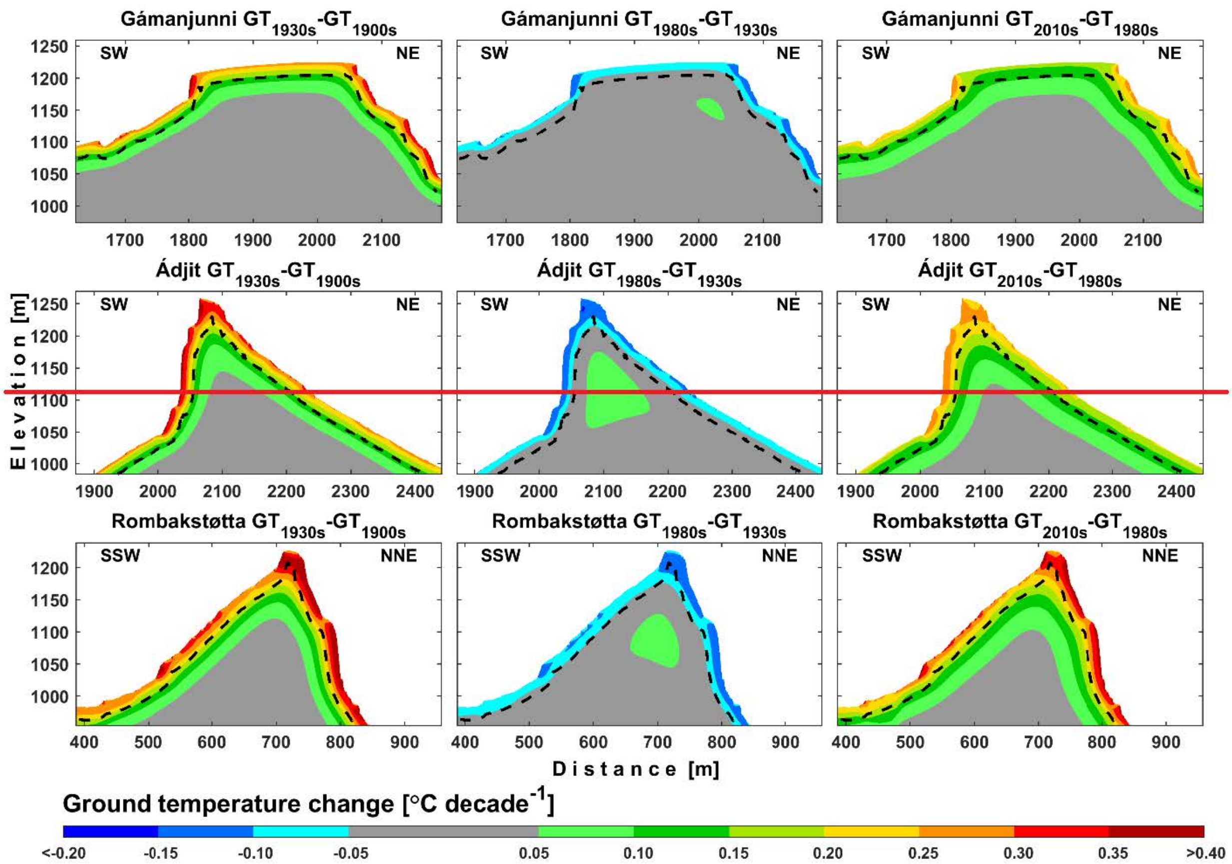

~~**Figure 9. Rate of change in 10 year mean GT for the profiles in the Northern Norway between the following decades: (1) the 1900s and the 1930s, (2) the 1930s and the 1980s, (3) the 1980s and the 2010s. 20 m depth is delineated by the black dashed lines.**~~

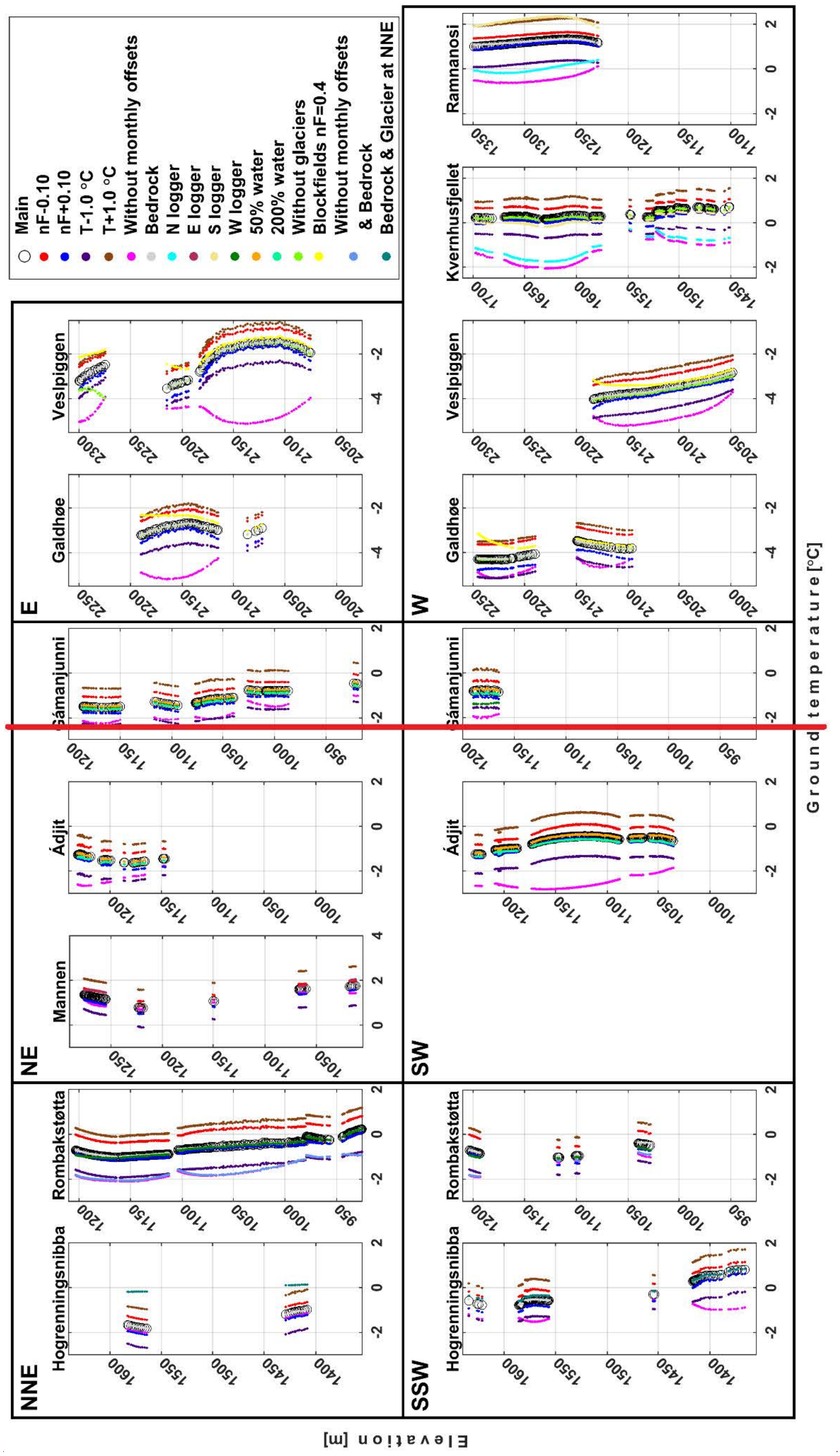

~~**Figure 10. GT in rock walls at 20 m depth simulated in the sensitivity scenarios for the 2010s. A cluster of values without any break elevation-wise usually represents a single rock wall.**~~

~~**Figure 11. Rates of SAT and GT change at approximately 20 m depth between the 1980s and the 2010s for all nodes below steep rock slopes (slope gradient > 60°). Lower subplots: Boxplots with SAT and GT rise between the 1980s and the 2010s for: (C-D) every profile, (E-F) 400 m elevation bins and (G-H) 2-degree latitude bins.**~~

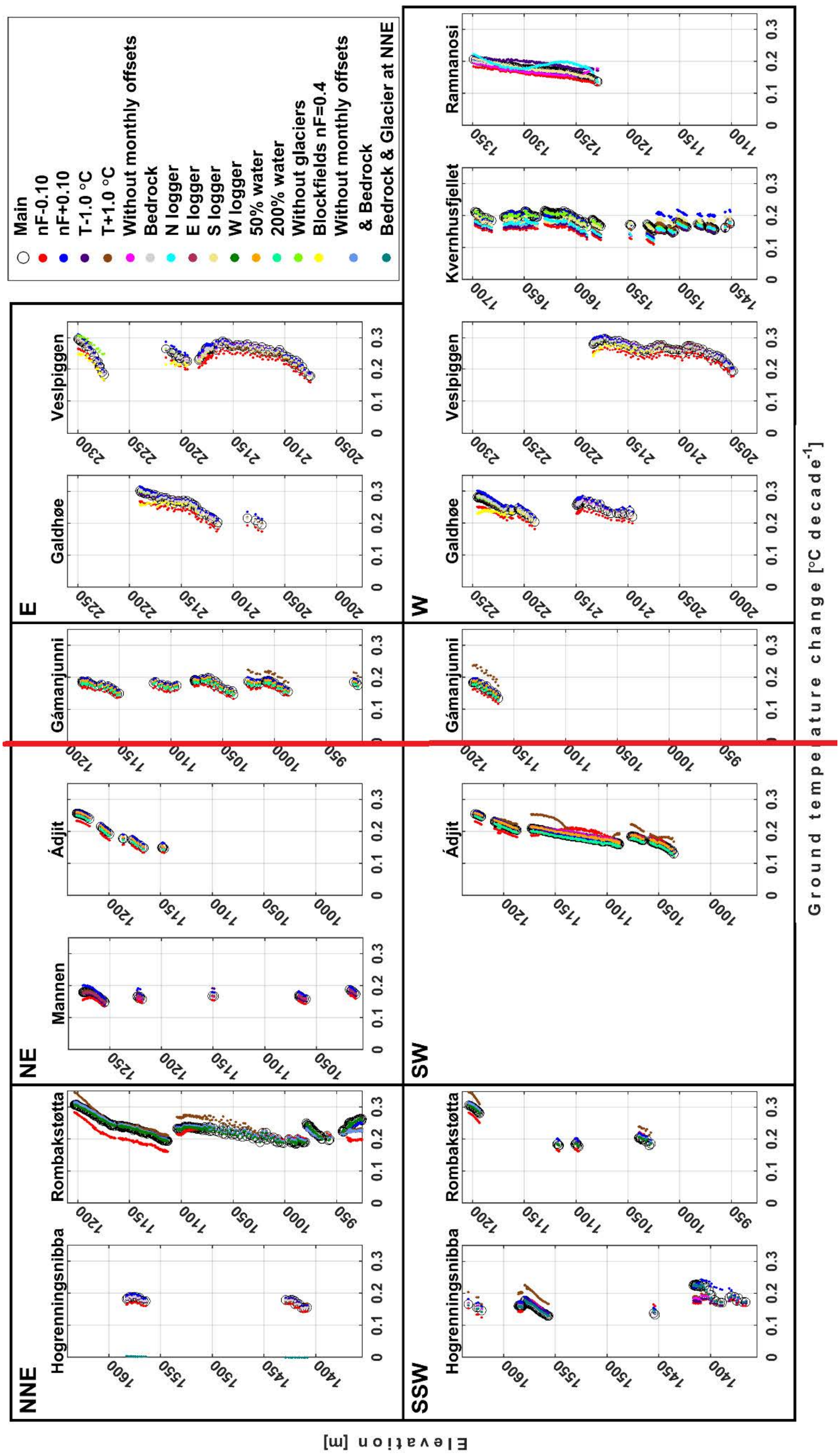

Main
nF-0.10
nF+0.10
T-1.0 °C
T+1.0 °C
Without monthly offsets
Bedrock
N logger
E logger
S logger
W logger
50% water
200% water
Without glaciers
Blockfields nF=0.4
Without monthly offsets
& Bedrock
Bedrock & Glacier at NNE
NNE
NE
E
SSW
SW
W
Hogrenningsnibba
Rombakstøtta
Mannen
Ádjit
Gámanjunni
Galdhøe
Veslpiggen
Kvernhusfjellet
Ramnanosi
Elevation [m]
Ground temperature change [°C decade-1]

Tables

~~**Tables**~~

~~Table 3. Assumed nF-factors along the profiles, which depend on the slope gradient.~~Table 1. Assumed nF-factors along the profiles.

Slope gradient [°] / Sediment or vegetation class	nF-factor		
	Western Norway	**Jotunheimen and Rombakstøtta**	**Gámanjunni and Ádjit**
<30	0.25	0.40 (based on data from Gisnås et al., 2014)	0.50 (based on data from Eriksen, 2018b)
30–40	0.50	0.55	0.60
40–50	0.70	0.70	0.75
50–60	0.90		
>60	1.00		
Blockfields (Jotunheimen)		0.70 (PACE, BH-1 and BH-2)	
Rock glacier (Ádjit)			0.80 (based on data from Eriksen, 2018a)
Broad-leaved forest	0.25 (Gisnås et al., 2017)		

Table ~~4~~2. Summary of the ~~exposures for the~~ rock ~~walls~~wall aspects and selected logger data along profiles. ~~The direction measuring system with respect to the north azimuth is used.~~ “Easternmost” - aspects between 0°–180°; “Westernmost” - aspects between 180°–360°.

Mountain, municipality	Main profile aspect of the westernmost rock wall [°]	Logger data for the ~~first~~westernmost rock wall	Main profile aspect of the easternmost rock wall [°]	Logger data for the ~~second~~easternmost rock wall
Mannen, Rauma	**None**		**38**	**Two ~~runs~~simulations: N (350°) as the main ~~run~~simulation and E (90°)**
Hogrenningsnibba, Stryn	**200**	**S (210°)**	**20**	**N (320°)**
Kvernhusfjellet, Stryn	**272**	**Three ~~runs~~simulations: W (270°) as the main ~~run~~simulation, N (320°) and S (210°)**	**None**	
Ramnanosi, Aurland	**271**	**Three ~~runs~~simulations: W (280°) as the main ~~run~~simulation, N (10°) and S (220°)**	**None**	
Veslpiggen, Lom	**294**	**W (297°)**	**85**	**Eh (89°)**
Galdhøe, Lom	**270**	**W (297°)**	**68**	**El (82°)**
Gámanjunni 3, Kåfjord	**260**	**Two ~~runs~~simulations: S (200°) as the main ~~run~~simulation and W (320°)**	**80**	**N (360°)**
Ádjit, Storfjord	**228**	**Sh (190°)**	**48**	**N (30°)**
Rombakstøtta, Narvik	**202**	**Two ~~runs~~simulations: E (100°) as the main ~~run~~simulation, because the west-facing logger is too cold, and W (270°)**	**37**	**N (25°)**

Table ~~5~~3. Sensitivity ~~scenarios~~simulations.

Scenario(s)	Modifications	Simulation type	Profiles
"nF-0.1"/ "nF+0.1"	We modify nF-factors by subtracting 0.1 or adding 0.1.	Uncertainty	All
"T-1 °C"/ "T+1 °C"	We subtract or add 1 °C to the forcing data before applying nF-factors.	Uncertainty	
"Without monthly offsets"	We ignore solar radiation and force the model directly with SAT; however, we still account for the nival offsets.	Test	
"N/E/S/W logger"	We test thermal influence of SOs measured in the other rock wall aspects as listed in Table ~~4~~2.	Uncertainty for Mannen~~,~~ and Gámanjunni; Test for Kvernhusfjellet, Ramnanosi, ~~Gámanjunni and~~ Rombakstøtta	Mannen, Kvernhusfjellet, Ramnanosi, Gámanjunni and Rombakstøtta
"50 % water"/ "200 % water"	The water fraction is reduced by 50 %/increased by 200 % compared to the values in the main ~~run~~simulation and the remaining fraction is added to/subtracted from the mineral fraction.	Uncertainty	Gámanjunni and Ádjit
"Bedrock"	We assume that the entire subsurface is composed of the bedrock.	Test	Ramnanosi, Hogrenningsnibba, Veslpiggen, Galdhøe and Rombakstøtta
"Without glaciers"	We remove glaciers and perennial snow along profiles.	Test	Galdhøe, Veslpiggen and Kvernhusfjellet
"Blockfields nF=0.4"	We change nF-factor for blockfields to 0.4.	Test	Galdhøe and Veslpiggen
"Snow patch"	At Hogrenningsnibba snow persisted until late summer in some years, hence we add a snow patch on the top of the mountain and partly along the north~~ern~~-facing slope.	Uncertainty	Hogrenningsnibba
"Bedrock & Glacier at NNE"	We test what happens if Hogrenningsnibba has no sediments	Test	

	and add a glacier at the NNE-facing slope.		
“**Without monthly offsets & Bedrock**”	We remove monthly surface offsets and assume that the subsurface consists only of bedrock.	Test	Rombakstøtta

~~**Table 1. Assumed depths of subsurface layers, along with volumetric fractions of the soil constituents for each layer: θ_w – volumetric water content; θ_m – volumetric mineral content; θ_o – volumetric content of organic matter; θ_a – volumetric air content; z – depth. All sediment classes are underlain by bedrock with the same ground composition as bedrock class (“a”).**~~

~~z [m]~~	~~θ_w [-]~~	~~θ_m [-]~~	~~θ_o [-]~~	~~θ_a [-]~~
~~**“a”: Bedrock (NGU code 130)**~~				
~~>0.0~~	~~0.05~~	~~0.95~~	~~0.00~~	~~0.00~~
~~**“b”: Thin till (NGU code 12);**~~ ~~**“c”: Thin colluvium (NGU code 82)**~~				
~~0.0–1.0~~	~~0.30~~	~~0.60~~	~~0.00~~	~~0.10~~
~~**“d”: Medium thick till**~~				
~~0.0–1.0~~	~~0.30~~	~~0.60~~	~~0.00~~	~~0.10~~
~~1.0–2.0~~	~~0.40~~	~~0.60~~	~~0.00~~	~~0.00~~
~~**“e”: Thick till (NGU code 11);**~~ ~~**“f”: Thick colluvium (NGU code 81)**~~				
~~0.0–2.0~~	~~0.30~~	~~0.60~~	~~0.00~~	~~0.10~~
~~2.0–10.0~~	~~0.40~~	~~0.60~~	~~0.00~~	~~0.00~~
~~**“g”: Weathered material**~~				
~~0.0–2.0~~	~~0.10~~	~~0.60~~	~~0.00~~	~~0.30~~
~~**“h”: Thin organic cover over bedrock or shallow regolith (NGU code 100)**~~				
~~0.0–0.5~~	~~0.40~~	~~0.50~~	~~0.10~~	~~0.00~~
~~**“i”: Thin regolith (NGU code 72)**~~				
~~0.0–1.0~~	~~0.10~~	~~0.60~~	~~0.00~~	~~0.30~~
~~1.0–2.0~~	~~0.40~~	~~0.60~~	~~0.00~~	~~0.00~~
~~**“j”: Medium thick regolith**~~				
~~0.0–1.0~~	~~0.20~~	~~0.60~~	~~0.00~~	~~0.20~~
~~1.0–4.0~~	~~0.40~~	~~0.60~~	~~0.00~~	~~0.00~~
~~**“k”: Fluvial/Alluvial sediments (NGU code 50)**~~				
~~0.0–1.0~~	~~0.10~~	~~0.60~~	~~0.00~~	~~0.30~~
~~1.0–10.0~~	~~0.40~~	~~0.60~~	~~0.00~~	~~0.00~~
~~**“l”: Blockfields (NGU code 73)**~~				
~~0.0–2.0~~	~~0.10~~	~~0.60~~	~~0.00~~	~~0.30~~
~~2.0–5.0~~	~~0.40~~	~~0.60~~	~~0.00~~	~~0.00~~
~~**“m”: Rock glacier (NGU code 88)**~~				
~~0.0–2.0~~	~~0.05~~	~~0.60~~	~~0.00~~	~~0.35~~
~~2.0–5.0~~	~~0.10~~	~~0.60~~	~~0.00~~	~~0.30~~
~~5.0–35.0~~	~~0.40~~	~~0.60~~	~~0.00~~	~~0.00~~
~~**“n”: Scree**~~				
~~0.0–5.0~~	~~0.02~~	~~0.40~~	~~0.00~~	~~0.58~~
~~5.0–various depths~~	~~0.60~~	~~0.40~~	~~0.00~~	~~0.00~~
~~**“o”: Fractured bedrock**~~				
~~0.0–10.0~~	~~0.05~~	~~0.80~~	~~0.00~~	~~0.15~~
~~10.0–various depths~~	~~0.10~~	~~0.90~~	~~0.00~~	~~0.00~~
~~**“p”: Heavily fractured bedrock**~~				
~~0.0–10.0~~	~~0.05~~	~~0.75~~	~~0.00~~	~~0.20~~
~~10.0–various depths~~	~~0.15~~	~~0.80~~	~~0.00~~	~~0.05~~
~~**“q”: Very thick colluvium**~~				
~~0.0–2.0~~	~~0.05~~	~~0.60~~	~~0.00~~	~~0.35~~
~~2.0–5.0~~	~~0.10~~	~~0.60~~	~~0.00~~	~~0.30~~
~~5.0–30.0~~	~~0.40~~	~~0.60~~	~~0.00~~	~~0.00~~

~~**Table 2. SAT records used to construct forcing along profiles.**~~

~~**Mountain, municipality**~~	~~**Meteorological station at the lower elevation along the profile (elevation; years with records)**~~	~~**Meteorological station on the mountain plateau (elevation; years with records)**~~	~~**Meteorological station(s) with the long-term temperature records (elevation; years with records)**~~
~~**Western Norway**~~			
~~Mannen, Rauma~~	~~Marstein (67 m; 2010–present)~~	~~Mannen (1294 m; 2010–present)~~	~~Bergen-Lungegårdshospitalet (17 m; 1861–1895); Bergen-Pleiestiftelsen (22 m; 1895–1926)~~
~~Hogrenningsnibba, Stryn~~	~~seNorge (200 m; 1957–present)~~	~~seNorge (1600 m; 1957–present)~~	
~~Kvernhusfjellet, Stryn~~			
~~Ramnanosi, Aurland~~	~~seNorge (40 m; 1957–present)~~	~~Klevavatnet (960 m; 2014–present)~~	
~~**Jotunheimen**~~			
~~Veslpiggen, Lom~~	~~Juvvasshøe (1894 m; 1999–present)~~	~~seNorge (2230 m; 1957–present)~~	~~Dombås II (643 m; 1864–1972)~~
~~Galdhøe, Lom~~			
~~**Northern Norway**~~			
~~Gámanjunni 3, Kåfjord~~	~~seNorge (250 m; 1957–present)~~	~~Gámanjunni (1237 m; 2016–present)~~	~~Tromsø I (38 m; 1872–1926)~~
~~Ádjit, Storfjord~~	~~Skibotn II (20 m; 2004–present)~~		
~~Rombakstøtta, Narvik~~	~~Straumsnes (200 m; 2011–present)~~	~~Narvik-Fagernesfjellet (1000 m; 2014–present)~~	

Videos

In the current version of the manuscript, videos are available through the University of Oslo's OneDrive account: https://uio-my.sharepoint.com/:f:/g/personal/justync_uio_no/EjO_zEqsoixAju0-h1198IgBbru2nFgngZuyDb0tl9KeMQ?e=dzmVrA . Note that the file is view-only. The videos can be viewed directly in any web browser, except for Internet Explorer 11, or downloaded (file size is 124 MB).